NATURAL CONVECTION FILM BOILING ON A VERTICAL SURFACE

Thesis by

David C.Sherman

In Partial Fulfillment of the Requirements

For the Degree of

Doctor of Philosophy

California Institute of Technology

Pasadena, California 91125

1980

(Submitted May 6,1980)

ACKNOWLEDGMENTS

I wish to extend my sincere thanks to Professor R.H.Sabersky for his guidance during the course of this investigation. I also wish to acknowledge the help of Professor C.Brennen in the area of hydrodynamic stability theory.

The assistance of Mr.S.Toner, Mr.W.Ledeboer, and Mr.C.Campbell in the design, construction and implementation of the experimental apparatus, and in the extraction of data therefrom is greatly appreciated.

My special thanks are extended to Ms.S.Berkley and others on the Caltech staff for their generous donations of time and effort.

ABSTRACT

Experimental results are presented for an investigation of free convection film boiling heat transfer to saturated ethanol, saturated Freon 113, and saturated distilled water from a vertical cylinder. High speed motion pictures of the vapor-liquid interface in film boiling have been obtained. All tests have been conducted at atmospheric pressure over a range of heat flux between 9000 and 37000 BTU/hr ft^2.

A study of the stability of the vapor-liquid interface is performed and the results are compared to the photographic data. Parameters influencing the heat transfer process are developed and the experimental data is used to determine their proper relationship.

The heat transfer coefficient in natural convection film boiling of saturated liquids on moderately long vertical surfaces at constant heat flux is shown to be insensitive to vertical position, and to be dependent only on the temperature differential and the fluid properties.

Large scale waves have been observed on the vapor-liquid interface: however, their effect on the heat transfer is minimal. It appears that intense vaporization at the interface plays an important role in the generation of these waves, while surface tension does not.

A strong possibility of liquid droplet entrainment in the vapor flow is indicated by the presence of a rough, wavy interface, a relatively high speed vapor-flow, and by the unexpectedly strong dependence of the heat transfer on the latent heat of vaporization.

TABLE OF CONTENTS

TABLE OF CONTENTS (CONTINUED)

LIST OF FIGURES

LIST OF FIGURES (CONTINUED)

LIST OF FIGURES (CONTINUED)

LIST OF FIGURES (CONTINUED)

LIST OF FIGURES (CONTINUED)

LIST OF TABLES

NOMENCLATURE

A_i	Cross-sectional area of insulation on thermocouple wire
a_L	Absorptivity of liquid
A_{tc}	Cross-sectional area of thermocouple wire
c	Dimensionless complex wave speed
c*	Complex wave speed
C	Heat transfer enhancement factor
c_F	Friction coefficient
c_P	Specific heat at constant pressure
$\overline{c^*_{R_{EXP}}}$	Experimentally determined average wave speed
D	Diameter
f	Friction factor
Fr	Froude number
g	Gravitational acceleration
h	Heat transfer coefficient
$\overline{h}$	Average heat transfer coefficient
h_c	Convective heat transfer coefficient
h_{fg}	Latent heat of vaporization
h'_{fg}	Modified latent heat of vaporization
h_R	Radiative heat transfer coefficient
$\langle h(t) \rangle$	Time averaged heat transfer coefficient
I	Current
$\hat{i},\hat{j}$	Unit vectors in the x and y directions, respectively
$\hat{k}$	Unit vector normal to plane of paper
k	Thermal conductivity

NOMENCLATURE (CONTINUED)

$\tilde{\tilde{kA}}$	Effective thermal conductance
L	Length
$m_{v,L}$	Mass flux in vapor or liquid normal to interface
$\dot{m}$	Mass flow rate
$\vec{n}$	Surface normal unit vector
N_{FB}	Film boiling number
Nu	Nusselt number
P	Pressure
p	Dimensionless pressure = $\frac{P}{\rho u_0^2}$
$\tilde{p}$	Dimensionless pressure disturbance amplitude
Pe	Peclet number
Pr	Prandtl number
$\bar{p}_v$	Undisturbed dimensionless pressure in vapor
P_0	Reference pressure
q	Heat flux
$\vec{q}_v$	Heat flux vector in vapor
R	Thermal resistivity
Re	Reynolds number
Re_δ	Vapor film Reynolds number
S	Dimensionless temperature disturbance amplitude
Sh	Superheat number
T	Temperature

NOMENCLATURE (CONTINUED)

T_S	Saturation temperature
t	Time, thickness
t^*	Time
$\vec{t}$	Surface tangent unit vector
ΔT_S	Difference between solid surface temperature and saturation temperature
u	Velocity, x-direction
u^+	Dimensionless velocity x-direction $= \dfrac{u}{\left(\dfrac{\tau_w}{\rho}\right)^{\frac{1}{2}}}$
u_0	Maximum vapor velocity, x-direction
V	Voltage
$\vec{V}$	Velocity vector
v	Velocity, y-direction
x, x^*	Vertical dimension
x_0	Reference vertical position
y, y^*	Horizontal dimension
y^+	Dimensionless horizontal dimension $= y \dfrac{\left(\dfrac{\tau_w}{\rho}\right)^{\frac{1}{2}}}{\left(\dfrac{\mu}{\rho}\right)^{\frac{1}{2}}}$
$A, B, b, b_1, b_2, c, c_0, c_1, K, m, m_1, m_2, n$	Numerical constants

NOMENCLATURE (CONTINUED)

α	Dimensionless wave number
α^*	Wave number
β	Numerical constant, thermocouple calibration coefficient
γ	Vapor to liquid density ratio
Δ	Difference
δ	Vapor film thickness
$\overline{\delta}$	Average vapor film thickness
ε	Dimensionless interfacial wave amplitude
ε_w	Emissivity of solid surface
η	Interfacial wave amplitude
$\overline{\eta}_{EXP}$	Experimentally determined average interfacial wave amplitude
θ	Dimensionless temperature difference
$\overline{\theta}$	Undisturbed dimensionless temperature profile
λ	Wavelength
$\overline{\lambda}_{EXP}$	Experimentally determined average interfacial wavelength
μ	Absolute viscosity
ρ	Density
σ	Surface tension
σ'	Stephan-Boltzmann constant
$\sigma_{v,L}$	Stress tensor in vapor or liquid
τ	Shear stress
φ	Dimensionless stream function disturbance amplitude
ψ	Dimensionless stream function

NOMENCLATURE (CONTINUED)

ψ^*	Stream function
$\overline{\psi}$	Undisturbed dimensionless stream function
ω	Dimensionless complex frequency
ω^*	Complex frequency

Subscripts

AC	Axial conduction
c	Critical
CRIT	Critical
D	Most dangerous
eff	Effective
EXP	Experimental
i	Interface, insulation
K-H	Kelvin-Helmholtz
L	Liquid
m	Metal
MAX	Maximum
MIN	Minimum
R	Radiative, real part
S	Saturation, steady-state
tc	Thermocouple
TP	Two-phase
v	Vapor
w	Wall

I. INTRODUCTION

The film boiling heat transfer process has become increasingly important in the last twenty years or so, primarily due to its applications to nuclear power reactors. Film boiling, however, occurs in a number of technological areas: For example, it is an important factor in the understanding of thermal stresses occurring during the quenching of hot metals, and in the field of cryogenics, where room temperature solids are brought into contact with extremely cold liquids.

Film boiling is a very inefficient heat transfer process, as large temperature differences are required to produce low to moderate heat flux rates. Perhaps for this reason, investigations into the phenomenon were practically nonexistent until the early 1950's, since film boiling seemingly was considered to be something to be avoided, rather than understood!

Film boiling is characterized by the presence of a vapor layer between a hot solid surface and a liquid at or below its saturation temperature for the system pressure. Since vapors, in general, have relatively low thermal conductivity, and since heat must flow through this vapor layer to reach the liquid, very high solid surface temperatures must be established to cause any significant heat transfer.

One can obtain some understanding of the problems associated with film boiling by studying the equilibrium pool boiling curve, Fig.1. This curve is a plot of the equilibrium heat flux at a given solid surface as a function of its temperature, when this temperature is above the saturation temperature of the liquid in which it is immersed. The curve is divided into four regions.

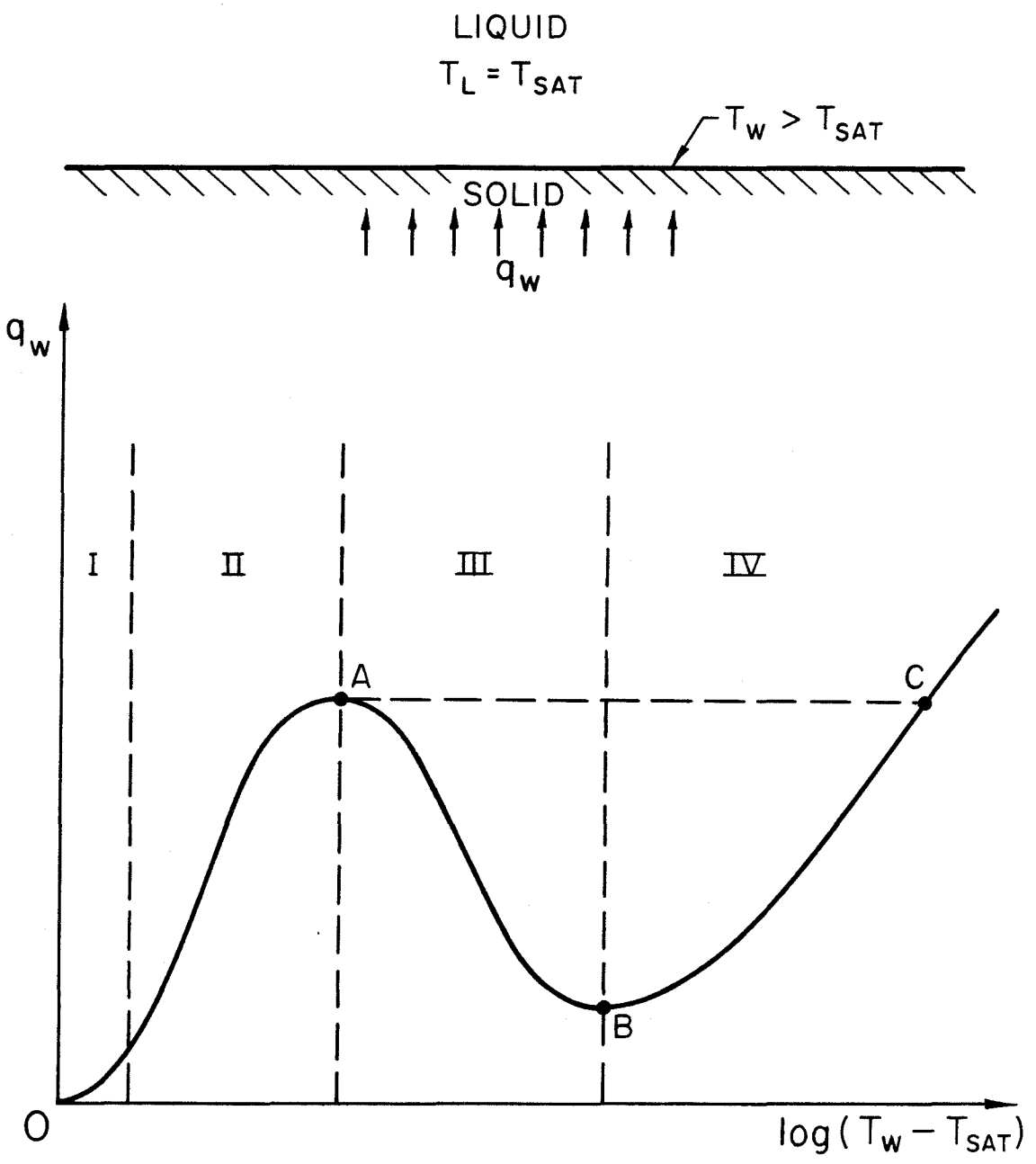

I. NATURAL CONVECTION
II. NUCLEATE BOILING
III. TRANSITION BOILING
IV. STABLE FILM BOILING

Figure 1. Equilibrium Pool Boiling Curve

Region I, in which the superheat of the solid surface (T_W-T_S) is only a few degrees, is characterized by natural convection with no phase change. The small temperature difference in this region does not provide enough heat flux to cause any vapor bubbles to form at nucleation sites in the liquid near the wall.

As the wall temperature, or alternatively the wall heat flux is further increased, Region II is entered, and small bubbles begin to form. This is the nucleate boiling regime, and as the temperature or heat flux is increased, bubble size and number density increase. It is believed that the fluid motions caused by the bubble activity are primarily responsible for the relatively large heat transfer rates occurring in nucleate boiling. As the point A in Fig.1 is approached the bubble action becomes very intense, and at the point A, there is so much vapor present near the wall that a further incremental increase in temperature will actually decrease the heat flux due to the insulating effect of further vapor generation. The heat flux associated with the point A is termed the critical heat flux or CHF.

Region III is called the transition boiling regime, and here the low vapor conductivity plays a very important role. Assuming that the temperature of the solid is being controlled, an increase in the solid surface temperature in this region produces a decrease in the resulting heat transfer to the liquid. This is primarily due to the fact that in this temperature range the additional vapor being generated tends to insulate the heated solid from the liquid. The vapor flow in this regime is very unstable and oscillatory. This trend of decreasing heat flux with increasing temperature continues until point B in Fig. 1 is approached. The surface is now

completely covered by a vapor layer and the temperature difference across the vapor begins to be large enough to counteract the insulating effect of further vapor generation.

The area in Fig.1 to the right of point B, labeled Region IV, is called the stable film boiling regime, and is the boiling regime which is the object of this study. The temperature associated with point B is called the minimum film boiling temperature, and is the minimum temperature for which a stable, continuous vapor blanket can exist between the solid surface and liquid bulk for a given liquid, liquid temperature, and system pressure. The equilibrium heat flux at this temperature is termed the minimum film boiling heat flux. In the stable film boiling regime, the heat flux again rises with increasing temperature since the resistance to heat transfer due to increased vapor generation increases more slowly than the driving temperature differential. The rate of increase of heat flux with temperature difference in stable film boiling, however, is much lower than that occurring in nucleate boiling. Eventually, the temperature of the solid surface will reach values at which thermal radiation becomes important and it will increasingly influence the heat transfer mechanism. (This temperature is of the order of several thousand degrees Farenheit for most liquids.)

In many applications involving boiling heat transfer, it is the heat flux which is controlled, not the surface temperature. This is the case, for example, where electric resistance heating is being employed, and the supply voltage is controlled, or in a nuclear reactor where each fuel element generates heat at a fixed rate.

If, in such an application, where normal operation is in the nucleate

boiling region of Fig.1, the heat flux is increased above the CHF point, a rapid increase in temperature will occur. As can be seen in Fig.1, for a heat flux greater than the critical value equilibrium is shifted to a temperature corresponding to point C or higher. This temperature is generally greater than the melting temperature of most metals, and this process results in the well-known phenomenon of "burnout".

The interest in the present study was originally stimulated by cooling problems arising in the design of nuclear reactors. In that case film boiling is expected to occur during a transient induced by loss of the liquid reactor coolant. After the coolant has been lost from the core, the nuclear fuel elements are surrounded by air and vapor providing a relatively poor natural convection heat transfer environment. Since these elements are still generating a substantial amount of heat, their temperatures can become very large. It is essential that, under these conditions, the temperature of the cladding of the fuel elements is kept below the melting point. In order to cool the reactor, liquid coolant is flooded into the core. However, the temperature of the fuel elements can be well above the minimum film boiling temperature, and thus the initial cooling of the reactor must be accomplished through film boiling heat transfer. Hence, knowledge of the heat transfer rates associated with film boiling is a key factor in determining the duration and effects of the cooling or reflood process.

Many factors have been found to influence heat transfer rates in film boiling. Among these are the orientation of the heating surface with respect to gravity, the subcooling of the liquid, and the liquid velocity. Each of these effects has been demonstrated in many different experiments,

[16],[30],[32],[36],[40],[46]-[49],[50],[51].

The emphasis of the present study is on the investigation of the behavior of the liquid-vapor interface and its effect on the heat transfer. It was felt that many of the basic aspects of this problem could be examined under relatively simple conditions in which the heating surface is vertical, the liquid is at the saturation temperature and all velocities are due to free convection only. These experimental conditions were therefore selected. The present study will include both analytical and experimental work on the film boiling process.

Stable film boiling probably lends itself more readily to an analysis than the other boiling mechanisms. Primarily, this is due to the relative orderliness of the process. In film boiling, the phases remain separated, and locally the vapor flow can be considered to depend on only one dimensional variable.

Much of the analytical work in film boiling has assumed that the vapor flow is laminar and that the vapor-liquid interface remains smooth, [3],[4],[9]-[11],[32],[34],[36],[39],[47],[49],[50]. The results of this type of analysis appear to agree with experiments of film boiling with cryogenic liquids such as liquid nitrogen or liquid argon on a vertical surface no longer than two or three inches. For other fluids, and for longer vertical surfaces, these analyses generally underpredict measured heat transfer coefficients.

Several investigators [8],[27],[28],[41], have noted that, after a relatively short flow length, the vapor Reynolds numbers become quite high indicating a probable turbulent transition within an inch or two of the bottom of a vertically oriented solid in film boiling. This may partially

explain the underprediction of heat transfer rates by a laminar analysis, as the heat transfer can be expected to be higher for a turbulent flow under the same external conditions. One of the objectives of this work is to gain a better understanding of the nature of the vapor flow and to develop the parameters which determine the heat transfer in film boiling.

In addition, many analyses also include the assumption that the vapor-liquid interphase boundary remains smooth, and that the vapor flows in a smooth channel formed by the wall and the interface. Several authors, however, [8],[27]-[29],[35],[37],[38],[41], have reported the observation of a wavy or irregular vapor-liquid interface through high-speed photography. Many attempts at explaining the effects of this observation have been made, none of which give entirely satisfactory agreement with experimental data.

There also has been much speculation concerning the question of the existence of liquid-solid contacts in stable film boiling. A few authors [12],[27],[34],[37],[38], have reported evidence, or made the assumption, that these contacts do occur for certain ranges of parameters, and such contact could greatly influence the heat transfer process.

The present investigation, as mentioned earlier, is concerned with the heat transfer in film boiling, especially when the film Reynolds number is high and the interface is wavy. The investigation is mainly experimental. Measurements were made to obtain heat transfer coefficients and high speed moving pictures were taken which allowed detailed examinations of the interface. In order to obtain data covering a wide range of fluid parameters, experiments were conducted using three fluids (distilled water, Freon 113, and ethanol).

Some analytical work has also been performed with the purpose of clarifying the mechanism responsible for causing the instability of the interface and devising parameters that could be used in the presentation of the data.

II. PREVIOUS WORK

The earliest recorded observations of film boiling were made by Leidenfrost [1], in 1756. He measured evaporation rates of water droplets on a heated, polished iron spoon. He noted that when the spoon was very hot, the evaporation times were quite long and the droplet remained almost spherical; whereas, when the spoon was not too hot, the drop immediately spread into a thin layer and evaporated much more rapidly. This relatively slow evaporation rate which occurs at large temperature differences is characteristic of film boiling.

In 1934, Nukiyama [43] performed boiling heat transfer experiments using an electrically heated platinum wire submerged in a pool of water. He reported that the heat transfer in boiling was not a monotonically increasing function of the heater temperature but exhibited a distinct maximum and minimum point. This work led to the conclusion that there exist three distinct modes of boiling heat transfer, nucleate, transition, and film boiling, and that each mode exhibits a different mechanism of heat transport.

An analytical approach to heat transfer in film boiling similar to Nusselts' laminar condensation analysis was suggested by many authors in the late 1940's [42]. L.A.Bromley [3] was the first to use this approach and published his results in 1950. He approached the film boiling problem with the following important assumptions:

1) The wall temperature is a constant.
2) The vapor flow is laminar and controlled by a balance of buoyancy and shear forces only.

3) Heat transfer is by conduction only, and all of the heat supplied to the vapor goes into evaporation of the liquid phase.

4) The vapor-liquid interface is smooth.

5) The liquid is uniformly at its saturation temperature.

6) The physical properties of the vapor can be evaluated at a temperature equal to the arithmetic average of the wall and liquid temperature.

The interfacial shear stress was evaluated by considering two extreme cases:

1) The vapor flows between two stationary, approximately parallel planes.

2) The liquid moves in such a way that there is no interfacial shear.

These last two assumptions alter the magnitude of the numerical coefficient in the expression obtained for the heat transfer coefficent and must serve as bounding cases for the evaluation of the effect of interfacial shear on laminar film boiling heat transfer rates. The result for the average heat transfer coefficient is:

$$\bar{h}=C_0\left[\frac{k_v^3 g\rho_v(\rho_L-\rho_v)h_{fg}}{L\mu_v(T_w-T_S)}\right]^{\frac{1}{4}} \qquad (1)$$

where

$$0.5 \le C_0 \le 0.732 \quad .$$

Bromley [3] later modified this expression by introducing an effective latent heat of vaporization

$$h_{fg}' = h_{fg}\left[1+0.34\,\frac{C_{P_v}(T_w-T_S)}{h_{fg}}\right]^2$$

to be used to account for the sensible heat of the vapor. He also suggested the following expressions

$$h_R = \frac{3}{4}\left[\frac{\sigma'}{\frac{1}{\varepsilon_w}+\frac{1}{a_L}-1}\right]\left(\frac{T_w^4-T_s^4}{T_w-T_s}\right) \qquad (2)$$

$$\bar{h}_{TOTAL} = \bar{h}+h_R$$

to account for radiative heat transfer, where σ' is the Stefan-Boltzmann constant, ε_w is the emissivity of the solid, and a_L is the absorptivity of the liquid, and $\bar{h}$ is given by Eq.(1).

Experiments by Ellion [4] and others have shown this result to be valid for very short lengths of the heated surface ($\approx 1''$ in water). For longer heated surfaces, this result generally underpredicts measured heat transfer rates.

A slight modification of the analysis by Bromley was made by Kutateladze [45] with respect to the effect of radiative heat transfer.

Another approach to modeling stable, laminar film boiling is the application of boundary layer analysis. Koh [9] considered laminar film boiling from a vertical flat plate by simultaneously solving the boundary layer equations for the vapor and liquid phases. The interfacial conditions of equal vapor and liquid velocities, shear stresses and momenta were used. These equations were solved for the case where the liquid bulk is at rest

for specific sets of fluid properties. Koh concluded that the interfacial shear stress in film boiling is quite different from zero, and that the parameter $[\rho_L \mu_L / \rho_v \mu_v]$ is important to the prediction of the heat transfer.

McFadden and Grosh [52], in a similar study, solved the boundary layer equations for vapor and liquid phases, but allowed for variable density and specific heat. The main result of this analysis was that, near the critical pressure, constant properties cannot be assumed. They stated that the expressions describing film boiling from a vertical plate heater and horizontal cylindrical heater were identical in reduced form to within a multiplicative constant.

Seetharamu et al [31] present a boundary layer analysis for film boiling from a vertical plate with nonuniform heat flux. Their equations could only be reduced to soluble form for the case where the heat flux varies inversely as the one-fourth power of vertical distance.

The effects of liquid subcooling have been included in boundary layer analyses of stable film boiling. Marschall and Moresco [39] present an analysis for constant wall temperature, variable properties, and liquid subcooling. Results for film boiling of water at atmospheric pressure, wall temperatures up to $1273^{o}K$ and water bulk temperatures from $343^{o}K$ to $373^{o}K$ are given. In another study, Sparrow and Cess [10] included the liquid buoyancy due to subcooling in the equation of motion of the liquid, and assumed that the vapor-liquid interface is not moving. They obtained numerical solutions relating the local Nusselt number to a parameter dependent on fluid properties, wall temperature and liquid subcooling. Nishikawa and Ito [11] modified the interfacial conditions of Sparrow and Cess by matching vapor and liquid velocities and shear stresses

at the interface. They obtained a stronger dependence on subcooling, and discussed the effects of vapor and liquid Prandtl numbers under various wall temperature conditions. Tachibana and Fukui [48] assumed velocity and temperature profiles for subcooled film boiling and obtained an expression for the heat transfer coefficient in terms of the boundary layer liquid velocity, and the liquid, vapor, and thermal boundary layer thicknesses. They also reported heat transfer data for film boiling of distilled water from a 0.0197 inch diameter horizontal wire. They found that the heat transfer coefficient increases with subcooling at a fixed value of wall superheat. Dhir and Purohit [36] have presented an analysis for subcooled film boiling from spheres, and present a semi-empirical correlation for average Nusselt number.

The effect of forced convection on film boiling, i.e., forced flow in the liquid phase, has been studied by several investigators. Bromley, Leroy and Robbers [47] extended Bromley's theory for natural convection to the case of liquid flow around regularly shaped bodies (cylinders and spheres) in which the liquid was assumed to have a velocity field satisfying the potential flow equations. Motte and Bromley [49] later considered the effect of subcooling on forced convection film boiling, and concluded that the primary mechanism of heat transfer in the liquid is eddy convection near the vapor-liquid interface. This model has not been developed very successfully. Many empirical relations for forced convection film boiling have been presented; however, these relations are generally limited in their applicability to the specific sets of system parameters and fluid properties from which they were obtained.

In 1958, Hsu and Westwater [7] published data for film boiling of

carbon tetrachloride, methanol, and benzene on vertical tubes having diameters between 3/8 and 3/4 inch, and lengths from 2.6 to 6.5 inches. Their data showed significant deviation from the theoretical predictions of Bromley [3].

In 1960 Hsu and Westwater [8] presented an analysis for turbulent film boiling of a saturated liquid on a vertical surface, explaining that the assumption of viscous flow in the vapor might account for the discrepancy between Bromley's analysis and their earlier measurements. They argued that at the lower end of the vertical surface the vapor mass flow rates are small, and hence, the assumptions of laminar vapor flow and a smooth interface may be valid in this region. However, beyond a certain height, or alternatively, beyond a critical vapor Reynolds number, transition to turbulent vapor flow with a wavy interface should be expected.

Thus they proposed that below an elevation, L_0, corresponding to a critical Reynolds number of 100, Bromley's results are valid. Above the height L_0, a laminar sublayer and a turbulent core was presumed to exist. In the upper portion of the flow Hsu and Westwater assume the following.

1) Heat is transferred by conduction across the laminar sublayer only.
2) There is no variation in velocity or temperature across the turbulent core of the vapor.
3) The velocity profile in the laminar sublayer is given by $u^+=y^+$, where

$$u^+ = \frac{u}{(\tau_w/\rho_v)^{\frac{1}{2}}} \quad ; \quad y^+ = y \frac{(\tau_w/\rho_v)^{\frac{1}{2}}}{(\mu_v/\rho_v)} \tag{3}$$

4) The interfacial shear is given by

$$\tau_i = \frac{1}{2} C_{F_{TP}} u_{max}^2 \rho_v \tag{4}$$

where $C_{F_{TP}}$ is an empirically determinal two-phase friction factor taken from data for concurrent flow of air and water at room temperature.

The results were

$$Nu = \frac{\bar{h} L}{k_v} = \frac{2h_{fg}' \mu_v Re_{CRIT}}{3k_v(T_W - T_S)}$$

$$+ \left(\frac{3B+1}{3A}\right)\left\{\left[\frac{2}{3}\left(\frac{3A}{3B+1}\right)(L-L_0) + \left(\frac{1}{y_{CRIT}}\right)^2\right]^{\frac{3}{2}} - \left(\frac{1}{y_{CRIT}}\right)^3\right\}$$

where

$$y_{CRIT} = \left[\frac{2\rho_v^2 Re_{CRIT}}{g\bar{\rho}_v(\rho_L - \bar{\rho}_v)}\right]^{\frac{1}{3}} \quad ; \quad L_0 = \frac{\mu_v Re_{CRIT} y_{CRIT} h_{fg}'}{2k_v(T_W - T_S)}$$

$$A = \left[\frac{g(\rho_L - \rho_v)}{\rho_v}\right]\left[\frac{\rho_v}{\mu_v Re_{CRIT}}\right]^2$$

$$B = \left[\frac{h_{fg}}{k_v(T_W - T_S)}\right]\left[\mu_v + \frac{1}{2} C_{F_{TP}} \left(\frac{\rho_v}{\bar{\rho}_v}\right) \mu_v Re_{CRIT} + \frac{k_v}{h_{fg}} (T_W - T_S)\right]$$

$\bar{\rho}_v$ = average density of vapor in laminar region

ρ_v = density of vapor in turbulent core

$$h_{fg}' = h_{fg}\left\{1+0.34\left[\frac{C_{p_v}(T_W-T_S)}{h_{fg}}\right]\right\}^2$$

Compared to Bromley's equation this result was in much better agreement with Hsu and Westwater's experimental data [7], which fell within ± 32% of the above predictive relation. Hsu and Westwater also report some limited interfacial wave data from high speed motion pictures.

This approximate model was modified in 1963 by Dougall and Rohsenow [54] to include thermal resistance in the turbulent core. Their results for heat transfer coefficient are ≈100% higher than the prediction by Bromley [3] and ≈50% lower than the results of Hsu and Westwater [8].

In 1969, Greitzer [53] built a water channel with walls modeled after the interfacial profiles reported by Hsu and Westwater [8]. He then injected a dye tracer in a water flow at an appropriate Reynolds number. His findings were that a large eddy formed in the wave crest, which apparently took fluid away from the laminar sublayer, making it thinner,and decreasing the thermal resistance of the vapor film. Simon et al [55] also argued that the time averaged thermal resistance in the presence of a wavy interface is smaller than one obtained from the mean film thickness. Coury [41] presented a similar hypothesis.

In 1970, Coury and Dukler [27] published a study of turbulent film boiling on vertical surfaces including the influence of interfacial waves. Their hypothesis was that the local Nusselt number is time independent even though the local heat transfer coefficient varies with time. Thus,

with the assumption of constant vapor thermal conductivity, the vapor film thickness must vary in such a way that the Nusselt number is constant, i.e.,

$$Nu = \frac{h(t)\delta(t)}{k_v} = \frac{h_s \delta_s}{k_v} \tag{6}$$

where the subscript, s, denotes equivalent steady-state values. Thus,

$$\langle h(t) \rangle = h_s \lim_{T\to\infty} \frac{1}{T} \int_0^T \frac{dt}{\left[\frac{\delta(t)}{\delta_s}\right]} \quad . \tag{7}$$

The ratio of the time averaged heat transfer coefficient to the equivalent steady-state heat transfer coefficient is called the heat transfer enhancement factor, C, and is defined by:

$$C = \frac{\langle h(t) \rangle}{h_s} \quad .$$

Assuming interfacial waves to be sinusoidal, Eq.(7) gives the following for the heat transfer enhancement factor:

$$C = \left(1 - \frac{\eta^2}{\bar{\delta}^2}\right)^{-\frac{1}{2}} \tag{8}$$

where η is the wave amplitude and $\bar{\delta}$ is the mean film thickness.

Coury and Dukler then took measurements of heat transfer rates for pool film boiling of saturated Freon 113 on a vertical surface, and compared this data to the results of their analysis. Choosing appropriate

values for interfacial roughness, they obtained approximately 12% mean deviation from theory, with 87% of points within ± 20% .

In a similar study, Suryanarayana and Merte [28], referring to the same result for heat transfer enhancement factor obtained by Coury and Dukler [27] (Eq.8), brought up the following considerations:

1) The amplitude of oscillations is a function of time.
2) The amplitude of oscillations is the same order of magnitude as the mean film thickness, and, for this range of η, the heat transfer enhancement factor, C, is very sensitive to small changes in amplitude.
3) The interfacial waves do not appear to show a regular sinusoidal pattern.

They suggest that the heat transfer enhancement factor may be expected to be a function of the vapor velocity, the vapor film thickness, the surface tension, gravity, and the liquid and vapor physical properties. As a simplification they proposed that the local Reynolds number of the vapor could be used as an indication of the amplitude of interfacial oscillations. Using data for film boiling of saturated liquid nitrogen at temperature differences between 100 and 315^{o}R from vertical cylinders 6 inches long and from 1 to $2\frac{1}{4}$ inches in diameter, the best fit was obtained by using

$$C=0.548\,Re^{0.187} \quad . \tag{9}$$

With this functional form for C, experimental values were within ± 30% of their analytical predictions. In the same paper, Suryanarayana and Merte present experimental measurements of the variation of vapor film thickness

with time and with height for film boiling of saturated liquid nitrogen from an isothermal vertical surface at a temperature difference of 315^{o}R.

Greitzer and Abernathy [29] present a laminar analysis of pool film boiling from a vertical surface where the vapor-liquid interface exhibits a three-dimensional wave structure. They state that their analytical model is not applicable when the dimension of the heating surface perpendicular to the vapor flow is much smaller than one wavelength. Their results for heat transfer coefficient were compared to the data of Hsu and Westwater [8] for pool film boiling of methanol, argon, and nitrogen, with a maximum discrepancy of about 20%. However, compared to data for pool film boiling of Freon 113 obtained during the present study, their analytical results for heat transfer coefficient were low by a factor of three to four, and did not accurately predict the variation of heat transfer coefficient with height.

Baum et al [35] observed film boiling of water and Freon 113 on vertical surfaces. They reported that, in the vertical direction, the interface is initially smooth, but, in a relatively small distance, takes on an oscillatory appearance. They also stated that in the film boiling studies, these interfacial oscillations appeared to be repelled before contacting the heating surface.

They propose a model wherein the heat removal capability of the vapor in film boiling is assumed to be directly proportional to the average vapor velocity. They account for the eddy diffusivity in turbulent flow by obtaining an effective thermal conductivity from the following relation:

$$k_{eff}=k_v\left\{1+\left[\frac{Re-Re_{CRIT}}{Re_{CRIT}}\right]\right\} \tag{10}$$

where Re_{CRIT} is the transition Reynolds number with a suggested value of 500.

By comparing their analytical results to experimental data for pool film boiling of Freon 113 at a pressure of 31 psia , they suggest a constant value of 1.22 for the heat transfer augmentation factor due to the presence of waves on the vapor-liquid interface. Thus, their expression for the heat transfer coefficient is:

$$h=1.22\ \frac{k_{eff}}{\delta} \tag{11}$$

where

$$\delta=\left\{\frac{1000q_w\mu_v}{h_{fg}\rho_v(\rho_L-\rho_v)}\right\}^{\frac{1}{2}}$$

and k_{eff} is given by Eq.(10).

It should be mentioned that the model proposed by Baum et al [35] assumes the average vapor film thickness and vapor Reynolds number to be invariant in the vertical direction. This seems to be in conflict with the fact that the local Reynolds number is proportional to the vapor mass flow rate, which must increase in the vertical direction, and with published data on the average vapor film thickness in film boiling, which is consistently reported to increase with elevation.

In another study, Andersen [37] proposes a laminar flow model of low-flow film boiling heat transfer from a vertical surface similar to

that of Bromley [3]. The basic assumption is that the film will not grow indefinitely, as is the case in the theory by Bromley, but will break down due to the Helmholtz instability. Assuming the liquid bulk to be at rest, the most unstable wavelength to the Helmholtz instability is given by

$$\lambda_D = 2\pi\sqrt{\frac{3\sigma\delta}{\rho_v u_0^2}} \quad . \tag{12}$$

He states that interfacial instabilities with a wavelength given by (12) are the most likely to occur. They will cause the film to break up, and the vapor will leave the interface as bubbles. A new film will then form and grow until it also becomes unstable. Andersen approximates the length L of the film by the most unstable wavelength given by (12) in Bromley's expression for average heat transfer coefficient [3]. Accordingly, the resulting equation is:

$$\bar{h} = c_1 \left\{ \frac{k_v^9 h_{fg}^2 \rho_v^3 (\rho_L - \rho_v)^4 g^4}{\mu_v^4 (T_W - T_S)^2 \sigma} \right\}^{\frac{1}{11}} \tag{13}$$

where $0.3321 \leq c_1 \leq 0.5498$.

Leonard et al [38] compare the expression for average heat transfer coefficient given by (13) with single rod quench tests conducted at the General Electric Company, with reasonably good agreement. However, when compared to data for film boiling of saturated ethanol, (13) was found to underpredict heat transfer coefficients by about 100%.

In 1966, Bradfield [12], reporting visual observations of droplet film boiling studies, concluded that liquid-solid contact exists in the

stable film boiling regime. Ten years later, Farrar and Marschall [34] presented experimental results for pool film boiling of a calcium sulfate solution at atmospheric pressure from a submerged sphere. They observed that at temperature differences above 850°C, the calcium sulfate was deposited on the sphere as small spots, indicating probable liquid-solid contacts. They postulate that, above this temperature, the interfacial wave activity is violent enough to propel liquid droplets across the vapor film and against the heated surface, where they are vaporized.

Borishanskii [14] reported data he had taken of film boiling of saturated ethanol and ethyl ether on a vertical graphite tube having a diameter of 6mm (0.236 in.) and a length of 270mm (10.63 in.). The most important aspect of this work was the discovery that the linear dimension of the heating surface did not affect the heat transfer. That is, for a constant wall heat flux over the entire surface, the measured temperatures did not significantly vary in the vertical direction. Borishanskii also suggests that Bromley's [3] expression for average heat transfer coefficient (1), may be valid when the quantity

$$\left[\frac{\sigma}{(\rho_L-\rho_v)g}\right]^{\frac{1}{2}}$$

is substituted for the linear dimension of the heated surface.

Borishanskii and Fokin [56] report data taken for free convection film boiling of ethyl ether, ethanol, n-hexane, water, and benzene on vertical stainless steel tubing from 3mm (0.118 in.) to 6mm (0.236 in.) in diameter and from 37mm (1.46 in.) to 287mm (11.3 in.) long. Through dimensional analysis they obtain for the convective heat transfer

coefficient:

$$h_c = 0.28 \left(\frac{g k_v^3 \rho_v \rho_L}{\mu_v^2} \right)^{\frac{1}{3}} \tag{14}$$

when

$$2 \times 10^4 < \frac{g \bar{\delta}^3 \rho_v \rho_L}{\mu_v^2} < 1.4 \times 10^6$$

where $\bar{\delta}$ is the average vapor film thickness.

III. ANALYSIS OF THE FILM BOILING HEAT TRANSFER PROCESS

The object of this section is to derive an expression for the heat transfer in free convection film boiling of a saturated liquid on a vertical surface. This analysis is undertaken with the intention of determining the physical parameters which affect the heat transfer. These parameters are then to be used as an aid in the presentation and discussion of the experimental data. No attempt is made to obtain a complete mathematical representation of the complicated film boiling process; the proper relationship of these parameters will be determined by experiment.

Previous investigators have derived heat transfer prediction methods on the basis of one of the following assumptions:

1) The vapor flow is laminar, and the vapor-liquid interface is smooth. The velocity and temperature profiles in the vapor can be obtained by solving the applicable forms of the Navier-Stokes and energy equations with appropriate boundary conditions.
2) The vapor flow is turbulent and the important flow features can be determined by comparison to similar turbulent flows such as in a turublent boundary layer on a flat plate.

It can be clearly demonstrated that the vapor Reynolds number becomes quite high in a relatively short length, and thus, turbulent flow appears to be a reasonably good assumption for long surfaces. However, previous analytical approaches to turbulent flow film boiling, such as that of Hsu and Westwater [8], do not correlate well with experimental measurements.

The present approach is similar to that suggested by S.G.Bankoff in the written discussion following the paper by Hsu and Westwater [8]. Accordingly a simple power relationship between the friction coefficient and Reynolds number is assumed. Bankoff suggests that the Blasius relation,

$$C_F = \frac{\tau_w}{\frac{1}{2}\rho_v u_0^2} = 0.046\, Re_\delta^{-1/4} \tag{15}$$

is applicable. However, one cannot expect the flow in film boiling to be precisely modeled by the turbulent boundary layer on a flat plate, and the exponent as well as the multiplier of the Reynolds number could well be different.

Considering the configuration illustrated in Fig.2, the total mass flow rate per unit width of the film can be expressed as:

$$\dot{m} = n\, \rho_v u_0 \delta \tag{16}$$

where u_0 is the maximum vapor velocity, and n is a numerical constant. Assuming zero vapor velocity at the wall $(y=0)$ and at the interface $(y=\delta)$, Eq.(16) holds with $n=2/3$ for laminar flow between parallel flat plates. Experimentally, Eq.(16) has been shown to be a good approximation with n equal to 7/8 for a turbulent flat plate boundary layer. Since Eq.(16) is valid for these two different types of flow having similar geometrical boundary conditions, it seems quite reasonable to assume that Eq.(16) is also applicable to the present problem.

Next, for the friction coefficient a relationship of the form

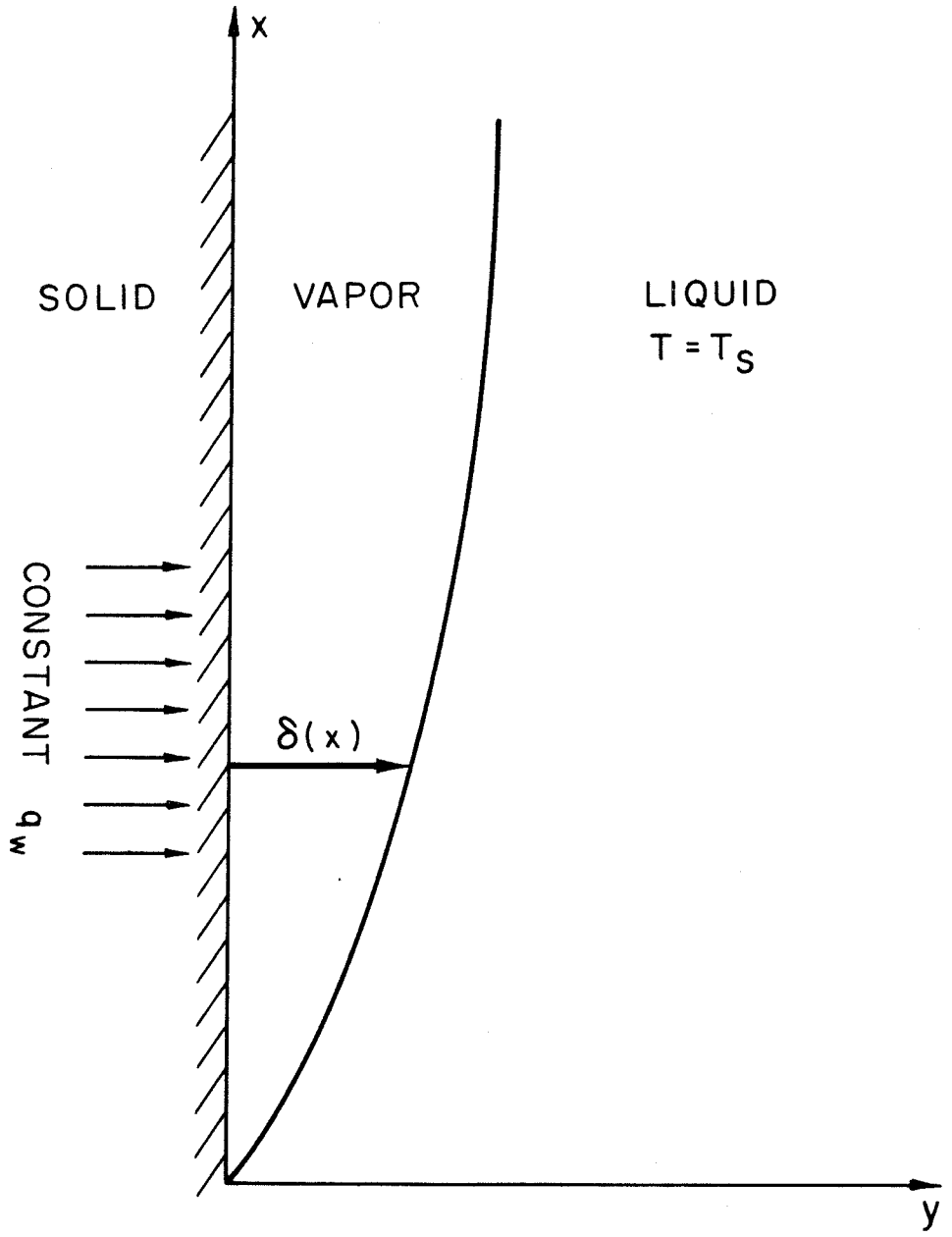

Figure 2. System Configuration for Analysis of Stable Film Boiling Heat Transfer

$$C_F = \frac{\tau_w}{\frac{1}{2}\rho_v u_0^2} = b\,Re_\delta^{-c} \tag{17}$$

is assumed. For a laminar flow between two stationary flat plates, b=8, and c=1; and, experimentally, for a turbulent boundary layer, b=0.046, and c=1/4. Since Eq.(17) is valid for these similar types of flow, it is reasoned that the general form of Eq.(17) will be suitable for the analysis. From Eq.(17),

$$\tau_w = \frac{b}{2}\rho_v u_0^2 \left(\frac{\mu_v}{u_0\rho_v\delta}\right)^c \tag{18}$$

A force balance in the vapor, ignoring changes in vapor momentum in the x-direction, and assuming equal wall and interfacial shear stresses, leads to

$$2\tau_w = (\rho_L - \rho_v)g\delta \approx \rho_L g\delta = b\rho_v u_0^2 \left(\frac{\mu_v}{u_0\rho_v\delta}\right)^c \quad . \tag{19}$$

And, solving Eq.(19) for δ gives,

$$\delta = \frac{b^{1/(1+c)}}{g^{1/(1+c)}} \left(\frac{\mu_v}{\rho_v}\right)^{c/(1+c)} \gamma^{1/(1+c)} u_0^{(2-c)/(1+c)} \tag{20}$$

where $\gamma = \rho_v/\rho_L$.

An energy balance for the vapor neglecting changes in vapor kinetic energy and enthalpy in the x-direction shows that

$$\frac{d\dot{m}}{dx} = \frac{q_w}{h_{fg}} \quad . \tag{21}$$

Substituting Eq.(16) into (21) gives

$$n\rho_v \frac{d}{dx}(u_0\delta) = \frac{q_w}{h_{fg}} \quad . \tag{22}$$

And, using Eq.(20) to eliminate δ from (22) one obtains

$$\frac{d}{dx}(u_0^{3/(1+c)}) = \frac{1}{nb^{1/(1+c)}}\left(\frac{g}{\rho_v\gamma\mu_v^c}\right)^{1/(1+c)} \frac{q_w}{h_{fg}} \quad . \tag{23}$$

Integrating Eq.(23) in x with $u_0(0)=0$ results in

$$u_0 = \frac{1}{n^{(1+c)/3}b^{1/3}}\left(\frac{g\mu_v}{\rho_v\gamma}\right)^{1/3}\left(\frac{q_w x}{\mu_v h_{fg}}\right)^{(1+c)/3} \quad , \tag{24}$$

and, Eq.(24) and (20) give,

$$\delta = \frac{b^{1/3}}{n^{(2-c)/3}}\left(\frac{\mu_v^2\gamma}{\rho_v^2 g}\right)^{1/3}\left(\frac{q_w x}{\mu_v h_{fg}}\right)^{(2-c)/3} \quad . \tag{25}$$

An expression for the Stanton number, C_H, analogous to Eq.(17) is now assumed to hold:

$$C_H = \frac{h}{\rho_v u_0 c_{P_v}} = \beta Re_\delta^{-c} Pr^{-m} \quad . \tag{26}$$

For laminar flow between two closely spaced, stationary flat plates, $\beta=1$, $c=1$, and $m=1$; and, experimentally for a turbulent boundary layer on a flat plate, $\beta=b/2=0.023$, $c=1/4$, and $m=2/3$. Following similar arguments to those justifying the use of Eq.(17), it is reasoned that the general

form of Eq.(26) will be applicable to this problem. Equation (26) then becomes

$$h=\beta\rho_v u_0 c_{P_v}\left(\frac{\mu_v}{\rho_v u_0 \delta}\right)^c Pr^{-m} \tag{27}$$

and, substituting (24) and (25) into (26) one obtains

$$h=\frac{\beta}{b^{1/3}n^{(1-2c)/3}}\rho_v^{2/3}c_{P_v}\mu_v^{1/3}g^{1/3}\gamma^{-1/3}Pr^{-m}\left(\frac{q_w x}{\mu_v h_{fg}}\right)^{(1-2c)/3} . \tag{28}$$

Constructing a dimensionless heat transfer coefficient, subsequently called the film boiling number, N_{FB} , Eq.(27) may be written

$$N_{FB}=\frac{h}{\rho_v c_{P_v}\left(\frac{\mu_v g}{\rho_v}\right)^{1/3}}=K\gamma^{-1/3}Pr^{-m}\left(\frac{q_w x}{\mu_v h_{fg}}\right)^{(1-2c)/3} \tag{29}$$

where $K=\frac{\beta}{b^{1/3}n^{(1-2c)/3}}$:

Noting that from Eq.(16)

$$Re_\delta=\frac{\rho_v u_0 \delta}{\mu_v}=\frac{\dot{m}}{\mu_v}$$

and that, for constant q_w , Eq.(21) integrates to

$$\dot{m}=\frac{q_w x}{h_{fg}} ,$$

we have

$$Re_\delta = \frac{1}{n} \frac{q_w x}{\mu_v h_{fg}} \quad . \tag{30}$$

Thus, Eq.(29) can be rewritten as

$$N_{FB} = A\gamma^{-1/3} Pr^{-m} Re_\delta^{(1-2c)/3} \tag{31}$$

where

$$A = \frac{\beta}{b^{1/3}}$$

and

$$N_{FB} = \frac{h}{\rho_v c_{P_v} \left(\frac{\mu_v g}{\rho_v} \right)^{1/3}} \quad .$$

For a laminar flow between closely spaced, parallel, stationary flat plates, $c=1$ and $m=1$, and therefore

$$N_{FB} = A\gamma^{-1/3} Pr^{-1} Re_\delta^{-1/3} \tag{32}$$

which is equivalent to the Bromley [3] solution for constant heat flux.

For a single phase, turbulent boundary layer on a flat plate, we have, experimentally, $c=1/4$, and $m=2/3$, giving,

$$N_{FB} = A\gamma^{-1/3} Pr^{-2/3} Re_\delta^{1/6} \quad . \tag{33}$$

Interestingly, taking $c=1/2$ in Eq.(31) produces the following expression:

$$N_{FB}=A\gamma^{-1/3}Pr^{-m} \quad . \tag{34}$$

In this case, the dependence of the heat transfer coefficient on vertical position has been eliminated.

As mentioned before the expression, Eq.(31),

$$N_{FB}=A\gamma^{-1/3}Pr^{-m}Re_{\delta}^{(1-2c)/3}$$

was derived with the intent of developing a relationship which would indicate the governing parameters of the problem, rather than with the expectation of obtaining an accurate prediction. The relationship represented by Eq.(31) does serve this function. Comparison with experiments will show the importance of these parameters.

IV. THE STABILITY OF THE VAPOR-LIQUID INTERFACE

Large scale waves have been observed on the vapor-liquid interface in film boiling, [8], [27]; however, their nature is not well understood. A Kelvin-Helmholtz approach (see Appendix E) gives wavelengths which are much smaller than those which are observed experimentally, possibly due to the following:

1) The vapor flow does not satisfy the potential flow equation.
2) There is significant mass transfer at the interface which is not taken into account.

A linearized stability analysis of film boiling similar to that followed by Ünsal and Thomas [19] for film condensation is suggested. This approach assumes viscous flow in the vapor, potential flow in the liquid, and includes the effect of vaporization on the force balance at the interface.

Given the configuration illustrated in Fig.3, the interface is mathematically defined by:

$$I(x^*,y^*,t^*)=y^*-\delta(x^*,t^*)=0 \tag{35}$$

where,

$$\delta(x^*,t^*)=\overline{\delta}(x^*)+\eta e^{i\alpha^*(x^*-c^*t^*)} \tag{36}$$

$\overline{\delta}$ is the mean vapor film thickness, η is the amplitude of interfacial oscillations, and an asterisk (*) denotes a dimensional quantity.

The normal to the interface, $\vec{n}$, is defined by:

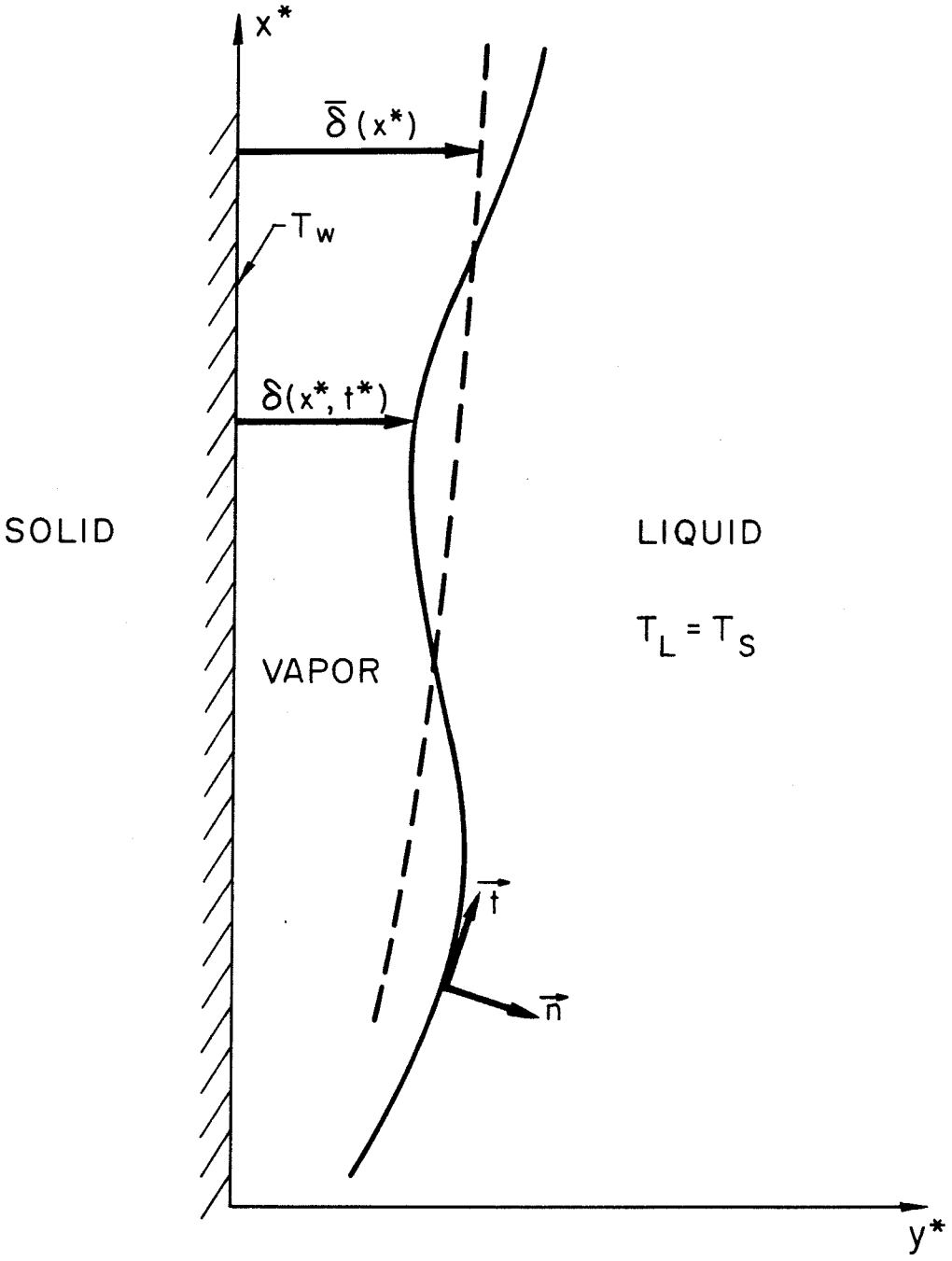

Figure 3. System Configuration for Linearized Stability Theory

$$\vec{n}= \frac{\nabla^*I}{|\nabla^*I|} = \frac{-\frac{\partial\delta}{\partial x^*}\hat{i}+\hat{j}}{[1+(\frac{\partial\delta}{\partial x^*})^2]^{\frac{1}{2}}} \approx -\frac{\partial\delta}{\partial x^*}\hat{i}+\hat{j} \tag{37}$$

where $\hat{i}$ and $\hat{j}$ are unit vectors in the x^*, and y^* directions, respectively.

The normal velocity of the interface, $\vec{v}_i \cdot \vec{n}$, is obtained by taking

$$\frac{DI}{Dt} = 0 = \frac{\partial I}{\partial t^*} + \vec{v}_i \cdot \nabla^* I \tag{38}$$

and dividing (38) by $|\nabla^* I|$.

$$\vec{v}_i \cdot \frac{\nabla^* I}{|\nabla^* I|} = \vec{v}_i \cdot \vec{n} = \frac{-\frac{\partial I}{\partial t^*}}{|\nabla^* I|} \approx \frac{\partial\delta}{\partial t^*} \quad . \tag{39}$$

Continuity of mass in the vapor phase is satisfied by letting

$$u=-\psi^*_{y^*} \quad \text{and} \quad v=\psi^*_{x^*} \quad . \tag{40}$$

Formulating the following dimensionless variables,

$$x= \frac{x^*}{\bar{\delta}} \; ; \; y= \frac{y^*}{\bar{\delta}} \; ; \; t= \frac{t^* u_0}{\bar{\delta}} \; ; \; \psi= \frac{\psi^*}{u_0 \bar{\delta}} \; ;$$

$$\theta= \frac{T-T_S}{T_W-T_S} \; ; \; p= \frac{P}{\rho_v u_0^2} \; ; \; \alpha=\alpha^*\bar{\delta} \; ; \; c= \frac{c^*}{u_0} \quad , \tag{41}$$

where u_0 is the maximum vapor velocity, gives the following equations of motion and energy for the vapor:

$$-\psi_{yt}+\psi_y\psi_{xy}-\psi_x\psi_{yy}=-p_x-\frac{1}{Re}(\psi_{yxx}+\psi_{yyy})-\frac{1}{Fr^2} \tag{42}$$

$$\psi_{xt}-\psi_y\psi_{xx}+\psi_x\psi_{xy}=-p_y+\frac{1}{Re}(\psi_{xxx}+\psi_{xyy}) \tag{43}$$

$$\theta_t-\psi_y\theta_x+\psi_x\theta_y=\frac{1}{Pe}(\theta_{xx}+\theta_{yy}) \tag{44}$$

where

$$Re=\frac{\rho_v u_0 \bar{\delta}}{\mu_v}\ ,\quad Fr=\frac{u_0}{\sqrt{g\bar{\delta}}}\ ,\quad \text{and}\quad Pe=\frac{\rho_v u_0 c_{p_v} \bar{\delta}}{k_v}\ .$$

It should be noted that the above governing equations limit the strict applicability of this analysis to laminar flow in the vapor film.

Continuity of normal mass flow across the interface gives:

$$m_v=m_L$$

where

$$m_v=\rho_v(\vec{v}_v-\vec{v}_i)\cdot\vec{n} \tag{45}$$

and,

$$m_L=\rho_L(\vec{v}_L-\vec{v}_i)\cdot\vec{n}$$

Neglecting surface tension (see Appendix E), the momentum theorem applied at the interface results in:

$$m_v\vec{v}_v-m_L\vec{v}_L=\vec{n}\cdot\sigma_L-\vec{n}\cdot\sigma_v \tag{46}$$

where $\sigma_{v,L}$ denotes the stress tensor in the vapor or liquid.

Assuming that the liquid is uniformly at its saturation temperature, and that the saturation temperature does not vary significantly due to small pressure oscillations at the interface results in the following interfacial conditions

$$\theta=0 \tag{47}$$

and

$$\vec{q}_v \cdot \vec{n} = m_v h_{fg} \tag{48}$$

where $\vec{q}_v$ is the heat flux vector in the vapor, defined as

$$\vec{q}_v = -k_v \nabla^* T = \frac{-k_v (T_W - T_S)}{\bar{\delta}} \nabla\theta \quad . \tag{49}$$

The liquid phase is assumed to be inviscid, thus,in the undisturbed state, the bulk of the liquid is at rest. Liquid velocities are therefore due only to the motion of the interface. Hence, liquid motion at the interface can have no tangential component. Therefore, continuity of tangential velocities at the interface gives,

$$\vec{v}_v \cdot \vec{t} = 0 \tag{50}$$

where $\vec{t} = \vec{n} \times \hat{k} = \hat{i} + \frac{\partial \delta}{\partial x^*} \hat{j}$ is the surface tangent unit vector.

Equations (45)-(50) combine to give:

$$\text{On} \quad y = 1 + \varepsilon e^{i\alpha(x-ct)} \quad \text{where} \quad \varepsilon = \frac{\eta}{\bar{\delta}} \quad ,$$

$$\psi_y = i\alpha\varepsilon e^{i\alpha(x-ct)} \psi_x \tag{51}$$

$$p_v = p_L + \frac{Sh^2}{Pe^2}(1-\gamma)\left(\theta_y - \theta_x \frac{\partial \delta}{\partial x^*}\right) \tag{52}$$

$$\theta = 0 \tag{53}$$

where

$$Sh = \frac{c_{P_v}(T_W - T_S)}{h_{fg}} \quad \text{and} \quad \gamma = \frac{\rho_v}{\rho_L} \quad ,$$

and, we have, on $y=0$

$$\psi_x = 0 \tag{54}$$

$$\psi_y = 0 \tag{55}$$

$$\theta = 1 \tag{56}$$

In the linear stability theory, the stream function, temperature, and pressure can be expressed in terms of base flow and disturbance quantities. Thus,

$$\begin{aligned} \psi &= \bar{\psi} + \varphi(y) e^{i\alpha(x-ct)} \\ \theta &= \bar{\theta} + S(y) e^{i\alpha(x-ct)} \\ p_v &= \bar{p}_v + \tilde{p}(y) e^{i\alpha(x-ct)} \end{aligned} \tag{57}$$

The base flow is steady, hence

$$\bar{\psi}_t = \bar{\theta}_t = \bar{p}_t = 0 \quad . \tag{58}$$

It is further assumed that the base flow is a parallel flow:

$$\bar{\psi}_x = \bar{\theta}_x = \frac{\partial \bar{\delta}}{\partial x^*} = 0 \tag{59}$$

It would be more accurate to say

$$\bar{\psi}_x \ll \bar{\psi}_y$$

$$\bar{\theta}_x \ll \bar{\theta}_y$$

$$\frac{\partial \bar{\delta}}{\partial x^*} \ll 1 \quad ,$$

since none of these quantities are truly equal to zero. However, it is felt that Eq.(59) is a useful simplification to the problem, and is a good approximation in that any errors introduced by this assumption may be expected to be of small relative magnitude.

Equations (57) are substituted into the equations of motion and energy (42)-(44), and terms which contain a complex exponential can be separated from terms which do not. Thus, the base flow equations are:

$$\bar{P}_x + \frac{1}{Re}\bar{\psi}_{yyy} + \frac{1}{Fr^2} = 0 \tag{60}$$

$$\bar{P}_y = 0 \tag{61}$$

$$\bar{\theta}_{yy} = 0 \quad . \tag{62}$$

And, the equations containing the disturbance quantities are:

$$\frac{1}{Re}(\varphi''' - \alpha^2\varphi') + i\alpha(c+\bar{\psi}_y)\varphi' - i\alpha\bar{\psi}_{yy}\varphi = -i\alpha\tilde{p} \tag{63}$$

$$-\frac{i\alpha}{Re}(\varphi'' - \alpha^2\varphi) + \alpha^2(c+\bar{\psi}_y)\varphi = -\tilde{p}' \tag{64}$$

$$S'' - \alpha^2 S = i\alpha Pe[\bar{\theta}_y\varphi - (c+\bar{\psi}_y)S] \tag{65}$$

To obtain the liquid pressure at the interface, it is assumed that the liquid flow satisfies the potential flow equations, and is due only to the motion of the interface. Therefore, at the interface

$$p_L = \frac{P_0}{\rho_v u_0^2} - \frac{g\bar{\delta}(x-x_0)}{\gamma u_0^2} - \frac{\alpha c^2 \varepsilon}{\gamma} e^{i\alpha(x-ct)} \tag{66}$$

where P_0 is the hydrostatic pressure at a reference elevation, x_0.

The interfacial boundary conditions (51)-(53) are applicable at $y=1+\varepsilon e^{i\alpha(x-ct)}$. Consistent with the linear stability theory, these conditions must be Taylor series expanded about, and applied at $y=1$, where terms of order α^2 and higher are neglected. This procedure results in the following:

$$\bar{p}_v = \frac{P_0}{\rho_v u_0^2} - \frac{g(x-x_0)\bar{\delta}}{\gamma u_0^2} + \frac{Sh^2}{Pe^2}(1-\gamma)\bar{\theta}_y^2 \quad \text{on } y=1 \tag{67}$$

$$\bar{\psi}_y = 0 \quad \text{on} \quad y=1 \tag{68}$$

$$\bar{\theta} = 0 \quad \text{on} \quad y=1 \tag{69}$$

$$\tilde{p} = -\frac{\alpha c^2 \varepsilon}{\gamma} + 2\frac{Sh^2}{Pe^2}(1-\gamma)S'\bar{\theta}_y \qquad \text{on} \quad y=1 \tag{70}$$

$$\varphi' = -\varepsilon \bar{\psi}_{yy} \qquad \text{on} \quad y=1 \tag{71}$$

$$S = -\varepsilon \bar{\theta}_y \qquad \text{on} \quad y=1 \tag{72}$$

and we have,

$$\bar{\psi}_y = 0 \qquad \text{on} \quad y=0 \tag{73}$$

$$\bar{\theta} = 1 \qquad \text{on} \quad y=0 \tag{74}$$

$$\varphi = 0 \qquad \text{on} \quad y=0 \tag{75}$$

$$\varphi' = 0 \qquad \text{on} \quad y=0 \tag{76}$$

$$S = 0 \qquad \text{on} \quad y=0 \tag{77}$$

The solution to the base flow problem equations (60)-(62), with boundary conditions (67),(68),(69),(73) and (74) is:

$$\bar{\psi}_y = 4y(y-1) \tag{78}$$

$$\bar{\theta} = 1-y \tag{79}$$

Differentiating Eq.(63) and combining with (64) to eliminate $\tilde{p}$ gives the Orr-Sommerfeld equation:

$$\varphi'''' - 2\alpha^2\varphi'' + \alpha^4\varphi = -i\alpha Re[(c+\bar{\psi}_y)(\varphi'' - \alpha^2\varphi) - \bar{\psi}_{yyy}\varphi] \tag{80}$$

Since (63) holds everywhere in the vapor, it is true in particular

on y=1. Thus it can be combined with boundary condition (70) to eliminate $\tilde{p}$, resulting in:

$$\varphi''' - \alpha^2\varphi' = i\alpha Re[\bar{\psi}_{yy}\varphi - (\bar{\psi}_y + c)\varphi' + \frac{\alpha c^2 \varepsilon}{\gamma} - 2\frac{Sh^2}{Pe^2}(1-\gamma)\, S'\bar{\theta}_y]$$

$$\text{on} \quad y=1 \quad . \tag{81}$$

Equations (80) and (65) along with boundary conditions (71),(72), (75),(76),(77), and (81) constitute the disturbance quantities problem, which must be solved for $\varphi(y)$ and $S(y)$.

$\varphi(y)$ and $S(y)$ are now expressed as power series in $\alpha=\alpha^*\bar{\delta}$ with the stipulation that α is small, i.e., that the film thickness is small compared to the wavelengths of interest. The series may be written as:

$$\varphi(y)=\varphi_0(y)+\alpha\varphi_1(y)+\alpha^2\varphi_2(y)+... \tag{82}$$

$$S(y)=S_0(y)+\alpha S_1(y)+\alpha^2 S_2(y)+... \tag{83}$$

Equations (82) and (83) are substituted into the disturbance equations and boundary conditions, and successive orders of solutions can be obtained by equating terms containing like powers of α, while neglecting terms containing higher powers of α.

The zeroth order solutions are:

$$\varphi_0 = -2\varepsilon y^2 \tag{84}$$

$$S_0 = \varepsilon y \quad . \tag{85}$$

And, the first order solutions are:

$$\varphi_1 = -i\varepsilon Re\left[\frac{2}{15}y^5 - \frac{c}{6}y^4 - \left\{\frac{\alpha c^2}{6\gamma} + \frac{1}{3}\frac{Sh^2}{Pe^2}(1-\gamma)\right\}y^3 + \left\{\frac{\alpha c^2}{4\gamma} + \frac{1}{3}(c-1) + \frac{1}{2}\frac{Sh^2}{Pe^2}(1-\gamma)\right\}y^2\right] \tag{86}$$

$$S_1 = i\varepsilon Pe\left[-\frac{1}{5}y^5 + \frac{1}{2}y^4 - \frac{c}{6}y^3 + (\frac{c}{6} - \frac{3}{10})y\right] \tag{87}$$

The second and higher order terms are considered to be negligibly small for sufficiently small values of the Reynolds number.

The quantity φ_0, corresponds to the disturbance to the dimensionless stream function, ψ, when the entire interface is displaced as a unit from $y=1$ to $y=1+\varepsilon$, that is for $\alpha=\alpha^*=0$. In this case,

$$\psi = \bar{\psi} + \varphi_0 = \frac{4}{3}y^3 - 2y^2 - 2\varepsilon y^2$$

and, at $y=1+\varepsilon$,

$$\psi = \frac{4}{3}(1+3\varepsilon) - 2(1+2\varepsilon) - 2\varepsilon = -\frac{2}{3} - 2\varepsilon \quad .$$

With no disturbance,

$$\psi(1) = -\frac{2}{3}$$

and thus displacement of the interface causes a change in the dimensionless stream function ψ by an amount

$$\Delta\psi = -2\varepsilon \quad .$$

This implies that there is an increase in volume flow rate in the film due to displacement of the interface away from the solid surface. This cannot be true, and is an artifact of the no slip boundary conditions imposed on the velocity combined with the restriction that the base flow remains unchanged when the interface is perturbed.

The error introduced is of the order $\frac{2\varepsilon}{2/3} = 3\varepsilon$ which is considered to be negligible for infinitesimal disturbances.

There is a concomitant artificial increase in the sensible heat of the vapor due to the zeroth order temperature perturbation $S_0(y)$ when the interface is displaced as a plane unit, and similar arguments hold in this case; i.e., the error introduced by holding the base temperature profile fixed as the interface is displaced is of small relative magnitude, and should not affect the resulting stability criteria.

The stability criteria can be considered by substitution of Eqs. (84)-(87) into the interfacial boundary condition (48). Equation (48) results in:

$$\frac{Sh}{Pe} S'(1)=i\alpha[\varphi(1)+\varepsilon c] \quad . \tag{88}$$

Applying (81) and (82) gives

$$\frac{Sh}{Pe} [S_0'(1)+\alpha S_1'(1)]=i\alpha[\varphi_0(1)+\alpha\varphi_1(1)+\varepsilon c] \quad . \tag{89}$$

And substituting (84)-(87) into (88) gives

$$\frac{\alpha Re}{12\gamma}(\alpha c)^2+\left\{\frac{\alpha Re}{6}+i\left(1+\frac{Sh}{3}\right)\right\}(\alpha c)-\frac{Sh}{Pe}-i\alpha\left(2+\frac{7}{10}Sh\right)$$

$$-\alpha^2 Re\left\{\frac{1}{5}-\frac{1}{6}\frac{Sh^2}{Pe^2}(1-\gamma)\right\}=0 \qquad (90)$$

Recalling that the disturbance quantities contain a complex exponential of the form

$$e^{i\alpha(x-ct)}=e^{i\alpha x}e^{-i\alpha ct} \quad ,$$

it is evident that it is the sign of the real part of the product $-i\alpha c$ which determines if these disturbances will grow or decay with time. Therefore, if the imaginary part of αc is nonzero and positive, the disturbance will grow with time.

If the nondimensional complex frequency, ω, is defined by

$$\omega=\alpha c=\frac{\omega^*\bar{\delta}}{u_0} \qquad (91)$$

the dispersion relation, Eq.(89), can be rewritten as

$$\frac{\alpha Re}{12\gamma}\omega^2+\left\{\frac{\alpha Re}{6}+i\left(1+\frac{Sh}{3}\right)\right\}\omega-\frac{Sh}{Pe}-i\alpha\left(2+\frac{7}{10}Sh\right)$$

$$-\alpha^2 Re\left\{\frac{1}{5}-\frac{1}{6}\frac{Sh^2}{Pe^2}(1-\gamma)\right\}=0 \qquad (92)$$

and disturbances will be:

$$\begin{aligned} &\text{Stable if} && \mathrm{Im}[\omega(\alpha)] < 0 \\ &\text{Oscillatory if} && \mathrm{Im}[\omega(\alpha)] = 0 \\ &\text{Unstable if} && \mathrm{Im}[\omega(\alpha)] > 0 \ . \end{aligned} \tag{93}$$

The behavior of $\omega(\alpha)$ is strongly dependent on the parameters Re, Sh, and Pe, and cannot easily be determined analytically.

A computer program has been written which solves Eq.(92) for any particular set of fluid and system properties. The results of this work are presented, compared to experimental measurements, and discussed in Section VIII-B. Some further considerations on the assumptions made in the derivation of Eq.(92), and on its region of validity, are presented in Appendix E.

V. EXPERIMENTAL APPARATUS

A. General Description

The equipment used in this study was selected and designed with the following objectives: 1) measurement of heat transfer rates and temperature differences occurring in pool film boiling of saturated liquids from a heated vertical cylinder at a pressure of one atmosphere; 2) simultaneous visual observation of the characteristics of the vapor-liquid interface. These observations were to be sufficiently accurate to allow comparisons with measured heat transfer conditions and with related analytical work.

The test chamber is designed so that an electrically heated cylinder can be suspended vertically along its centerline. The chamber is a rectangular pyrex glass vessel with a machined aluminum top. The chamber is placed inside a protective rectangular enclosure fabricated from plexiglass and perforated metal. The enclosure has two doors on opposite sides which can be opened for photographic observation. A high speed motion picture camera is mounted on a tripod next to the enclosure. A 500 watt medium-flood lamp is placed on the other side of the enclosure to provide illumination for the photographic observations.

The test chamber is equipped with an immersion heater to establish operating temperatures in the bulk of the fluid. This temperature (usually the saturation temperature) is maintained by a 500 watt disk heater in place below the test vessel.

The test section consists of an electrically heated cylinder, which is held near its top end by an asbestos part which is machined to fit into

the aluminum top of the test vessel. The aluminum top, with the test section in place, is raised and lowered from the outside of the protective enclosure by a simple offset sliding arm mechanism with a screw clamp to secure the top in place. A photograph of the installation is included as Fig.4.

It should be noted that there is some physical danger associated with immersion in a liquid of a cartridge heater of the type used in this investigation. If the sheath material is flawed in any way which allows liquid to penetrate into the internal heating area, rapid vaporization can cause the heater to rupture violently. This occurred during one test run, and glass and hot fluid were sent flying in the laboratory. Thus, a protective enclosure was provided as described and goggles were used during this type of experimentation.

The wall temperature of the test section is measured by several thermocouples distributed along the outside of the rod, and the test vessel is equipped with a free thermocouple to measure the fluid bulk temperature.

The voltage supplied to the test section is controlled by a variable autotransformer, and the power consumption rate is measured with a digital voltmeter and an AC ammeter appropriately placed in the circuit. This is represented schematically in Fig.5.

B. Test Section

The test section used in this investigation is an electric cartridge heater manufactured by the Rama Corporation in San Jacinto, California. The heater is cylindrical, and is 12 inches in length and 0.5 inches in diameter. The heating is supplied by passing electric current through nichrome resistance wire which is wrapped in a coil around a ceramic core.

The wire wrapped core is surrounded by an Incalloy 800 sheath having a thickness of 1/16 inch and is electrically insulated from the sheath by a magnesium oxide packing. One end of the sheath is closed with a welded cap and the other end is sealed with ceramic, with the two electrical leads protruding.

The test section is designed to operate on 120 volts AC with a rated power output of 1200 watts. The heating is uniformly distributed over the surface, with the exception of about 1/2 inch at the lower (capped) end of the rod. The heating coil terminates just above this capped portion so that the tip of the rod is not directly heated. A photograph of the test section is presented in Fig.6.

C. Controls and Instrumentation

The voltage supplied to the test section is controlled by a Powerstat model 1126 variable transformer with 120V input, and 0-135 volts output, with a 15 amp maximum current rating. The supply voltage is measured with a Hewlett-Packard model 3465A digital multimeter, and the current supplied to the rod is measured with a Weston model 904 alternating current ammeter.

The surface temperature of the test section is obtained by measuring the voltage generated by thermocouples which are spot welded to the outside of the Incalloy 800 sheath. From four to eight 0.020 inch diameter chromel-alumel thermocouple junctions are distributed along the surface of the cartridge heater. These junctions are made by spot welding a chromel wire to the selected point on the heater, and then welding an alumel wire approximately 1/8 inch away from the first weld at the same elevation on the rod. This method of thermocouple attachment assures that the measured temperature

as actually that of the surface. It also produces a smaller irregularity in the heater surface than does the method of attaching both wires at the same spot, and hence, minimizes the amount by which the thermocouple junction disturbs the vapor flow.

The bulk temperature of the fluid is measured by a free thermocouple constructed by butt welding 0.020 inch chromel and alumel wire. Each of the thermocouples has in its circuit another thermocouple maintained at $32^{o}F$ in an ice-water bath. By an appropriate connection of the wires, one obtains an output voltage proportional to the temperature difference between the two junctions in each circuit. Each thermocouple is calibrated against a precision thermometer.

All of the thermocouple wires have a fiberglass insulating sheath. Each of these wires passes through a separate hole in the asbestos rod holder, and out of the protective enclosure where they are attached to a Leeds and Northrup thermocouple switch. This thermocouple switch allows selection of any one of the thermocouples for measurement. The output of the thermocouple switch is connected to a Hewlett-Packard 3465A digital multimeter for instantaneous voltage measurement, and to a Hewlett-Packard 17501A strip chart recorder for the study of the variation of thermocouple voltage output with time.

D. Photographic Equipment

High-speed motion pictures of the structure of the vapor-liquid interface are taken with a Fastax WF-3 16mm camera. The camera is mounted on a tripod next to one of the doors of the protective enclosure (see Fig.7). The tripod is equipped with a special aluminum mounting platform which allows greater horizontal leeway for camera placement than does the

standard platform. A 500 watt medium flood light mounted on the opposite side of the protective enclosure from the camera provides sufficient illumination.

The camera is capable of film speeds of up to 8000 frames per second. The speed of the camera is controlled by a special transformer which was supplied by the manufacturer of the camera. A film speed of 2500 frames per second was considered appropriate for observation of the relevant phenomena. Kodak 2498 RAR black and white reversal film processed negative was selected for its high contrast and sensitivity. An electronically controlled timing light is mounted inside the Fastax camera, and flashes with a period of 1 millisecond. This timing light produces dark bands on the edge of the film, the spacing of which determines the exact framing rate.

Quantitative measurements and qualitative observations of the photographic records were made using a Richardson Camera Corporation Model R-100 film viewer. The magnification of the camera and film viewer combined produced an image on the screen of the viewer which is about 7.5 times actual size. The film viewer allows the user to observe the film one frame at a time, or to observe the recorded motions over a wide range of speeds.

E. Fluid Selection and Related Details

It was considered desirable to perform tests using three fluids exhibiting a wide range of certain physical properties in order to determine the parameters which are important in film boiling. Water was selected as one of these fluids because of its universal usage. Freon 113 and ethanol were chosen as the other two fluids primarily for the following reasons: 1) These fluids provide a good physical contrast to water mainly

because of the differences in the latent heat of vaporization, and in the densities of the liquid and vapor. These physical properties have been clearly shown to play a large role in film boiling heat transport. 2) There is some data for film boiling of these fluids in the literature. This provides information for comparative purposes, and for determination of the repeatability and accuracy of film boiling heat transfer measurements of the type undertaken in this study.

The use of ethanol and Freon 113 as test fluids presented some practical problems. Ethanol is flammable under certain conditions, and since a very hot solid was being immersed in the alcohol, some fire preventative measures were indicated. The solution of this problem was to flood the top of the test chamber with low pressure nitrogen gas through ports machined into the aluminum top of the vessel. This drastically reduced the oxygen concentration in the neighborhood of the free surface of the ethanol, thus effectively prohibiting combustion.

Additionally, the vapors of ethanol and especially Freon 113, while having very low toxicity, are unpleasant to breathe, and since the presence of one or more persons during the tests was mandatory, some measures had to be taken to eliminate the accumulation of these vapors in the laboratory. A fan was installed in the window of the laboratory, and flexible ducting was run from the inlet of this fan and suspended directly above the test vessel. In this way the vapor concentration in the room was maintained at an acceptable level during the experiments.

VI. EXPERIMENTAL PROCEDURE

A. Preparation

The cartridge heater with attached thermocouples to be used as the test section as discussed in Section V, was first cleaned with acetone to remove any deposits or oxidation which had formed on its surface during previous tests. The test vessel was then rinsed with water and cleaned with acetone. The test section was then placed in its asbestos holder and mounted in the aluminum top of the test vessel which was in its raised position for preheating, (see Fig.7). The electrical connections for heating and thermocouple measurements were then made. The reference thermocouples were placed within sealed glass tubes filled with water, and these tubes were inserted into an ice-water mixture and the temperature of the water in the tubes was allowed to reach an equilibrium value of $32^{o}F$.

The test vessel was filled with the selected liquid and placed inside the protective enclosure and on top of the disk heater. The fume removal system was activated. If photographic data was to be taken, the cold rod was lowered into the fluid and the camera was focused. The rod was then removed and the immersion heater was placed inside the test vessel and was switched on along with the disk heater. The temperature of the liquid in the vessel was monitored with the free thermocouple. This heating continued until the liquid was uniformly at its saturation temperature.

While the liquid was being heated, the preheating of the test section was begun. The objective was to bring the wall temperature of the test section as close as possible to the temperature it would attain during the

film boiling test at the selected conditions. Since the heat transfer conditions were poorer during the preheating in still air than during the test with the rod immersed in the liquid, the initial heating was accomplished at a power level lower than that which would be employed during the test. The temperatures along the surface of the test section were monitored by measuring the output voltages of the attached thermocouples.

If photographic recording was planned, the camera was loaded with film, and the floodlight switched on. The camera transformer voltage was adjusted to select the desired film speed.

When the liquid and test section were at the desired temperatures, the test procedure was begun.

B. Test Procedure

After the initial preparation of the system was completed, as described in part A of this section, the liquid in the vessel was at the desired temperature, and the cartridge heater, with the exception of the unheated tip, was at a temperature estimated to be near the temperature it would attain during the test. The presence of a cold section near the bottom of the rod was considered undesirable, since this section would not be transferring heat in the film boiling regime, but in nucleate boiling, and the exact location of the inception of film boiling would be difficult to determine. For this reason, the unheated tip of the rod was heated externally with a propane torch to a temperature somewhat higher than the rest of the section. In this way, there was sufficient heat stored in the tip of the rod to keep its temperature above the minimum film boiling temperature and the rod completely surrounded by vapor for several

minutes, which proved to be a more than adequate interval to complete the desired measurements. Additionally, the rate of change of temperature with time in the tip section of the rod was sufficiently small, and the closest thermocouple was still sufficiently far away from the tip so that the effect of non-steady conditions at the tip of the rod could be considered negligible. In the region where measurements were made, this non-steady effect was, in fact, not measurable.

At this point, the voltage applied to the test section was increased to the desired level, and the section, in place in the aluminum top of the test vessel, was lowered into the liquid using the sliding arm mechanism, and the set screw was tightened to secure the rod in place. For ethanol tests, the valve controlling the nitrogen gas flow into the top of the test vessel was opened slightly to prevent combustion.

The output of the thermocouples on the test section was monitored with the strip chart recorder. When the output of all of the thermocouples no longer varied with time, each of the thermocouple readings was recorded. The test section voltage and current were also recorded at this point.

If high-speed movies were to be taken, the timing light was switched on and the camera was activated. When the photographic film was exhausted, it was removed and stored for development.

Often, several runs could be made before the tip of the rod cooled down below the temperature at which a stable vapor film could be maintained. The power input to the test section was changed by adjusting the variable transformer setting, the camera was reloaded, and the temperature of the rod was monitored with the strip chart recorder. When steady temperature readings were again reached, the test procedure could be repeated.

C. Test Conditions

Tests were conducted using three fluids, distilled water, ethanol, and Freon 113 at their saturation temperatures of 212°F, 173°F, and 117°F respectively. Measurements of wall temperatures were made in saturated Freon 113 at several values of wall heat flux between 9,950 $\frac{BTU}{hr\ ft^2}$ and 36,380 $\frac{BTU}{hr\ ft^2}$. This corresponded to a range of voltage between 70.67 and 136.26 volts and of current between 5.41 and 10.25 amperes.

In saturated ethanol, wall temperature measurements were made over a range of wall heat flux between 15,640 and 36,880 $\frac{BTU}{hr\ ft^2}$, corresponding to applied voltages between 81.6 and 136.2 volts, and currents between 6.88 and 10.39 amperes.

For saturated distilled water, temperature measurements were taken for a wall heat flux in the neighborhood of 35,500 $\frac{BTU}{hr\ ft^2}$ corresponding to an applied voltage of 135 volts and a current of 10.1 amperes. Because of the power limitations of the rod, and the high value of the minimum film boiling heat flux for water, the range of heat flux over which measurements could be made in water was limited.

In saturated Freon 113, high-speed motion pictures were taken at several positions on the rod at heat flux values of 20,050 and 11,040 $\frac{BTU}{hr\ ft^2}$. In ethanol, high-speed movies were taken at several elevations at heat flux values of 35,870 and 23,110 $\frac{BTU}{hr\ ft^2}$. The motion pictures for water were taken at a heat flux of about 35,500 $\frac{BTU}{hr\ ft^2}$, as indicated above.

VII. EXPERIMENTAL RESULTS

A. Heat Transfer Measurements

The results of all film boiling measurements are presented in Table 1 . This table lists for all thermocouple locations and for all experiments the measured values of the heat flux, the wall temperature, and the calculated values of the heat transfer coefficients. Three different heat transfer coefficients are given, one for the total heat transfer, one for the radiative portion, and one for the convective part.

The variation of the convective heat transfer coefficient with vertical position at fixed values of heat flux, for selected experiments covering the available range of heat flux, are presented graphically in Figs.8-28. The points plotted represent the averages of heat transfer measurements at the same thermocouple location for values of heat flux within ±5% of the value indicated in the figures.

The convective heat transfer coefficient is obtained by calculating the total heat transfer coefficient from the measured wall heat flux and temperature, and then subtracting the radiation component as obtained from the Bromley formula, Eq.(2). Section II, assuming a solid surface emissivity of 0.8, and liquid absorptivity of 1.0.

Also plotted on Figs. 8-28 are some expressions for heat transfer coefficients proposed by other investigators, and some modified results of the analytical work presented in Section III. These will be discussed in detail in Section VIII-A.

Of special note in Figs. 8-28 is the marked insensitivity of the measured heat transfer coefficients to vertical position. The largest

on the vapor-liquid interface which are recorded in Table 9 represent the average of all measured wavelengths at a given set of experimental conditions, and at a given elevation on the test section. Each motion picture recorded the image of the interface for several seconds, during which many hundreds of waves passed through the field of view. There was substantial variation in the wavelengths measured, especially at higher elevations on the test section. In addition, as the interface was often undergoing violent motions at higher elevations, disturbances were exhibiting time varying lengths and amplitudes. Thus, it was quite difficult at times to specify the length or amplitude of disturbances with a high degree of accuracy. It should be understood, therefore, that the data reported for interfacial wave characteristics represent the average of many individual measurements, and should be treated as mean or most prevalent values with an accuracy limitation of no less than ± 30% , and a standard deviation of at least 20% of the mean.

The variation of average wavelengths with elevation for all photographic experiments is presented in Figs.34-38. The most interesting feature here is that the measured average wavelengths increase noticeably with elevation, but have only a very weak dependence, if any, on heat transfer rate over the range for which data was taken.

Also on Figs. 34-38 are plotted some results of the analysis presented in Section IV. These results will be discussed in detail in Section VIII-B.

2. Qualitative Observations

High-speed motion pictures showed drastic changes in the nature of

the vapor-liquid interface when viewed at different elevations. Near the lower end of the test section (within 1 inch of the bottom, or so) the interface appeared smooth, almost glassy, with small regularly spaced waves traveling upwards and growing slightly (see Fig.39).

Somewhat higher along the test section (one to three inches from the bottom for Freon 113, two to four inches for ethanol and water) these waves increased in amplitude to the order of the test section diameter. The surface no longer appeared smooth as smaller waves and ripples were superimposed on the larger wave structures. The large-amplitude waves no longer exhibited a regular sinusoidal shape, but appeared very much like ocean waves about to break towards the lower end of the rod, while propagating upward (see Fig.40). Occasionally one of these large waves would grow or collapse sharply. Frequently the tip of one of these large, finger-like waves would break off into the surrounding liquid as a vapor bubble and float away. Some of these bubbles were recaptured by the vapor farther upstream. The irregular nature of the interface in this region made measurements increasingly difficult.

At the higher end of the test section (greater than three inches from the bottom for Freon 113, four inches for water and ethanol) the interface appeared highly irregular, continuing, however, to exhibit wave-like motions. The larger waves were very unusually shaped, having very large peaks extending into the liquid, and troughs having lengths and amplitudes much smaller than those of the peaks (see Fig.41). Often, a relatively calm area would appear between waves which seemed to have a length about equal to that of the wave peak which had just passed. Just as often, however, a large wave peak would be followed by a small

depression, and then by another large peak with no intervening relatively undisturbed areas.

Additionally, the bubbles in the liquid adjacent to the interface at the higher end of the test section were quite numerous, having been torn from interfacial wave peaks at lower elevations. These bubbles, unfortunately, obstructed the view of the interface to a great extent making quantitative data very difficult to extract.

In fact, above six or seven inches from the bottom of the twelve inch test section, the interface could hardly be distinguished, which made meaningful measurements of the wave characteristics impossible in this region.

Some frames from the high-speed motion pictures have been enlarged and are presented as Figs.39-47. Each of these figures contains the description of the experimental conditions under which the image was obtained.

VIII. DISCUSSION OF RESULTS

A. Heat Transfer Measurements

1. Experimental Results

The effect of certain variables on the heat transfer in film boiling of a saturated liquid on a vertical cylinder can be obtained directly from the experimental data. An inspection of Figs. 8 - 28 which graphically illustrate the variation in convective heat transfer coefficient with elevation on the test cylinder, clearly shows the following: for a constant heat flux in free convection film boiling of a saturated liquid on a vertical cylinder, the heat transfer coefficient is insensitive to position, at least over the first ten to twelve inches. In other words, under these conditions, a constant heat flux surface is roughly equivalent to a constant temperature surface.

This result leads to three possible simplifications in the reduction of the data. First, no correction to measured heat transfer coefficient for axial conduction in the solid need be made, since there is insufficient axial temperature gradient to produce significant heat flow in that direction. Secondly, since the temperatures of the heating surface and the liquid do not vary substantially in the vertical direction, it is reasonable to assume that the mean temperature of the vapor film is also fairly constant. Thus, convection of heat in the vapor in the vertical direction can be assumed to be minimal and can be neglected with respect to the heat transfer across the vapor. Thirdly, since the mean or film temperature of the vapor is nearly constant, and the pressure in the vapor does not vary significantly except for very long cylinders, it is not necessary to allow for variations

in vapor properties over the length of the heating surface. This simplifies analysis and allows the analytical and empirical results to be more easily scrutinized for other, more pertinent effects.

Figure 29 graphically illustrates the variation of average heat transfer coefficient with wall heat flux for film boiling of three different saturated liquids. These results show a slight increase in heat transfer coefficient with increasing heat flux in the data for ethanol and for Freon 113. Power limitations prevented the collection of data for water over a sufficiently large heat flux range to be conclusive in terms of the dependence of heat transfer coefficient on the wall heat flux. However, it is reasonable to infer, based on the available experimental evidence, that the dependence of the heat transfer coefficient on heat flux is relatively very weak, compared to say, that which occurs in nucleate boiling.

A comparison of the average heat transfer coefficient for the three saturated liquids at a heat flux value of $36{,}000 \frac{BTU}{hr\ ft^2}$ is made in Table 2. These results show that, at the same heat flux, the heat transfer coefficient for saturated ethanol has the highest value of $51.9 \frac{BTU}{hr\ ft^{2\circ}F}$, the heat transfer coefficient for saturated water is somewhat lower having a value of $45.9 \frac{BTU}{hr\ ft^{2\circ}F}$, and the heat transfer coefficient for Freon 113 is lowest at $40.6 \frac{BTU}{hr\ ft^{2\circ}F}$. The difference between the measured heat transfer coefficients for ethanol and Freon 113 at the same heat flux is much greater than the difference between the heat transfer coefficients obtained in Freon 113 when the heat flux is varied by a factor of almost four.

Yet, the differences in the coefficients for the different fluids is

still surprisingly small, considering the wide variations in the physical properties. With the system geometry and pressure fixed, the only variable parameters are the applied heat flux, and the location at which temperatures are measured. Having shown the relative insensitivity of the heat transfer coefficient to both of these system parameters, combined with the observed sensitivity to the choice of fluid, one is led to the conclusion that, for pool film boiling of a saturated liquid on a vertical cylinder at one atmosphere, the heat transfer coefficient is primarily a function of the fluid properties. Of course, many of the fluid properties are temperature dependent, which implies an indirect dependence on the heat flux.

2. Comments on Previous Work

Figures 8-28, which present data obtained in this study for local heat transfer coefficients (minus the estimated radiation component) as a function of position, also contain published analytical results obtained by several previous investigators. One of the curves plotted in Figs.8-28 represent the Bromley [3] equation for the local heat transfer coefficient. This equation consistently underpredicts measured heat transfer coefficients by 50 to 75%. It must be realized, however, that Bromley's work is based on the assumption of laminar vapor flow and this condition exists only for a small portion of the data, and was never intended to be applicable beyond this range. As will be discussed later in this section, there may, however, be other complicating effects which may contribute to the limitations of this equation.

The analytical results obtained by Hsu and Westwater [8], Eq.5,

Section II, for turbulent film boiling on a vertical surface is also plotted on Figs. 8-28. It is clear that this expression generally overpredicts measured heat transfer rates, especially when compared to the data for ethanol and for Freon 113. One of the main assumptions in this analysis is that the total thermal resistance of the vapor is directly proportional to the thickness of the laminar sublayer adjacent to the heated surface. Comparison to other turbulent flows indicates that this may be a valid assumption. The overprediction of the heat transfer may be due in part to the method of estimating the laminar sublayer thickness and/or the model selected for the velocity profile. Additionally, the turbulent core of the vapor film may provide significant thermal resistance as shown by Dougall and Rohsenow [54].

Also appearing in Figs. 8-28 are curves representing the analytical work of Andersen [37] for free convection laminar film boiling on a vertical surface. As mentioned in Section II, Andersen assumes that the film will not grow indefinitely, but will break down due to the Kelvin-Helmholtz instability, and start anew, forming a further stretch of laminar flow. Photographic data obtained in the present study showed no evidence of contact between the liquid bulk and the heated solid. It is felt that an occurrence of this sort would have been easily observed, and thus the vapor film does not completely "break down" under the conditions selected in this experimental investigation. Additionally, the observed interfacial waves have substantially larger wavelengths than those which are predicted by a Kelvin-Helmholtz approach. Based on these observations, it is concluded that any laminar analysis will be inadequate for prediction of heat transfer rates on moderately long vertical surfaces, since the uninterrupted

flow path of the vapor is sufficiently long to make turbulent flow a virtual certainty. As can be seen in Figs.8-28 , the curves representing the equation derived by Andersen consistently underpredict measured heat transfer coefficients.

The correlation obtained by Borishanskii and Fokin [56], Eq. (14), Section II, for free convection film boiling from a vertical surface is plotted in Figs. 8-28. It should be noted that this correlation exhibits no dependence on the vertical dimension of the heated surface, which is consistent with the experimental evidence. This correlation predicts the measured heat transfer coefficients well for film boiling of ethanol and water; however, it overpredicts the heat transfer coefficients for film boiling of Freon 113. This result will be discussed in greater detail in the following subsection.

It is clear, from comparison of the experimental data obtained in this investigation to the analytical expressions and experimental corelations obtained by prior investigators, that a truly accurate prediction method for the heat transfer rates in natural convection film boiling from a vertical surface does not yet exist. This is probably due to a lack of complete understanding of the heat transfer mechanisms.

3. Comments on Analytical Results and Comparison with Data

The semi-empirical approach to turbulent free convection film boiling heat transfer on a vertical surface undertaken in Section II was based on the assumption of a simple power relation between the friction coefficient, C_F , and the vapor Reynolds number (Eq.17) of the form

$$C_F = b\,Re_\delta^{-c}$$

along with an analogous expression (Eq.26) for the Stanton number,

$$C_H = \beta\,Re^{-c}Pr^{-m} \quad .$$

These assumptions led to the following expression (Eq.31) for the film boiling number, N_{FB}:

$$N_{FB} = \frac{h_c}{\rho_v c_{P_v}\left(\frac{g\mu_v}{\rho_v}\right)^{1/3}} = A\gamma^{-1/3}Pr^{-m}Re_\delta^{(1-2c)/3} \quad .$$

For single-phase, forced convection, turbulent flow over a flat plate, c and m are usually taken to be equal to 1/4 and 2/3 respectively, giving (Eq.33),

$$N_{FB} = A\gamma^{-1/3}Pr^{-2/3}Re_\delta^{1/6}$$

where A is a constant. Recalling that $Re_\delta \propto \frac{q_w x}{\mu_v h_{fg}}$, this result implies a one sixth power dependence of the heat transfer coefficient on the vertical dimension. Experimental measurements have shown practically no variation of the heat transfer coefficient with elevation; certainly the dependence, if any, seems to be even weaker than a one sixth power relation. However, the experiments undertaken in this work involve heat transfer measurements covering only one foot or less of heated surface, and perhaps measurements on a longer surface might show some dependence on the vertical dimension. Therefore, it was felt that Eq.(33) might be one

of the possible correlations which may describe the present data as well as data which may be taken in the future, and it will be used for comparison with the present results. In addition, it was considered to be pertinent to further develop Eq.(31) to see which exponent would lead to an expression that would be independent of height.

Using $c=1/2$ in Eqs. (16) and (26) leads to Eq.(34)

$$N_{FB}=B\gamma^{-1/3}Pr^{-m}$$

where B is a constant. This expression provides for a heat transfer coefficient which is completely insensitive to position, which agrees well in that respect with experimental results. The selection of different values of c may appear to be somewhat arbitrary, yet it is to be realized that the flow in the film is certainly different from that in the boundary layer of a flat plate and a value for c different from $1/4$ should certainly not be unexpected.

Equations (33) and (34) were compared to experimental data to obtain appropriate values of the constants A and B. It was found, however, that neither Eq.(33) or (34) could fully account for the measured fluid-to-fluid variations in heat transfer coefficient. The quantity N_{FB} is, at the same heat flux in all three fluids, high for water, in a middle range for ethanol, and low for Freon 113. This variation of N_{FB} with the different fluids could not be fully accounted for by the right hand sides of either Eq.(33) or (34).

At this point it should be noted that the correlation obtained by Borishanskii and Fokin [56], Eq.(14), Section II, can be rewritten in the

following form:

$$N_{FB}=0.28\gamma^{-1/3}Pr^{-1} \qquad (14')$$

This expression is of very similar form to Eq.(34), especially since the Prandtl number of most vapors is very nearly unity. Of special interest is the fact that Eqs. (34) and (14′) were derived in entirely different ways. Equation (14′) is based on the results of a dimensional analysis using the laminar flow equations combined with some rather pragmatic assumptions, and on the results of an extensive experimental investigation. These findings were then used to determine the relationship between the parameters obtained. Equation (34) results from the application of empirically determined parametric relationships for single phase forced convection, with some modifications, to the film boiling process.

While Eqs. (14′) or (34) will satisfactorily model the process for the data taken by Borishanskii and Fokin for ethyl ether, n-hexane, and benzene, and for ethanol and water, they are quite inaccurate when applied to film boiling of Freon 113, producing heat transfer coefficients which are high by approximately 100%. It is felt that this anomaly is due to an aspect of the film boiling heat transfer process which has not been taken into account, and which becomes quite evident when measurements are taken using a fluid with an unusually low latent heat of vaporization. Freon 113 has such a low value of latent heat of vaporization which is approximately 7% of the value for water, 33% of the value for ethanol, and 45% of the value for n-hexene.

This unknown aspect of the heat transfer process probably, then, has to do with phase change, as the latent heat of vaporization is clearly

a parameter. Further data analysis has pointed out that the temperature of the heated surface, or alternatively, the wall heat flux must also be involved. One possibility is that, with high vapor velocities near a wavy vapor-liquid interface, small droplets of the liquid are torn from the interface and entrained in the vapor flow. These droplets could either be propelled onto the hot solid, as reported by Farrar and Marschall [34], or be vaporized by the surrounding superheated vapor. In either case, the heat transfer mechanism would be modified by the presence of this moisture and the heat transfer coefficients would be higher than expected in the absence of droplet entrainment. This type of phenomenon would tend to explain the higher than expected values of N_{FB} for film boiling of water, and the lower than expected values of N_{FB} for film boiling of Freon 113.

The very high latent heat of vaporization of water would indicate that any additional vaporization associated with droplet entrainment could significantly decrease the temperature difference required to dissipate the heat generated in the solid. And, conversely, the very low latent heat of vaporization of Freon 113 would indicate that the occurrence of vaporization away from the interface would not greatly improve the relative efficiency of the heat transfer process.

A precise quantification of this effect would require knowledge of the volume fractions of liquid drops, along with a method of specifying their rate of vaporization. This information is not available at the present time.

Since neither an applicable theory nor experimental verification and measurements of liquid droplet entrainment characteristics were available, it was proposed that the effect of possible vaporization away from

the interface might be accounted for by one additional dimensionless parameter. An effort was made to obtain a logical grouping of relevant quantities. A dimensionless parameter relating the enthalpy associated with heating a unit mass of vapor from its saturation temperature to the wall temperature to the latent heat of vaporization was constructed. This quantity, which has occurred in other two-phase flow analyses in somewhat different connections, is generally called the superheat number and is defined by:

$$Sh = \frac{c_{P_v}(T_W - T_S)}{h_{fg}} \quad .$$

It was proposed that some power of the superheat number, Sh , could, at least in part, account for the effect of possible vaporization away from the vapor-liquid interface. Thus Eqs. (33) and (34) were modified to the following forms:

$$N_{FB} = A\gamma^{-1/3} Pr^{-m_1} Re_\delta^{1/6} Sh^{b_1} \tag{94}$$

$$N_{FB} = B\gamma^{-1/3} Pr^{-m_2} Sh^{b_2} \quad . \tag{95}$$

As can be seen, it was decided to allow the exponent of the Prandtl number to float in both equations. The data was reanalyzed to obtain the best-fit values of A, b_1, m_1, and B, b_2 and m_2. This resulted in the following set of expressions:

$$N_{FB}=0.074\gamma^{-1/3}Pr^{-0.50}Re_{\delta}^{1/6}Sh^{-0.39} \quad (96)$$

$$N_{FB}=0.22\gamma^{-1/3}Pr^{-0.65}Sh^{-0.23} \quad (97)$$

Equation (96) results from letting $c=1/4$ in Eq.(31) and (97) results from letting $c=1/2$ in (31). Both of these expressions represent the present results in a satisfactory manner.

The experimental results for convective heat transfer coefficient along with the predictions of Eq.(96) are presented in Tables 3,4, and 5 for all data points. The experimental results for average convective heat transfer coefficient along with the predictions of (97) are listed in Tables 6,7 and 8.

Curves illustrating the variation of convective heat transfer coefficient with vertical position as given by Eqs. (96) and (97) are plotted in Figs. 8-28 along with the experimental data and labeled present work. The curves representing (96) are labeled $c=1/4$, and those representing (97) are labeled $c=1/2$. Both expressions fit the data to within $\pm 20\%$ for 90% of all points.

While both Eq.(96) and (97) model the process quite well for the experimental data obtained during this study, preference must be given to the functional form of the latter, Eq.(97). Equation (97) more precisely models the measured insensitivity of heat transfer coefficient to vertical position and to heat flux and more clearly isolates the influence of the latent heat of vaporization. Equation (96) is not preferred since it contains the vapor film Reynolds number, which depends on the wall heat

flux, and the vertical position, i.e.,

$$Re_\delta = \frac{\rho_v u_0 \delta}{\mu_v} \alpha \frac{q_w x}{\mu_v h_{fg}} \quad .$$

Equation (96) is presented in graphical form in Figs. 30,31, and 32 for the data for ethanol, Freon 113, and water, respectively. Similarly, Eq.(97) is presented in Fig.33 for the data taken for film boiling of all three fluids. Figures 30-33 provide a comparison of experimental measurements to the correlations Eq.(96) and (97) for all of the data in dimensionless form. As can be seen, the comparison is quite satisfactory. The majority of those points which deviate from calculated values by more than 20% represent data taken within one inch of the lower end of the test section. In this region, the assumption of turbulent flow may not be a good one, resulting in poor agreement with Eqs.(96) and (97), and the predictions of a laminar analysis, such as that due to Bromley [3], may be adequate. Additionally, at the lower end of the test section, the interface is relatively smooth, and the vapor flow rate is small, decreasing the probability of liquid droplet entrainment in the film.

B. Interfacial Wave Characteristics

1. Comments on Theory of Section IV

In Section IV, the following dispersion relation for interfacial waves (Eq.92) was derived:

$$\frac{\alpha Re}{12\gamma}\omega^2+\left\{\frac{\alpha Re}{6}+i\left(1+\frac{Sh}{3}\right)\right\}\omega-\frac{Sh}{Pe}-i\alpha\left(2+\frac{7}{10}Sh\right)$$

$$-\alpha^2 Re\left\{\frac{1}{5}-\frac{1}{6}\frac{Sh^2}{Pe^2}(1-\gamma)\right\}=0 \quad .$$

This result was derived on the basis of certain simplifying assumptions with respect to the nature of the vapor flow, which,it is felt, are reasonable approximations, although they may not be entirely consistent with the actual physical process. The assumption of parallel flow in particular may not be completely justified as mentioned in the derivation. However, any errors generated by this assumption are not believed to affect the present development in a major way, since the vapor velocity and the temperature gradients in the vertical direction must be small in comparison to the horizontal gradients, and the angle between the interface and vertical is small except near the region of film boiling inception. The conditions are generally met and hence, the errors introduced by the parallel flow assumption are considered to be acceptable.

Certainly the use of the laminar flow equations limits the strict applicability of Eq.(92) to the small region of vapor flow near the lower end of a vertical surface wherein the flow is known to be viscous. However, it was hoped that some information derived from this equation could be used to interpret the phenomena observed in the turbulent flow areas. This interpretation might then serve as some indication as to the validity of mechanisms which were assumed to generate the wave motion.

2. Results of Theory

A computer program was designed and implemented to solve Eq.(92)

for various sets of fluid properties and system parameters. The program had access to files containing the values of the vapor properties as a function of the vapor film temperature. The program initially required specification of the fluid, the wall heat flux, the wall temperature, and the position of interest on the test section. After this information was accepted by the program, an upper limit, lower limit and incremental value for the nondimensional wave number, α, were supplied. The program would then generate the dimensionless complex frequencies, ω, corresponding to the selected values of α.

Since the flow was considered to be turbulent in the regions of interest, an approximate turbulent profile consistent with the heat transfer analysis of Section III was entered in the program. This profile was used only to obtain the maximum vapor velocity, u_0, and the average vapor film thickness, $\bar{\delta}$.

Of primary interest is the variation of the imaginary part of the dimensionless complex frequency, ω, with the dimensionless wave number. The general form of the results is presented graphically in Fig.48, wherein $Im(\omega)$ is plotted against α. There are several important features in Fig.48. First, the value of α for which $Im(\omega)=0$ is termed the critical wave number, α_c, and is the theoretical stability boundary. All waves having lower wave numbers (higher wavelengths) are predicted to be stable, and all waves having higher wave numbers (lower wavelengths) should grow to finite amplitudes.

Secondly, the value of α corresponding to the maximum of $Im(\omega)$ is termed the "most unstable" or "most dangerous" wave number, α_D. Waves having this wave number (or corresponding wavelength $\lambda_D=2\pi\bar{\delta}/\alpha_D$) should,

in theory, grow most rapidly, at least initially.

Of note is the fact that the curve is rather flat in the region of maximum growth rate, and thus one might expect to see a spectrum of waves of finite amplitude having wave numbers in the neighborhood of α_D, whereas, if α_D corresponded to a very sharp peak in $Im(\omega)$, one would expect to observe waves having the corresponding wavelength, λ_D, almost exclusively.

Also of interest is the variation of the locations of α_C and α_D with the vapor Reynolds number. As the Reynolds number is increased, both α_D and α_C attain lower values. This indicates that one should expect to observe longer wavelengths at higher elevations, and at higher values of heat flux, since the Reynolds number will increase in either case.

3. Experimental Results and Comparison to Theory

High-speed motion pictures of free convection film boiling on a vertical cylinder in three saturated fluids were analyzed for the purpose of extracting data on the characteristics of waves on the vapor-liquid interface. Motion pictures were taken at various elevations in saturated ethanol at wall heat flux values of 35870 $\frac{BTU}{hr\,ft^2}$ and 23110 $\frac{BTU}{hr\,ft^2}$, in saturated Freon 113 at wall heat flux values of 20060 $\frac{BTU}{hr\,ft^2}$ and 11040 $\frac{BTU}{hr\,ft^2}$, and in saturated distilled water at a wall heat flux of 35430 $\frac{BTU}{hr\,ft^2}$. The pictures were enlarged and measurements of wavelength ($\bar{\lambda}_{EXP}$), wave speed ($\bar{c}^*_{R_{EXP}}$), wave amplitude ($\bar{\eta}_{EXP}$), and minimum film thickness (δ_{MIN}) were made. These results are presented in Table 9. As mentioned in Section VII, these results are averages of many measurements, and should be treated as statistical mean values, giving an indication of the order of magnitude of the most prevalent characteristic features of

the interfacial disturbances under a given set of experimental conditions.

It is clear, from Table 9, that there is, indeed, an increase in average measured wavelength with increasing elevations in all cases. Additionally, the wave amplitudes increase rapidly in the vertical direction attaining values of the order of the test section diameter (0.5 inches), concurring with the qualitative observations. The minimum film thickness increases in the vertical direction, as expected from a simple heat balance.

The effect of heat flux on the observed wavelengths appears to be minimal, in contrast to theoretical predictions. However, the range of heat flux over which data was obtained is deemed insufficiently broad for conclusive evidence as to the effect of heat flux on interfacial wave characteristics.

The critical wavelengths, λ_c, and the "most dangerous" wavelengths, λ_D, corresponding to the experimental conditions under which data was taken were computed according to the theory of Section IV, and as discussed earlier in this section. These computations are presented in Table 10, along with the experimentally determined average wavelength, $\overline{\lambda}_{EXP}$, and the average vapor film thickness, $\overline{\delta}$, maximum vapor velocity, u_0, and vapor film Reynolds number used in the calculations. The theoretical values of both critical and "most dangerous" wavelengths are listed along with the computed oscillatory frequency of the waves, labeled Real $[\omega^*_D]$.

It should be pointed out that the wavelengths computed by the theory of Section IV are substantially larger than those obtained using a Kelvin-Helmholtz approach (see Appendix E). This indicates that vaporization at the interface is an important aspect of the formation of interfacial waves, and should not be neglected in the stability theory. This, in fact, is

considered to be the principal finding of this analysis.

Although wave frequencies were difficult to measure due to the irregular nature of the interface, the predicted frequencies are consistent with the film speeds required to sufficiently slow down the interfacial activity.

Comparison of the measured average wavelength, $\bar{\lambda}_{EXP}$, to the computed value of the "most dangerous" wavelength, λ_D, and the critical wavelength, λ_C, is available in Table 10, and graphical comparison can be made in Figs. 34-38. The measured and computed "most dangerous" wavelengths seem to compare well at elevations of less than one inch in all cases. However, as the elevation is increased, the measured wavelengths fall substantially lower than the predicted value of λ_D. As can be seen in Figs. 34-38, all measured wavelengths however, are well within the region of unstable waves, even though they do not coincide with the waves computed to have the highest initial growth rates.

To quantify this deviation of measurement from theory, the growth rate, $Im[\omega]$, theoretically corresponding to the measured average wavelength is compared to the maximum growth rate, $Im[\omega_D]$, corresponding to the calculated "most dangerous" wavelength, λ_D, in Table 11. The rightmost column in these tables presents the ratio of the dimensionless growth rate theoretically corresponding to the measured average wavelength, $Im[\omega(\bar{\alpha}_{EXP})]$, to the maximum calculated dimensionless growth rate, labeled $Im(\omega_D)$. As can be seen, the ratio is near unity at the lowermost end of the test section, decreasing to 0.2 to 0.5 at higher elevations. Thus, while the computed and measured wavelengths may differ by a factor of fifty or more, the associated theoretical growth rates only vary by a factor

of about four.

This result is indicative of the fact that, as mentioned earlier, the curve relating $Im(\omega)$ to α is not very steep in the region of α_D (see Fig.48). Therefore, the prediction of α_D, or alternatively λ_D, is very sensitive to small errors in the values of vapor velocity, u_0, average film thickness, $\overline{\delta}$, and various vapor properties used in the calculations.

Again, one has to consider the assumptions discussed earlier and the fact that the actual waves are certainly nonlinear. The fact that the observed waves have lengths different from the "most dangerous" one, λ_D, is, therefore, not surprising. In fact, it is easy to imagine that although λ_D is the wavelength with the highest initial growth rate, a different wavelength may be the most likely one to reach a given finite amplitude. It is, however, believed to be significant that the observed wavelengths are within the region of the wavelengths which were calculated to be unstable. This fact seems to indicate that the theory presented, even though very simplified, is able to describe the main features of the wave generating process. In particular, it appears probable that the evaporation from the interphase boundary is an important feature in the formation of the waves whereas surface tension is not, as was pointed out earlier.

C. Effect of Interfacial Waves on Heat Transfer

Qualitative observations and experimental data indicate that there are drastic changes in the nature of the vapor-liquid interface with elevation in natural convection film boiling of a saturated liquid on vertical, uniform heat flux surfaces having lengths greater than an inch or so (see Figs. 39-47). At lower elevations the interface is smooth, with regularly

spaced, low amplitude waves traveling in the vertical direction. At the higher end of the surface, the interface is most irregular, with longer waves having very large amplitudes, and curved, finger-like shapes. The surrounding liquid is laden with vapor bubbles, and the entire area is characterized by violent, large-scale motions.

It is most interesting to note, however, that while the nature of the interface undergoes such extreme changes with vertical position, inspection of the heat transfer measurements made simultaneously indicate no significant variation in heat transfer coefficient over the same range of elevation.

As mentioned in Section II, Coury and Dukler [27] and Suryanarayana and Merte [28] have investigated the effect of large-amplitude interfacial oscillations on the heat transfer in film boiling on a vertical surface. The experimental data of Coury and Dukler [27] for film boiling of saturated Freon 113, and of Suryanarayana and Merte [28] for film boiling of saturated nitrogen, also show no significant variation of heat transfer coefficient with height (above one inch or so), agreeing well with the experimental results of the present investigation.

Assuming that the interfacial waves are sinusoidal, and that they do not disturb the dimensionless temperature profile in the vapor film, Coury and Dukler [27] introduce an analytical heat transfer enhancement factor, C, representing the ratio of the mean heat transfer coefficient with an oscillating film to the heat transfer coefficient with a steady film at the mean film thickness as follows:

$$C=(1-\varepsilon^2)^{-1/2}$$

where ε is the dimensionless amplitude of oscillation, that is, the ratio of the wave amplitude to the mean film thickness.

Suryanarayana and Merte [28] obtain the same analytical result as Coury and Dukler [27];however, it is modified empirically. They propose that the heat transfer enhancement is proportional to some power of the film Reynolds number and experimentally obtain the following form:

$$C=0.548\,Re_{\delta}^{0.187}$$

The expressions above indicate that the effect of large interfacial waves is an augmentation of the heat transfer. Since the amplitude and violence of the interfacial waves increase in the vertical direction, one would expect to measure relatively large increases in the measured heat transfer coefficients if, indeed, interfacial waves were to cause an augmentation of the heat transport mechanism. As mentioned before, these increases are not borne out by experiment.

Based on the present experimental evidence, then, it may be concluded that under conditions of natural convection film boiling of a saturated fluid on a vertical surface, there is no enhancement of the heat transfer as a direct result of the presence of large-amplitude waves on the vapor-liquid interface, at least over the first foot or so. The waviness of the interface may induce liquid droplet entrainment in the film, which would improve the efficiency of the heat transfer mechanism, and this was assumed in the formulation of Eq.(97). It appears doubtful, however, that the presence of the waves alone will increase the heat transfer coefficient as compared to that which would be obtained with a

smooth interface. In fact, it is quite feasible that the presence of interfacial waves diminishes the efficiency of the heat transfer process, if one considers the following possibility.

One of the difficulties in theoretically predicting film boiling heat transfer coefficients may be that the actual interfacial waves observed are very large. As a consequence, adjacent to the wave peaks, there can be very little transfer of heat from the wall to the liquid. The significant portion of the heat transfer must be occurring in the small wave troughs, and in the intermittent calm areas, which appear to cover no more than half the vertical length of the heated section at any given time. The vapor generated in these sections must be the major contributing factor in the growth of the wave peaks.

The vapor present near the peaks and in the pocket-like shapes formed by the peaks is probably effectively stagnant. As a consequence, the vapor mass flow which is involved in the transport of heat from the solid surface to the interface might be significantly smaller than that which is calculated from a simple model in which quasi-parallel vapor flow is assumed. Experimentally, it can be shown that the time averaged thickness of the vapor film is much greater than that predicted in the absence of interfacial waves. Thus the average velocity of the vapor may be significantly smaller than expected. This would increase the temperature difference required to transfer the generated heat and could cause the heat transfer coefficients to vary more slowly with position than expected from a turbulent flow-smooth channel analysis, which predicts a heat transfer coefficient which increases with height.

The above explanation is highly speculative, and a great deal of

experimental and analytical verification would be required to substantiate these arguments. However, it is clear at this point that the large waves do not directly augment the heat transfer.

D. Areas for Future Study

As a result of this investigation it is clear that the present level of understanding of the film boiling heat transfer process is still imperfect especially when the geometry involves long vertical surfaces. The nature of the vapor flow in the film is still somewhat in question, as are the characteristics and effects of the interfacial waves. Further investigations are certainly justified and a few suggestions are offered.

Experimentally, some investigation into the nature of interfacial waves is indicated. One can envisage a series of experiments in which the vapor flow in film boiling is approximated by injecting a gaseous substance at an appropriate rate through a vertical surface and into a pool of liquid. Comparison of the nature of the gas-liquid interface under these conditions to the interfacial oscillations occurring under actual film boiling conditions would shed more light on the effect of vaporization on the interfacial waves. This comparison would also test the hypotheses underlying the present explanation. Additionally, this kind of experimentation could easily lend itself to measurement of liquid entrainment characteristics [60].

Another approach which would reveal any possible impingement of entrained liquid droplets would involve film boiling of a scaling salt solution on a long vertical surface, similar to the experiments of Farrar and Marschall [34] with spheres. Under these condtions, any droplets which

impinge on the solid surface will leave a salt deposit providing a clear indication of contact.

Film boiling experiments involving very long vertical surfaces would be enlightening in terms of the nature and effect of extremely large amplitude interfacial waves, and would provide more information on the film boiling process at very high vapor Reynolds numbers. One would like to see hot wire anemometry involved in such a setup to measure turbulence levels and perhaps actual vapor velocities.

These studies would, hopefully, lead to a quantitative understanding of the effects of interfacial waves on the heat transfer, including the possible reduction of average velocities and heat transfer surface area, the effect of possible liquid droplet entrainment, and the possible role of droplets actually impinging on the solid surface.

Other aspects of film boiling are also in need of further investigation, both experimental and analytical. Among these are the effects of subcooling, forced convection, and the influence of gravity and system pressure. The present state of quantitative information in the area of film boiling, and in fact, in all regimes of boiling, is still quite incomplete. The need for improved information will continue to exist, particularly in order to assess problems associated with nuclear power generation, the operation of large cryogenic facilities, and perhaps, the development of improved heat treating processes for large structures.

IX. SUMMARY AND CONCLUSIONS

Surface temperatures in pool film boiling of three saturated liquids (ethanol, Freon 113, distilled water) on a 0.50 inch diameter, 12 inch long electrically heated vertical cylinder have been measured as a function of position and applied heat flux. High-speed motion pictures of the interfacial wave patterns accompanying the heat transfer have been recorded and analyzed for qualitative and quantitative information on the nature of interfacial disturbances.

A semi-empirical analysis of the heat transfer in turbulent pool film boiling of a saturated liquid on a vertical surface has been performed, and the results compared with heat transfer measurements. The results of the analysis were modified to better represent the empirical data. The modification is thought to represent the effects of possible liquid droplet entrainment in the vapor film.

A linearized stability analysis of the vapor-liquid interface in laminar flow film boiling has been performed. This analysis includes the effects of mass transfer on the force balance at the vapor-liquid interface. The results are extrapolated into the region of turbulent flow film boiling for comparison to measured interfacial wave characteristics.

On the basis of the experimental and analytical results, the following conclusions can be made:

(1) The measured heat transfer coefficient for free convection pool film boiling of a saturated liquid on a moderately long vertical cylinder exhibits little, if any, variation with vertical position, and only a relatively weak dependence on

the heat flux from the solid surface.

(2) The heat transfer data for three saturated fluids (ethanol, Freon 113, and distilled water) may be predicted well from the following experimentally modified analytical relation:

$$N_{FB}=0.22\gamma^{-1/3}Pr^{-0.65}Sh^{-0.23}$$

where,

$$N_{FB}=\frac{h_c}{\rho_v c_{P_v}\left(\frac{g\mu_v}{\rho_v}\right)^{1/3}},$$

$$\gamma=\frac{\rho_v}{\rho_L}$$

$$Pr=\frac{\mu_v c_{P_v}}{k_v}$$

and

$$Sh=c_{P_v}\frac{(T_W-T_S)}{h_{fg}}$$

(3) There is a possibility of liquid droplet entrainment in the vapor film indicated by the dependence of the measured heat transfer coefficients on certain fluid properties, most notably, on the latent heat of vaporization.

(4) The nature of the vapor-liquid interface exhibits drastic changes with elevation, being very smooth and showing only small, gentle disturbances at lower elevations, while

becoming extremely violent with a very large amplitude and irregular wave structure at higher elevations.

(5) No contact seemed to occur between the bulk of the liquid and the heated vertical surface under the experimental conditions employed in this investigation.

(6) Evaporation from the vapor-liquid interface is an important feature in the generation of interfacial waves, while surface tension is not.

(7) The interfacial activity does not directly augment the heat transfer, as had been expected from some previous analytical results. In fact, there is a good probability that these waves tend to lower heat transfer coefficients due to the significant amounts of relatively stagnant vapor located in the large wave peaks. However, the waves may have an indirect augmenting effect by enhancing the rate of liquid droplet entrainment in the vapor film.

BIBLIOGRAPHY

1) Leidenfrost, J.G., "DeAquae Communis Nonullis Qualitatibus Tractus," Duisburg, 1756; Int.J.Heat Mass Transfer, 9, 1156-1166 (1966).

2) Drew, T.B., and Mueller, A.C., "Boiling," Trans.Amer.Inst.Chem.Eng., 33, 449-473 (1937).

3) Bromley, L.A., "Heat Transfer in Stable Film Boiling," Chem.Eng.Progr., 46 (5), 221-227 (1950).

4) Ellion, M.E., "A Study of the Mechanisms of Boiling Heat Transfer," Memo 20-88, Jet Propulsion Laboratory, Pasadena, California (1954).

5) Zuber, N., "Hydrodynamic Aspects of Boiling Heat Transfer," AEC U-4439, (1959).

6) Zuber, N., and Tribus, M., "Further Remarks on the Stability of Boiling Heat Transfer," AEC U-3631, (1958).

7) Hsu, Y.Y., and Westwater, J.W., "Film Boiling from Vertical Tubes," AIChE J., 4(1), 58-62 (1958).

8) Hsu, Y.Y., and Westwater, J.W., "Approximate Theory for Film Boiling on Vertical Surfaces," Chem.Eng.Progr., Symp.Ser., 56(30), 15-24(1960).

9) Koh, J.C.Y., "Analysis of Film Boiling on Vertical Surfaces," J.Heat Transfer, 84C(1), 55-62 (1962).

10) Sparrow, E.M., and Cess, R.D., "The Effect of Subcooled Liquid on Laminar Film Boiling," J.Heat Transfer, 84C(2), 149-156 (1962).

11) Nishikawa,K., and Ito, T., "Two-Phase Boundary-Layer Treatment of Free Convection Film Boiling," Int.J.Heat Mass Transfer, 9(2), 103-115(1966).

12) Bradfield, W.S., "Liquid-Solid Contact in Stable Film Boiling," Ind. Eng.Chem.Fundam., 5(2), 200-204 (1966).

13) Gallant, R.W., "Physical Properties of Hydrocarbons. Part 21 — Halogenated Hydrocarbons," Hydrocarbon Processing, 47(2), 113-121 (1968).

14) Borishanskii, V.M., "Experimental Investigation of Heat Transfer in Film Boiling on Horizontal and Vertical Tubes," in Problems of Heat Transfer and Hydraulics of Two-Phase Media: A Russian Symposium, Pergamon Press, NY, 152-162 (1969).

15) Jordan, D.P., "Film and Transition Boiling," Advan.Heat Transfer, 5, 55-128 (1968).

16) Price, C.E., and Sauer, H.J., Jr., "Film Boiling of Nitrogen from Inclined Flat Plates," ASHRAE Paper No.2143, ASHRAE Annual Meeting, Kansas City, Missouri, 58-63, (1970).

17) Bergles, A.E., and Thompson, W.G., Jr., "The Relationship of Quench Data to Steady-State Pool Boiling Data," Int.J.Heat Mass Transfer, 13, 55-68 (1970).

18) Plesset, M.S., "Note on the Flow of Vapor Between Liquid Surfaces," J.Chem.Phys., 20(5), 790-793 (1952).

19) Ünsal, M., and Thomas, W.C., "Linearized Stability Analysis of Film Condensation," J.Heat Transfer, 100, 629-634 (1978).

20) Marschall, E., and Lee, C.Y., "Stability of Condensate Flow Down a Vertical Wall," Int.J.Heat Mass Transfer, 16, 41-48 (1973).

21) Yih, C.S., "Stability of Liquid Flow Down an Inclined Plane," Physics of Fluids, 6, 321-334 (1963).

22) Betchov, R., and Criminale, W.O., Stability of Parallel Flows, Academic Press, NY (1967).

23) CRC Handbook of Chemistry and Physics, 58th Ed., CRC Press, Cleveland, Ohio (1977).

24) Hsieh, D.Y., "Effects of Heat and Mass Transfer on the Rayleigh-Taylor Instability," ASME J.Basic Eng., 94, 156-162 (1972).

25) Clements, L.D., and Colver, C.P., "Natural Convection Film Boiling Heat Transfer," Industrial and Engineering Chemistry, 62(9), 26-46 (1970).

26) Clements, L.D., and Colver, C.P., "Generalized Correlation for Film Boiling," J.Heat Transfer, 94, 324-326 (1972).

27) Coury, G.E., and Dukler, A.E., "Turbulent Film Boiling on Vertical Surfaces. A Study Including the Influence of Interfacial Waves," Paper B.3.6, Proceedings International Heat Transfer Conference, Paris (1970).

28) Suryanarayana, N.V., and Merte, H., Jr., "Film Boiling on Vertical Surfaces," J.Heat Transfer, 94, 377-384 (1972).

29) Grietzer, E.M., and Abernathy, F.H., "Film Boiling on Vertical Surfaces," Int.J.Heat Mass Transfer, 15, 475-491 (1972).

30) Nagendra, H.R., "Laminar Film Boiling on Inclined Isothermal Flat Plates," AIAA Journal, 2(1), 72-79 (1973).

31) Seetharamu, K.N., Krishnamurthy, M.V., and Ramachandran, A., "Free Convection Laminar Film Boiling from a Vertical Plate with Nonuniform Heat Flux," Israel Journal of Technology, 10(3), 201-205 (1972).

32) Sauer, H.J., and Shih-Chang, L., "Effect of Inclination on Film Boiling," Paper B.3.7, Proceedings Fifth International Heat Transfer Conference, Tokyo, Japan (1974).

33) Kalinin, E.K., Berlin, I.I., and Kostyuk, V.V., "Film Boiling Heat Transfer," Advan.Heat Transfer, 12, 51-194 (1975).

34) Farrar, L.C., and Marschall, E., "Film Boiling in a Scaling Liquid," J.Heat Transfer, 98, 173-177 (1976).

35) Baum, A.J., Purcipile, J.C., and Dougall, R.S., "Transition and Film Boiling Heat Transfer from Vertical Surfaces," ASME Paper 77-HT-82 (1977).

36) Dhir, V.K., and Purohit, G.P., "Subcooled Film Boiling Heat Transfer from Spheres," ASME Paper 77-HT-78 (1977).

37) Andersen, J.G.M., "Low-Flow Film Boiling Heat Transfer on Vertical Surfaces, Part I: Theoretical Model," AIChE Symp.Ser., 73(164), 2-6 (1976).

38) Leonard, J.E., Sun, K.H., and Dix, G.E., "Low-Flow Film Boiling Heat Transfer on Vertical Surfaces, Part II: Empirical Formulations and Applications to BWR-LOCA Analysis," AIChE Symp.Ser., 73(164), 7-13 (1976).

39) Marschall, E., and Moresco, L.L., "A Variable Property Analysis of Laminar Film Boiling on Vertical Plates," Numerical Heat Transfer (1970).

40) Groeneveld, D.C., and Gardiner, S.R.M., "Post-CHF Heat Transfer Under Forced Convective Conditions," ASME Symposium on the Thermal and Hydraulic Aspects of Nuclear Reactor Safety, Vol.I, 43-73 (1977).

41) Coury, G.E., Ph.D.Dissertation, University of Houston, Houston, Texas (1968).

42) Westwater, J.W., "Boiling of Liquids," Advan.Chem.Eng., 2, 1-31 (1958).

43) Nukiyama, S., "Maximum and Minimum Values of Heat Transfer from Metal to Boiling Water Under Atmospheric Pressure," Nippon Kikai Gakkai Rombunshu, 37(206), 367 (1934): Int.J.Heat Mass Transfer, 9(12), 1419-1433 (1966).

44) Hsu, Y.Y., "A Review of Film Boiling at Cryogenic Temperatures," Advances in Cryogenic Engineering, 17, 361-381 (1972).

45) Kutateladze, S.S., Fundamentals of Heat Transfer, Academic Press, NY (1963).

46) Hamill, T.D., and Baumeister, K.J., "Effect of Subcooling and Radiation on Film Boiling Heat Transfer from a Flat Plate," NASA TN D-3925, (1967).

47) Bromley, L.A., Leroy, N.R., and Robbers , J.A., "Heat Transfer in Forced Convection Film Boiling," Ind.Eng.Chem., 45(11), 2639-2646 (1953).

48) Tachibana, F., and Fukui, S., "Heat Transfer in Film Boiling to Subcooled Liquids," International Developments in Heat Transfer, Proceedings ASME Heat Transfer Conference, 219-223 (1961).

49) Motte, E.I., and Bromley, L.A., "Film Boiling of Flowing Subcooled Liquids," Ind.Eng.Chem., 49, 1921-1928 (1957).

50) Cess, R.D., "Forced Convection Film Boiling on a Flat Plate with Uniform Heat Flux," J.Heat Transfer, 84, 395 (1962).

51) Farahat, M.M., and Madbouly, E.E., "Stable Film Boiling Heat Transfer from Flat Horizontal Plates Facing Downwards," Int.J.Heat Mass Transfer, 20, 269-277 (1977).

52) McFadden, P.W., and Grosh, R.J., "An Analysis of Laminar Film Boiling with Variable Properties," Int.J.Heat Mass Transfer, 1, 325-335 (1961).

53) Greitzer, E.M., Ph.D.Dissertation, Harvard University, Cambridge, Massachusetts, (1969).

54) Dougall, R.S., and Rohsenow, W.M., "Film Boiling on the Inside of Vertical Tubes with Upward Flow of the Fluid at Low Qualities," Report No. MIT-TR-9079-26, Massachusetts Institute of Technology, Cambridge, Massachusetts (1963).

55) Simon, F.F., Papell, S.S., and Simoneau, R.J., "Minimum Film Boiling Heat Flux in Vertical Flow of Liquid Nitrogen," NASA TN D-4307 (1968).

56) Borishanskii, V.M., and Fokin, B.S., "Heat Transfer During Film Boiling on a Vertical Surface under Conditions of Free Convection in a Large Volume," in Convective Heat Transfer in Two-Phase and One-Phase Flows, V.M.Borishanskii and J.J.Paleev, Eds.; AEC tr-6877, 185-197 (1969).

57) Sparrow, E.M., "Error Estimates in Temperature Measurements," in Measurements in Heat Transfer, E.R.G.Eckert and R.J.Goldstein, Eds., Hemisphere Publishing Corp., Washington, D.C., 1-23 (1976).

58) Jakob, M., Heat Transfer, Vol.II, John Wiley and Sons, NY (1957).

59) Hennecke, D.K., and Sparrow, E.M., "Local Heat Sink on a Convectively Cooled Surface-Application to Temperature Measurement Error," Int.J. Heat Mass Transfer, 13,287-304 (1970).

60) Brennen, C.E., California Institute of Technology, Pasadena, California, Private Communication, January 1980.

61) Lamb, Sir Horace, Hydrodynamics, 6th Ed., Dover Press, New York, (1945).

APPENDIX A

EXPERIMENTAL APPARATUS

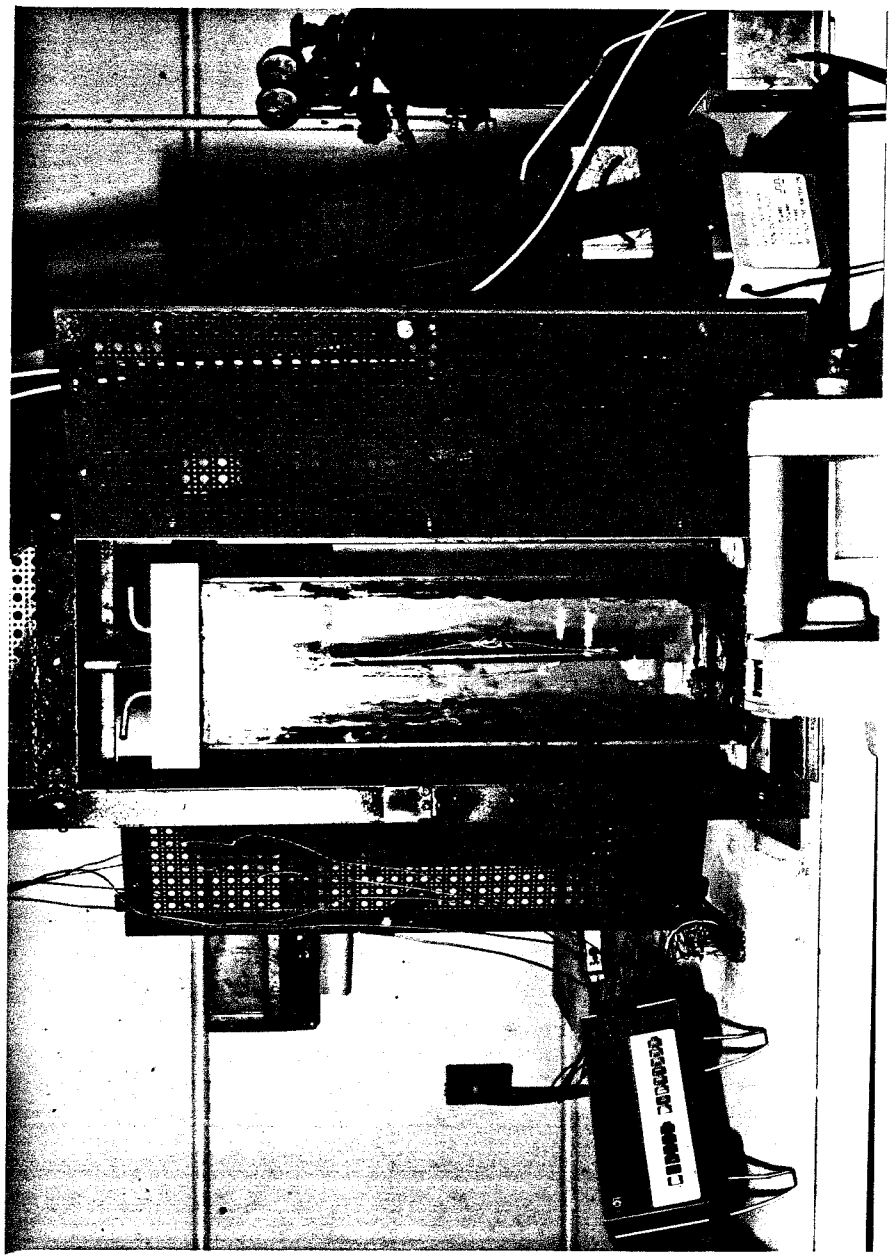

Figure 4. Photograph of Experimental Installation

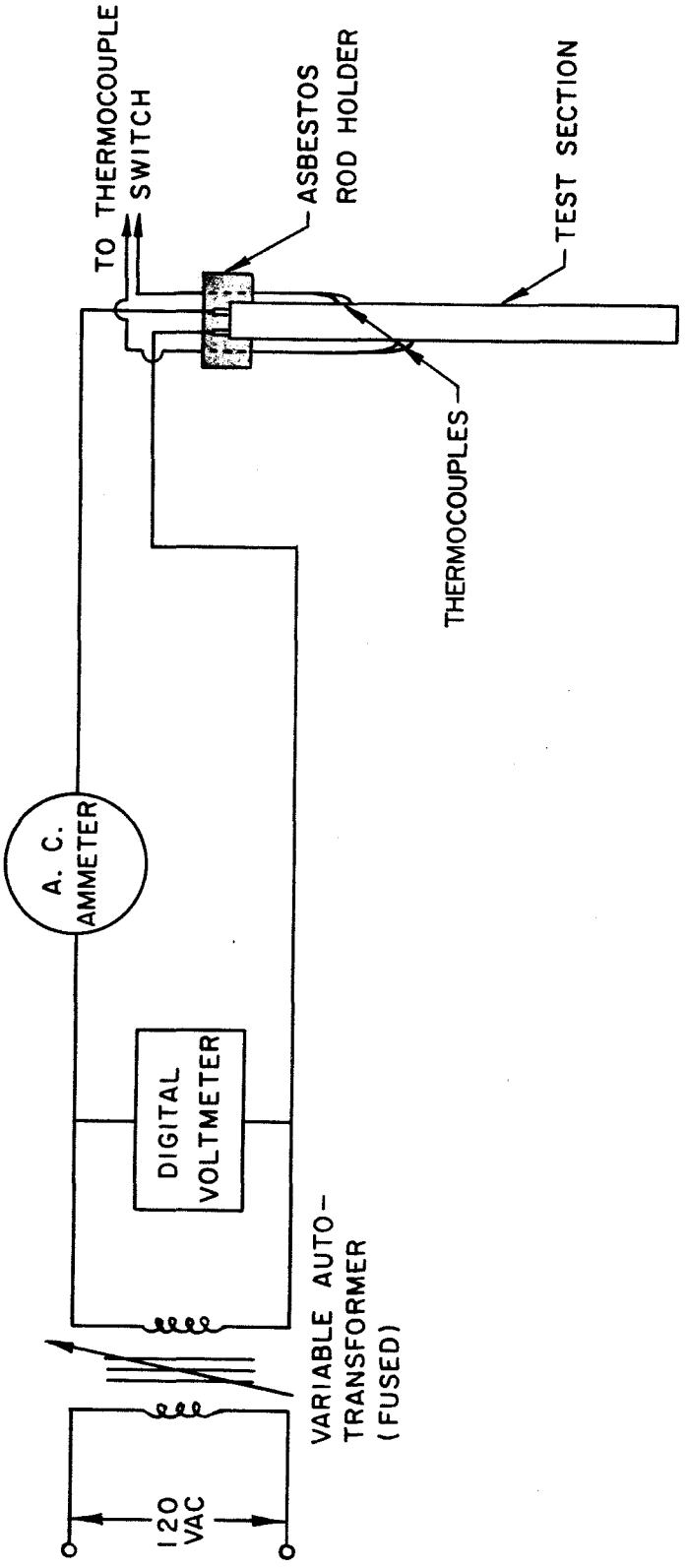

Figure 5. Schematic Diagram for Electrical Controls and Measurements

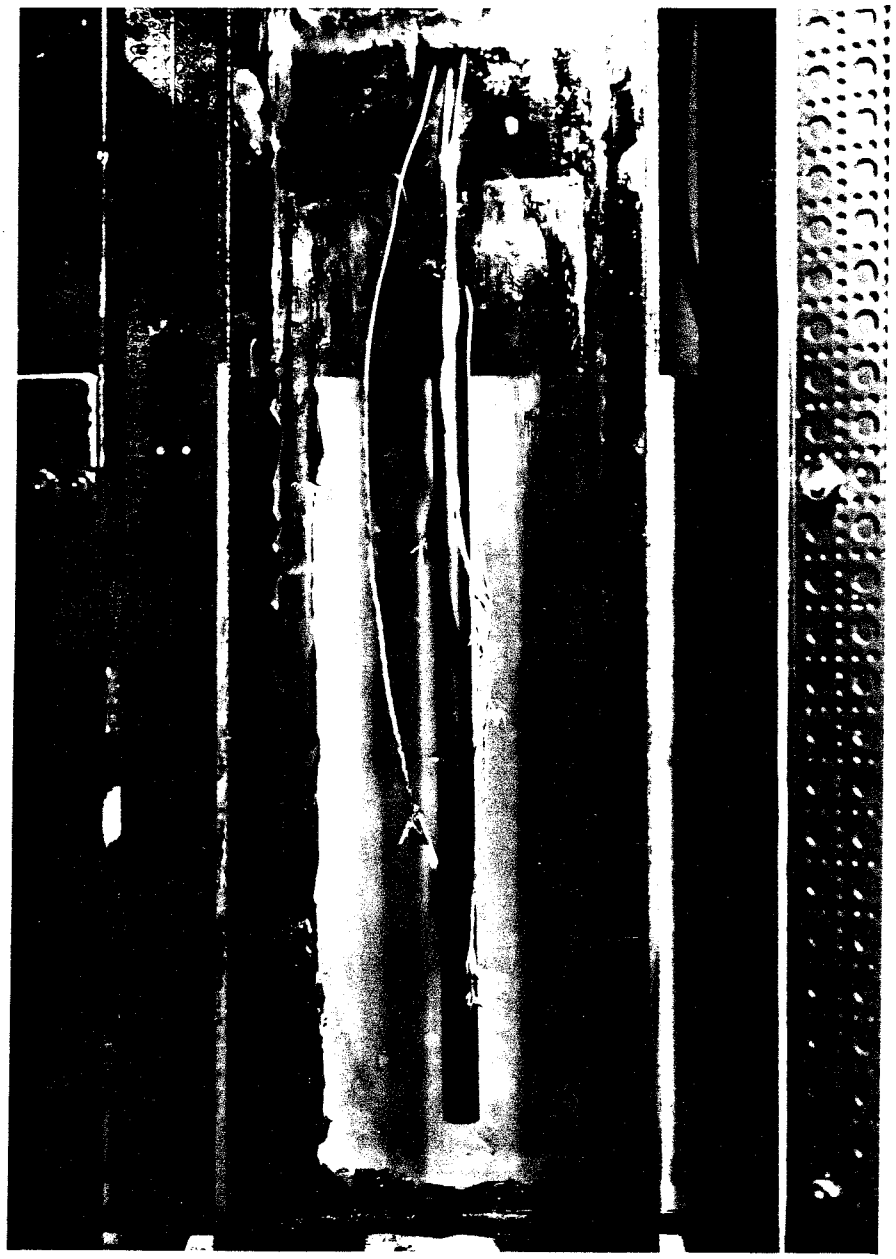

Figure 6. Photograph of Test Section and Vessel

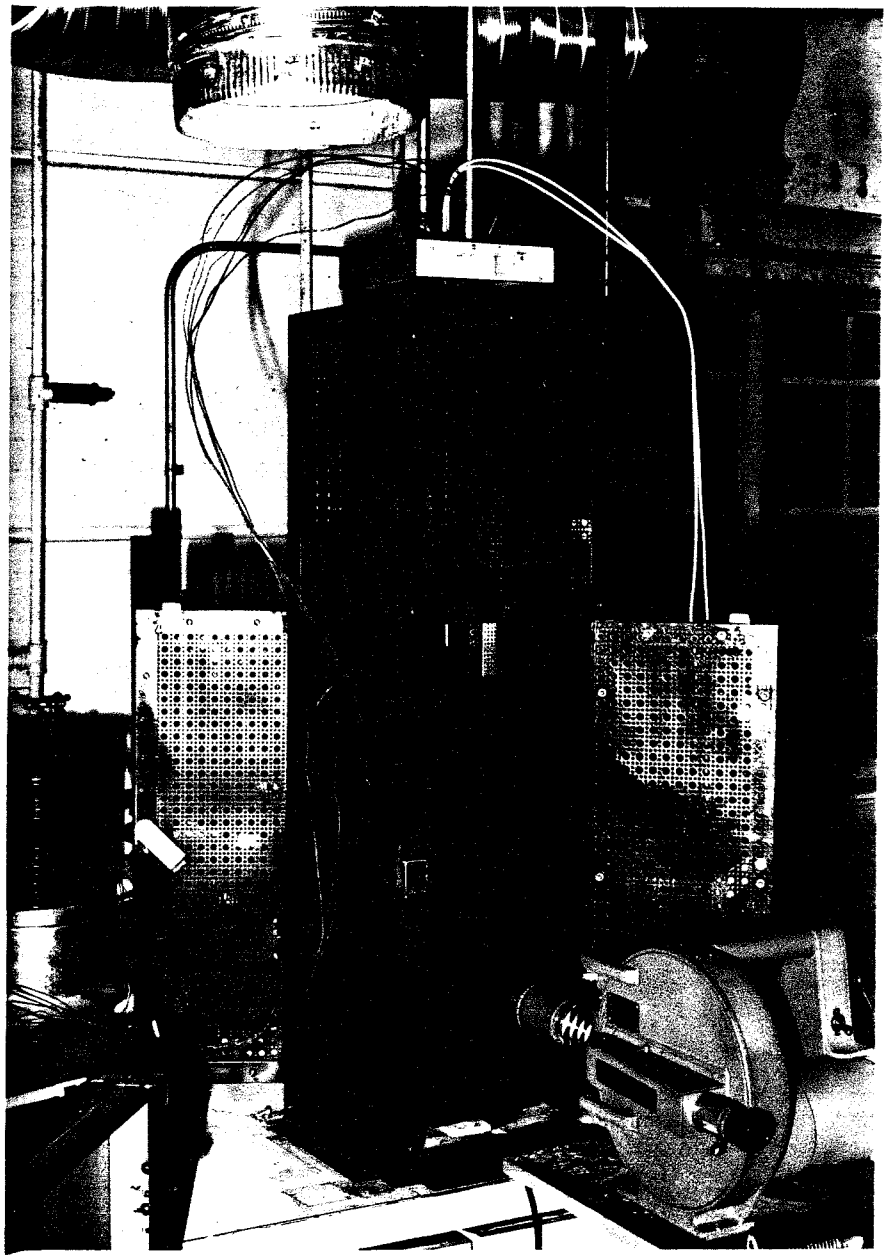

Figure 7. Photograph of Experimental Apparatus Including Fastax Camera

APPENDIX B

HEAT TRANSFER RESULTS

TABLE 1. HEAT TRANSFER EXPERIMENTAL DATA

SATURATED ETHANOL

$Q_W\left(\frac{BTU}{hr\ ft^2}\right)$	x(in)	$T_W(^oF)$	$h_{TOTAL}\left(\frac{BTU}{hr\ ft^{2o}F}\right)$	$h_R\left(\frac{BTU}{hr\ ft^{2o}F}\right)$	$h_c\left(\frac{BTU}{hr\ ft^{2o}F}\right)$
35010	1.5	962	44.4	5.1	39.3
35010	3.0	923	46.7	4.8	41.9
32440	1.5	914	43.8	4.7	39.1
32440	3.0	879	46.0	4.5	41.5
30080	1.5	873	43.0	4.4	38.6
30080	3.0	837	45.3	4.1	41.2
26340	1.5	794	42.4	3.8	38.6
26340	3.0	766	44.4	3.6	40.8
23530	1.5	730	42.3	3.4	38.9
23530	3.0	703	44.4	3.2	41.2
34860	4.5	890	48.6	4.5	44.1
34860	6.06	914	47.1	4.7	42.4
34862	7.44	848	51.7	4.2	47.5
31550	4.5	836	47.6	4.1	43.5
31550	6.06	859	46.0	4.3	41.7
31550	7.44	793	50.9	3.8	47.1
29170	4.5	794	47.0	3.8	43.2
29170	6.06	817	45.3	4.0	41.3
29170	7.44	764	49.4	3.6	45.8
25880	4.5	731	46.4	3.4	43.0
25880	6.06	758	44.3	3.6	40.7
23040	4.5	676	45.8	3.0	42.8
23040	6.06	709	43.0	3.3	39.7
34980	4.5	909	47.6	4.7	42.9
	6.0	918	47.0	4.8	42.4
	7.5	841	52.4	4.2	48.2
31960	4.5	870	45.9	4.4	41.5
	6.0	874	45.6	4.4	41.2

TABLE 1. (CONTINUED)

SATURATED ETHANOL(CONT'D)

$Q_W\left(\frac{BTU}{hr\ ft^2}\right)$	x(in)	$T_W(^oF)$	$h_{TOTAL}\left(\frac{BTU}{hr\ ft^{2o}F}\right)$	$h_R\left(\frac{BTU}{hr\ ft^{2o}F}\right)$	$h_c\left(\frac{BTU}{hr\ ft^{2o}F}\right)$
31960	7.5	808	50.4	4.0	46.4
29540	4.5	826	45.3	4.1	41.2
	6.0	830	45.0	4.1	40.9
	7.5	773	49.3	3.7	45.6
26140	4.5	749	45.4	3.5	41.9
	6.0	764	44.2	3.6	40.6
	7.5	731	46.9	3.4	43.5
23530	4.5	698	44.8	3.2	41.6
23530	6.0	714	43.5	3.3	40.2
34360	1.0	854	50.5	4.3	46.2
	2.0	920	46.0	4.7	41.3
	3.0	931	45.4	4.9	40.5
	4.5	858	50.2	4.3	45.9
	6.0	842	51.4	4.2	47.2
	7.5	845	51.2	4.2	47.0
	9.0	861	50.0	4.3	45.7
	10.5	854	50.5	4.3	46.2
31640	1.0	827	48.4	4.0	44.4
	2.0	884	44.5	4.5	40.0
	3.0	896	43.8	4.6	39.2
	4.5	813	49.5	4.0	45.5
	6.0	795	50.9	3.8	47.1
	7.5	795	50.9	3.8	47.1
	9.0	826	48.5	4.1	44.4
	10.5	825	48.6	4.1	44.5
34940	1.0	891	48.7	4.5	44.2
	2.0	953	44.8	5.0	39.8
	3.0	955	44.7	5.1	39.6

TABLE 1. (CONTINUED)

SATURATED ETHANOL (CONT'D)

$Q_W\left(\frac{BTU}{hr\ ft^2}\right)$	x(in)	$T_W(^oF)$	$h_{TOTAL}\left(\frac{BTU}{hr\ ft^{2o}F}\right)$	$h_R\left(\frac{BTU}{hr\ ft^{2o}F}\right)$	$h_c\left(\frac{BTU}{hr\ ft^{2o}F}\right)$
34940	4.5	852	51.5	4.3	47.2
	6.0	836	52.7	4.1	48.6
	7.5	863	50.7	4.3	46.4
	9.0	905	47.8	4.7	43.1
	10.5	878	49.6	4.4	45.2
31780	1.0	832	48.2	4.0	44.2
	2.0	890	44.4	4.6	39.8
	3.0	895	44.0	4.5	39.5
	4.5	799	50.8	3.9	46.9
	6.0	777	52.6	3.6	49.0
	7.5	809	50.0	3.9	46.1
	9.0	850	47.0	4.2	42.8
	10.5	861	46.2	4.3	41.9
28900	1.0	769	48.5	3.6	44.9
	2.0	829	44.1	4.1	40.0
	3.0	833	43.8	4.1	39.7
	4.5	746	50.5	3.5	47.0
	6.0	727	52.2	3.4	48.8
	7.5	759	49.4	3.6	45.8
	9.0	805	45.8	3.9	41.9
36880	1.0	940	48.1	4.9	43.2
	2.0	1017	43.7	5.6	38.1
	4.5	857	53.9	4.2	49.7
	6.0	932	48.6	4.8	43.8
	7.5	866	53.2	4.3	48.9
	9.0	904	50.5	4.7	45.8
33120	1.0	867	47.8	4.4	43.4
	2.0	945	42.9	4.9	38.0

TABLE 1. (CONTINUED)

SATURATED ETHANOL (CONT'D)

$Q_W\left(\frac{BTU}{hr\ ft^2}\right)$	x(in)	$T_W(^oF)$	$h_{TOTAL}\left(\frac{BTU}{hr\ ft^{2o}F}\right)$	$h_R\left(\frac{BTU}{hr\ ft^{2o}F}\right)$	$h_c\left(\frac{BTU}{hr\ ft^{2o}F}\right)$
33120	4.5	796	53.2	3.8	49.4
	6.0	872	47.4	4.4	43.0
	7.5	819	51.3	4.0	47.3
30380	1.0	802	48.3	3.9	44.4
	2.0	885	42.7	4.5	38.2
	4.5	743	53.3	3.5	49.8
	6.0	822	46.8	4.0	42.8
	7.5	835	45.9	4.1	41.8
36290	1.0	889	50.7	4.5	46.2
	2.0	972	45.4	5.2	40.2
	3.0	930	48.0	4.9	43.1
	4.5	829	55.5	4.1	51.3
	6.0	894	50.4	4.6	45.8
	7.5	827	55.5	4.0	51.5
	9.0	844	54.1	4.2	49.9
	10.5	796	58.3	3.9	54.4
32880	1.0	826	50.4	4.1	46.3
	2.0	900	45.2	4.6	40.6
	3.0	860	47.9	4.3	43.6
	4.5	778	54.4	3.7	50.7
	6.0	837	49.5	4.1	45.4
	7.5	775	54.6	3.6	51.0
36430	1.0	905	49.8	4.6	45.2
	2.0	986	44.8	6.3	38.5
	3.0	946	47.2	5.0	42.2
	4.5	833	55.2	4.1	51.1
	6.0	904	49.9	4.7	45.2
	7.5	832	55.3	4.0	51.2

TABLE 1. (CONTINUED)

SATURATED ETHANOL (CONT'D)

$Q_W\left(\frac{BTU}{hr\ ft^2}\right)$	x(in)	$T_W(^oF)$	$h_{TOTAL}\left(\frac{BTU}{hr\ ft^{2o}F}\right)$	$h_R\left(\frac{BTU}{hr\ ft^{2o}F}\right)$	$h_c\left(\frac{BTU}{hr\ ft^{2o}F}\right)$
36430	9.0	837	54.9	4.1	50.8
	10.5	883	51.3	4.4	46.9
33190	1.0	833	50.3	4.1	46.2
	2.0	924	44.2	4.8	39.4
	3.0	880	47.0	4.5	42.5
	4.5	782	54.5	3.7	50.8
	6.0	849	49.1	4.2	44.9
	7.5	786	54.2	3.8	50.4
29650	1.0	759	50.6	3.6	47.0
	2.0	854	43.6	4.3	39.3
	3.0	812	46.4	3.9	42.5
	4.5	725	53.7	3.3	50.4
	6.0	789	48.2	3.8	44.4
27330	1.0	698	52.1	3.2	48.9
	2.0	803	43.4	3.9	39.5
	3.0	765	46.2	3.6	42.6
	4.5	682	53.7	3.1	50.6
	6.0	756	46.9	3.6	43.3
24310	1.0	617	54.8	2.8	52.0
	2.0	736	43.2	3.4	39.8
	3.0	702	46.0	3.2	42.8
	4.5	632	53.0	2.8	50.2
21300	1.0	507	63.8	2.2	61.6(?)
	2.0	658	44.0	3.0	41.0
	3.0	626	47.1	2.8	44.3
	4.5	578	52.6	2.5	50.1
36300	1.0	889	50.7	4.5	46.2
	2.0	968	45.7	5.2	40.5

TABLE 1. (CONTINUED)

SATURATED ETHANOL(CONT'D)

$Q_W\left(\frac{BTU}{hr\ ft^2}\right)$	x(in)	$T_W(^oF)$	$h_{TOTAL}\left(\frac{BTU}{hr\ ft^{2o}F}\right)$	$h_R\left(\frac{BTU}{hr\ ft^{2o}F}\right)$	$h_c\left(\frac{BTU}{hr\ ft^{2o}F}\right)$
36300	3.0	909	49.3	4.6	44.7
	4.5	823	55.9	4.1	51.8
	6.0	872	52.0	4.4	47.6
	7.5	791	58.8	3.8	55.0
	9.0	803	57.6	3.8	53.8
	10.5	778	60.0	3.7	56.3
32970	1.0	830	50.2	4.1	46.1
	2.0	898	45.5	4.6	40.9
	3.0	838	49.6	4.1	45.5
	4.5	763	55.9	3.6	52.3
	6.0	813	51.5	3.9	47.6
	7.5	724	59.9	3.4	56.5
	9.0	774	54.9	3.7	51.2
29930	1.0	764	50.7	3.7	47.0
	2.0	823	46.1	4.1	42.0
	3.0	774	49.8	3.7	46.1
	4.5	717	55.0	3.3	51.7
	6.0	771	50.1	3.7	46.4
	7.5	678	59.3	3.1	56.2
27180	1.0	693	52.3	3.2	49.1
	2.0	759	46.4	3.6	42.8
	3.0	702	51.4	3.2	48.2
	4.5	666	55.2	3.0	52.2
	6.0	719	49.8	3.3	46.5
	7.5	669	54.8	3.0	51.8
24440	1.0	616	55.2	2.7	52.5
	2.0	674	4818	3.0	45.8
	3.0	622	54.5	2.8	51.7
	4.5	611	55.8	2.7	53.1
	6.0	660	50.2	3.0	47.2

TABLE 1. (CONTINUED)

SATURATED DISTILLED WATER

$Q_W\left(\frac{BTU}{hr\ ft^2}\right)$	x(in)	$T_W(^oF)$	$h_{TOTAL}\left(\frac{BTU}{hr\ ft^{2o}F}\right)$	$h_R\left(\frac{BTU}{hr\ ft^{2o}F}\right)$	$h_c\left(\frac{BTU}{hr\ ft^{2o}F}\right)$
37380	1.0	982	48.6	5.5	43.1
	2.0	1095	42.3	6.5	35.8
	3.0	1021	46.2	5.8	40.4
	4.5	1060	44.1	6.2	37.9
	6.0	1121	41.1	6.8	34.3
	7.5	956	50.2	5.2	45.0
	10.5	938	51.5	5.1	46.4
31530	1.0	860	48.7	4.5	44.2
	2.0	990	40.5	5.5	35.0
	3.0	934	43.7	5.1	38.6
	4.5	964	41.9	5.3	36.6
	7.5	847	49.7	4.4	45.3
36540	1.0	1012	45.7	5.8	39.9
	2.0	1064	42.9	6.3	36.6
	3.0	1008	45.9	5.7	40.2
	4.5	1012	45.7	5.8	39.9
	6.0	1104	41.0	6.7	34.3
	9.0	1025	45.0	5.9	39.1
35610	2.0	1082	40.9	6.4	34.5
	3.0	1016	44.3	5.8	38.5
	4.5	1025	43.8	5.9	37.9

TABLE 1. (CONTINUED)

SATURATED DISTILLED WATER

$Q_W\left(\frac{BTU}{hr\ ft^2}\right)$	x(in)	$T_W(^oF)$	$h_{TOTAL}\left(\frac{BTU}{hr\ ft^{2o}F}\right)$	$h_R\left(\frac{BTU}{hr\ ft^{2o}F}\right)$	$h_c\left(\frac{BTU}{hr\ ft^{2o}F}\right)$
35610	6.0	1095	40.3	6.5	33.8
	9.0	1055	42.4	6.1	36.1
35430	3.0	986	45.8	5.5	40.3
	5.0	912	50.6	4.9	45.7
	7.0	1010	44.4	5.7	38.7
	3.0	964	47.1	5.3	41.8
	5.0	903	51.3	4.8	46.5
	7.0	1012	44.3	5.8	38.5
35080	3.0	986	45.3	5.5	39.8
	5.0	916	49.8	4.9	44.9
	7.0	1021	43.4	5.9	37.5
35480	3.0	1025	43.6	5.9	37.7
	5.0	938	48.9	5.1	43.8

TABLE 1. (CONTINUED)

SATURATED FREON 113

$Q_W\left(\frac{BTU}{hr\ ft^2}\right)$	x(in)	$T_W(^oF)$	$h_{TOTAL}\left(\frac{BTU}{hr\ ft^{2o}F}\right)$	$h_R\left(\frac{BTU}{hr\ ft^{2o}F}\right)$	$h_c\left(\frac{BTU}{hr\ ft^{2o}F}\right)$
36380	1.0	1074	38.0	5.8	32.3
	2.0	1096	37.2	6.0	31.2
	3.0	1042	39.4	5.6	33.8
	4.5	939	44.3	4.7	39.6
	6.0	1022	40.2	5.3	34.9
	7.5	938	44.4	4.7	39.7
	9.0	989	41.8	5.1	36.7
14020	1.0	495	37.2	2.0	35.2
	2.0	502	36.5	2.0	34.5
	3.0	452	41.9	1.7	40.2
	4.5	445	42.8	1.7	41.1
	6.0	488	37.9	2.0	35.9
	7.5	433	44.5	1.7	42.8
19480	1.0	666	35.5	2.8	32.7
	2.0	677	34.8	2.8	32.0
	3.0	624	38.5	2.6	35.9
	4.5	572	42.9	2.3	40.6
	6.0	626	38.2	2.6	35.6
	7.5	595	40.8	2.4	38.4
24540	1.0	801	35.9	3.6	32.3
	2.0	817	35.1	3.7	31.4
	3.0	764	38.0	3.4	34.6
	4.5	682	43.5	2.9	40.6
	6.0	769	37.7	3.4	34.3
19530	1.0	667	35.6	2.8	32.8
	2.0	705	33.2	3.0	30.2
	3.0	654	36.4	2.7	33.7
	4.5	600	40.5	2.5	38.0

TABLE 1. (CONTINUED)

SATURATED FREON 113 (CONT'D)

$Q_W\left(\frac{BTU}{hr\ ft^2}\right)$	x(in)	$T_W(^oF)$	$h_{TOTAL}\left(\frac{BTU}{hr\ ft^{2o}F}\right)$	$h_R\left(\frac{BTU}{hr\ ft^{2o}F}\right)$	$h_c\left(\frac{BTU}{hr\ ft^{2o}F}\right)$
19530	6.0	640	37.4	2.7	34.7
	7.5	561	44.1	2.3	41.8
	9.0	545	45.7	2.2	43.5
	10.5	490	52.5	2.0	50.5
24440	1.0	807	35.4	3.6	31.8
	2.0	835	34.1	3.9	30.2
	3.0	780	36.9	3.5	33.4
	4.5	702	41.8	3.0	38.8
	6.0	756	38.3	3.3	35.0
	7.5	677	43.7	2.9	40.8
	9.0	729	40.0	3.2	36.8
28540	1.0	897	36.6	4.3	32.3
	2.0	926	35.3	4.5	30.8
	3.0	871	37.9	4.1	33.8
	4.5	776	43.4	3.5	39.9
	6.0	843	39.4	4.0	35.4
	7.5	850	39.0	4.0	35.0
13960	1.0	546	32.6	2.2	30.4
	2.0	548	32.5	2.2	30.3
	3.0	495	37.0	2.0	35.0
	4.5	453	41.6	1.7	39.9
	6.0	516	35.1	2.1	33.0
11860	1.0	469	33.8	1.9	31.9
	2.0	471	33.6	1.9	31.7
	3.0	420	39.2	1.6	37.6
	4.5	400	42.0	1.6	40.4
9951	1.0	392	36.3	1.6	34.7
	2.0	391	36.4	1.5	34.9

TABLE 1. (CONTINUED)

SATURATED FREON 113 (CONT'D)

$Q_W\left(\frac{BTU}{hr\ ft^2}\right)$	x(in)	$T_W(^oF)$	$h_{TOTAL}\left(\frac{BTU}{hr\ ft^{2o}F}\right)$	$h_R\left(\frac{BTU}{hr\ ft^{2o}F}\right)$	$h_c\left(\frac{BTU}{hr\ ft^{2o}F}\right)$
9951	3.0	340	44.8	1.4	43.4
	4.5	347	43.4	1.4	42.0
34930	1.0	1050	37.5	5.6	31.9
	2.0	1132	34.4	6.4	28.0
	3.0	1100	35.6	6.1	29.5
	4.5	934	42.8	4.6	38.2
	6.0	981	40.5	5.0	35.5
	7.5	945	42.2	4.7	37.5
	9.0	1050	37.5	5.6	31.9
	10.5	1109	35.2	6.1	29.1
31770	1.0	1002	35.9	5.1	30.8
	2.0	1073	33.2	5.8	27.4
	3.0	1044	34.3	5.5	28.8
	4.5	878	41.8	4.2	37.6
	6.0	922	39.5	4.5	35.0
	7.5	898	40.7	4.3	36.4
23240	1.0	786	34.8	3.6	31.2
	2.0	848	31.8	3.9	27.9
	3.0	824	32.9	3.8	29.1
	4.5	694	40.3	2.9	37.4
	6.0	738	37.5	3.3	34.2
13180	1.0	517	33.0	2.0	31.0
	2.0	565	29.5	2.3	27.2
	3.0	553	30.3	2.2	28.1
	4.5	463	38.2	1.8	36.4
9396	1.0	394	34.0	1.6	32.4
	2.0	438	29.3	1.7	27.6
	3.0	431	30.0	1.7	28.3

TABLE 1. (CONTINUED)

SATURATED FREON 113 (CONT'D)

$Q_W\left(\frac{BTU}{hr\ ft^2}\right)$	x(in)	$T_W(^oF)$	$h_{TOTAL}\left(\frac{BTU}{hr\ ft^{2o}F}\right)$	$h_R\left(\frac{BTU}{hr\ ft^{2o}F}\right)$	$h_c\left(\frac{BTU}{hr\ ft^2F}\right)$
9396	4.5	367	37.7	1.5	36.2
11260	1.0	440	34.9	1.7	33.2
	2.0	492	30.0	2.0	28.1
	3.0	494	30.7	2.0	28.7
	4.5	420	37.2	1.6	35.6
11540	1.0	450	34.7	1.8	32.9
	2.0	508	29.6	1.9	27.5
	3.0	499	30.2	1.9	28.3
	4.5	425	37.5	1.6	35.9
	6.0	443	35.5	1.8	33.7
	7.5	430	36.9	1.7	35.2
	9.0	447	35.0	1.8	33.2
	10.5	416	38.7	1.7	37.0
13150	1.0	491	35.2	1.9	33.3
	2.0	554	30.2	2.3	27.9
	3.0	537	31.4	2.2	29.2
	4.5	456	38.9	1.8	37.1
	6.0	475	36.8	1.9	34.9
	7.5	462	38.2	1.8	36.4
	9.0	488	35.5	1.9	33.6
	10.5	496	34.8	2.0	32.8
15550	1.0	561	35.1	2.3	32.8
	2.0	624	30.7	2.6	28.1
	3.0	608	31.7	2.5	29.2
	4.5	515	39.1	2.0	37.1
	6.0	536	37.2	2.2	35.0
	7.5	520	38.6	2.0	36.6
	9.0	575	34.0	2.3	31.7

TABLE 1. (CONTINUED)

SATURATED FREON 113 (CONT'D)

$Q_W\left(\frac{BTU}{hr\ ft^2}\right)$	x(in)	$T_W(^oF)$	$h_{TOTAL}\left(\frac{BTU}{hr\ ft^{2o}F}\right)$	$h_R\left(\frac{BTU}{hr\ ft^{2o}F}\right)$	$h_c\left(\frac{BTU}{hr\ ft^{2o}F}\right)$
18460	1.0	652	34.6	2.8	31.8
	2.0	712	31.1	3.1	28.0
	3.0	691	32.2	2.9	29.3
	4.5	586	39.4	2.4	37.0
	6.0	610	37.5	2.5	35.0
	7.5	599	38.4	2.5	35.9
16160	1.0	566	36.0	2.2	33.8
	2.0	619	32.2	2.5	29.7
	3.0	598	33.6	2.4	31.2
	4.5	502	42.1	2.0	40.1
	6.0	543	38.0	2.2	35.8

TABLE 2

AVERAGE HEAT TRANSFER COEFFICIENTS FOR FILM BOILING OF THREE SATURATED FLUIDS AT THE SAME HEAT FLUX VALUE OF $36{,}000 \frac{BTU}{hr\ ft^2}$

Fluid	h_{TOTAL} $\frac{BTU}{hr\ ft^2\ ^\circ F}$	h_c $\frac{BTU}{hr\ ft^2\ ^\circ F}$
Ethanol	51.9	47.5
Freon 113	40.6	35.3
Distilled Water	45.9	40.2

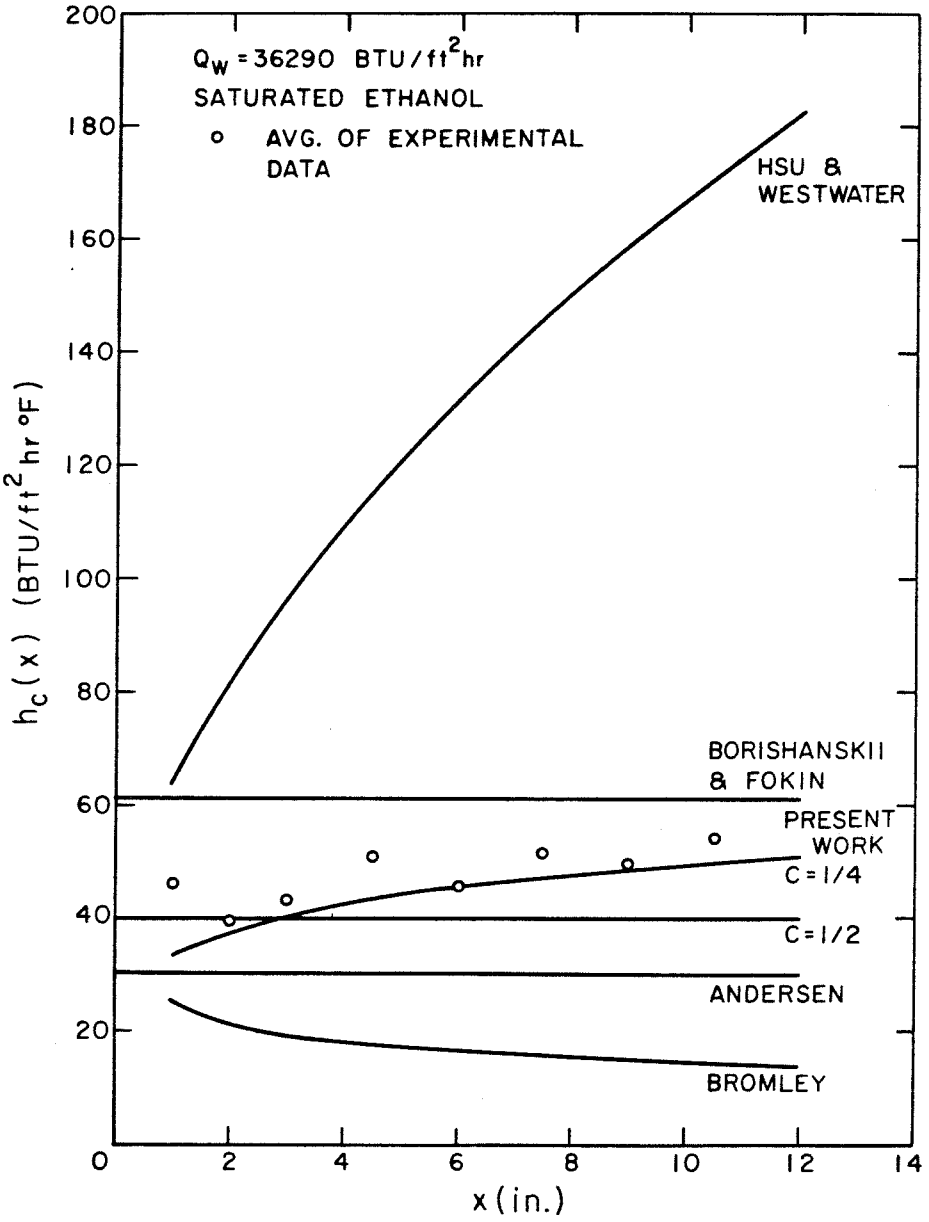

Figure 8. Convective Heat Transfer Coefficient vs. Vertical Position for Free Convection Film Boiling of Saturated Ethanol on a Vertical Cylinder

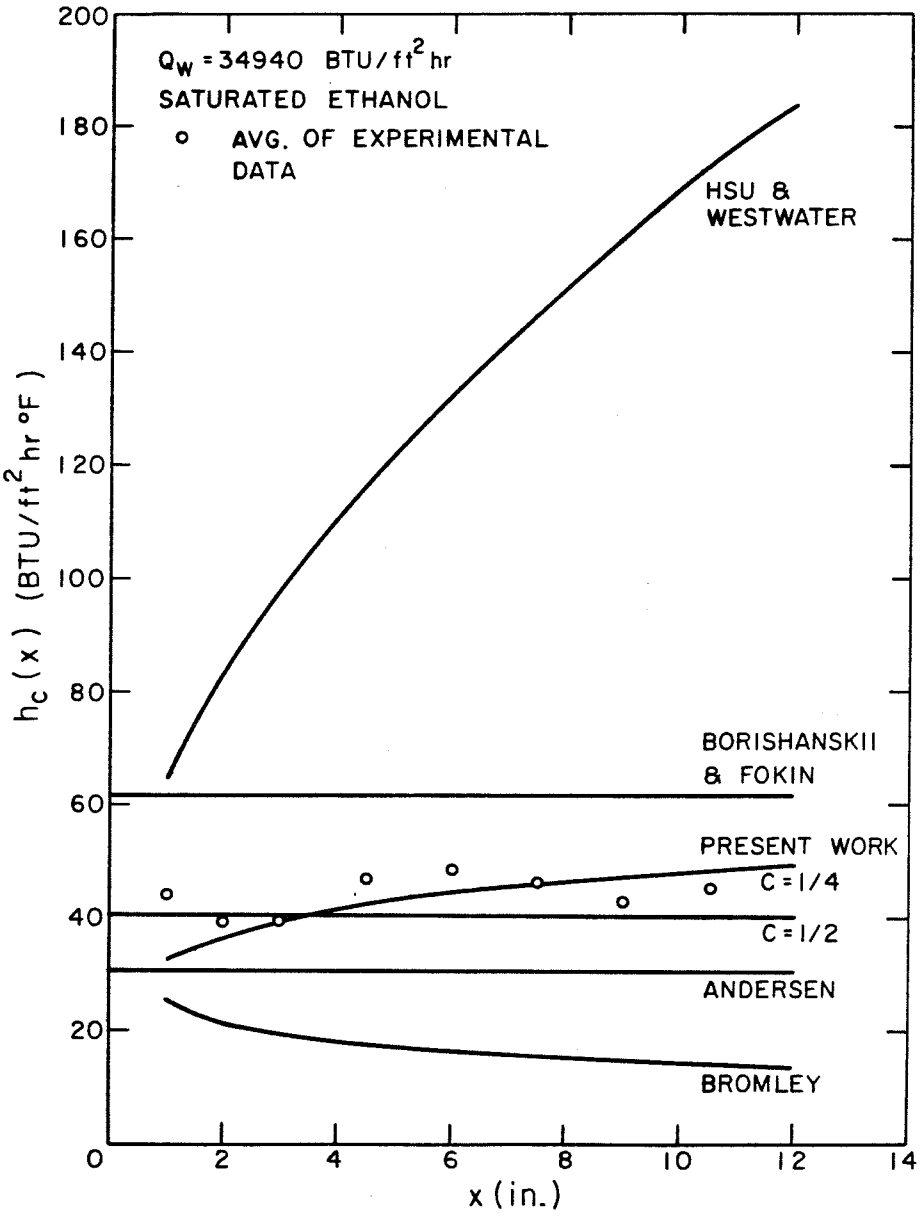

Figure 9. Convective Heat Transfer Coefficient vs. Vertical Position for Free Convection Film Boiling of Saturated Ethanol on a Vertical Cylinder

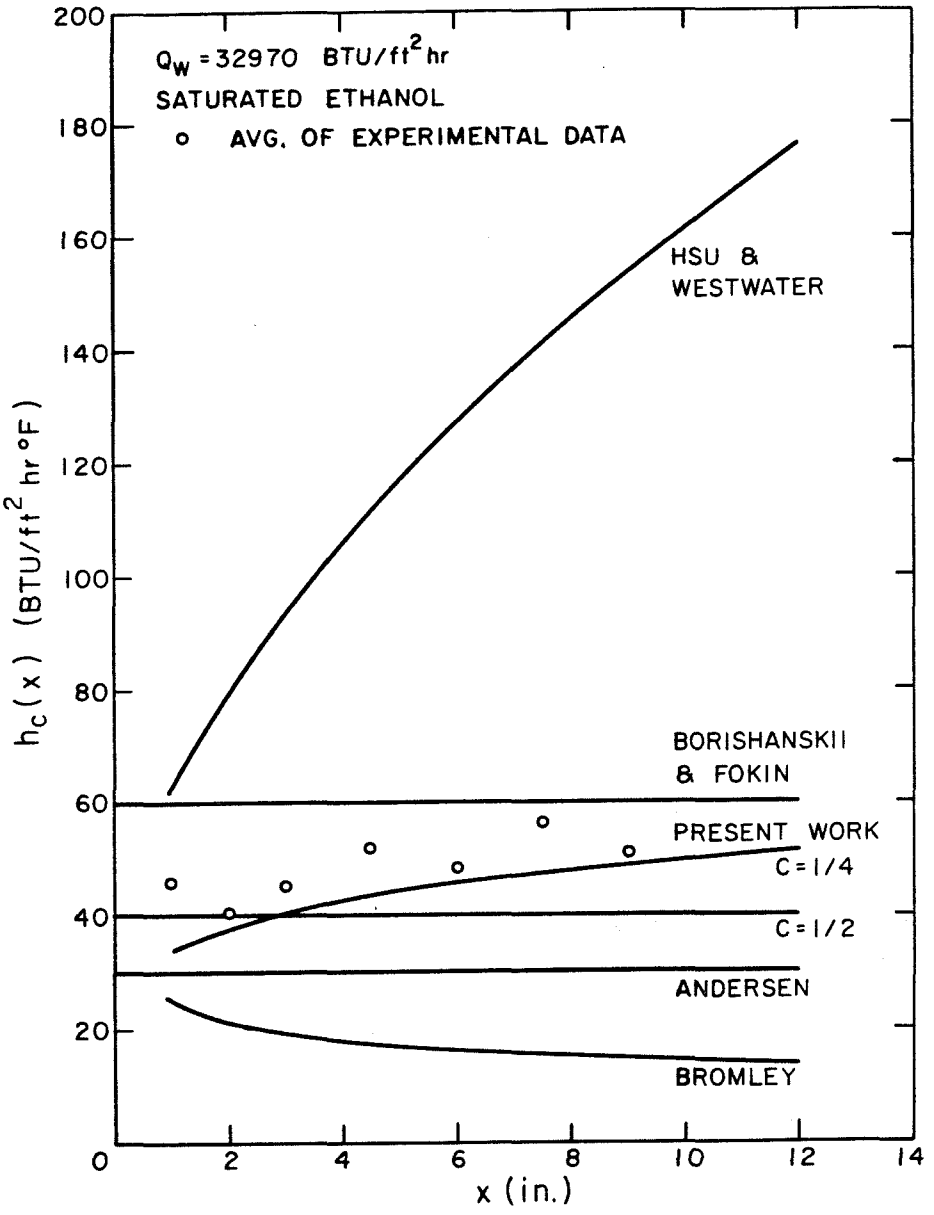

Figure 10. Convective Heat Transfer Coefficient vs. Vertical Position for Free Convection Film Boiling of Saturated Ethanol on a Vertical Cylinder

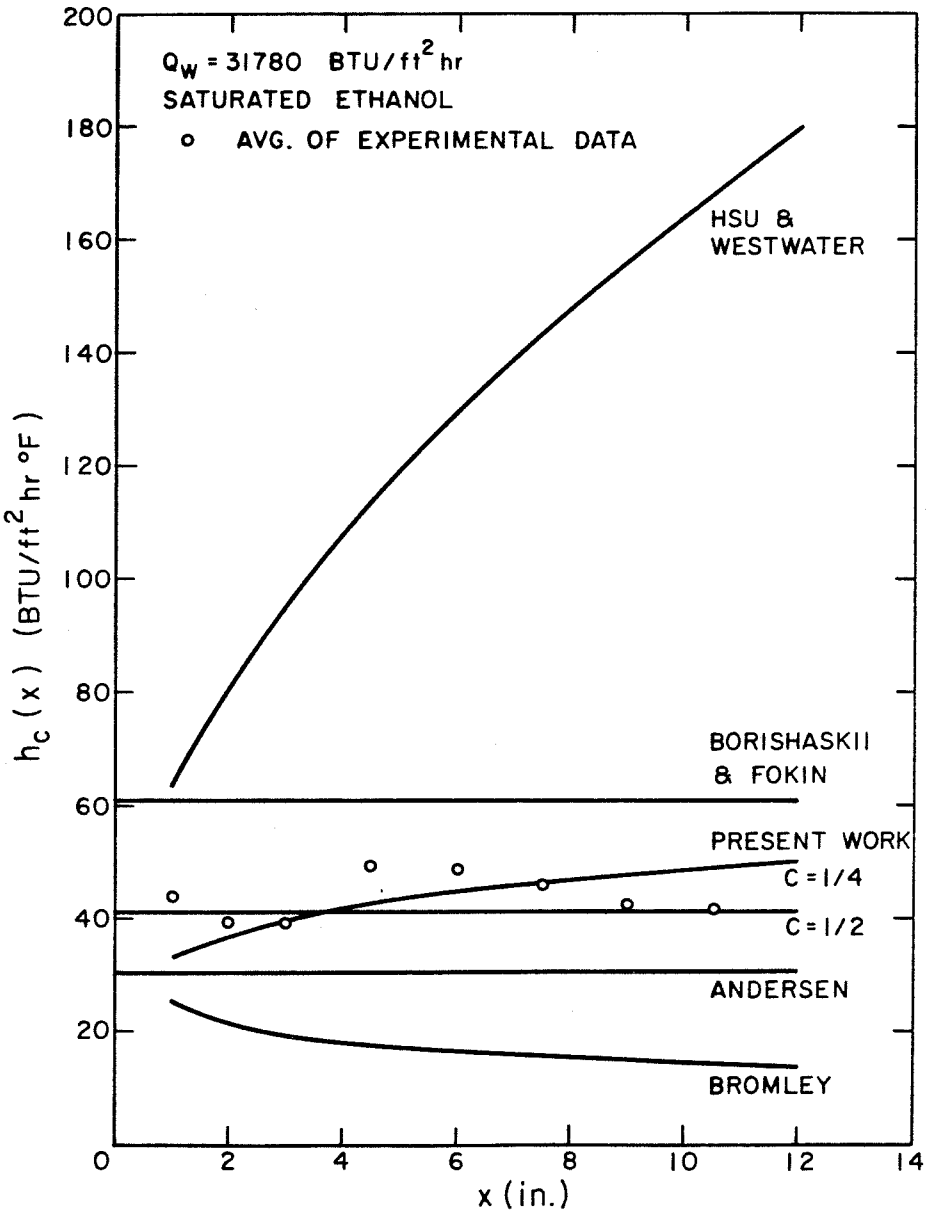

Figure 11. Convective Heat Transfer Coefficient vs. Vertical Position for Free Convection Film Boiling of Saturated Ethanol on a Vertical Cylinder

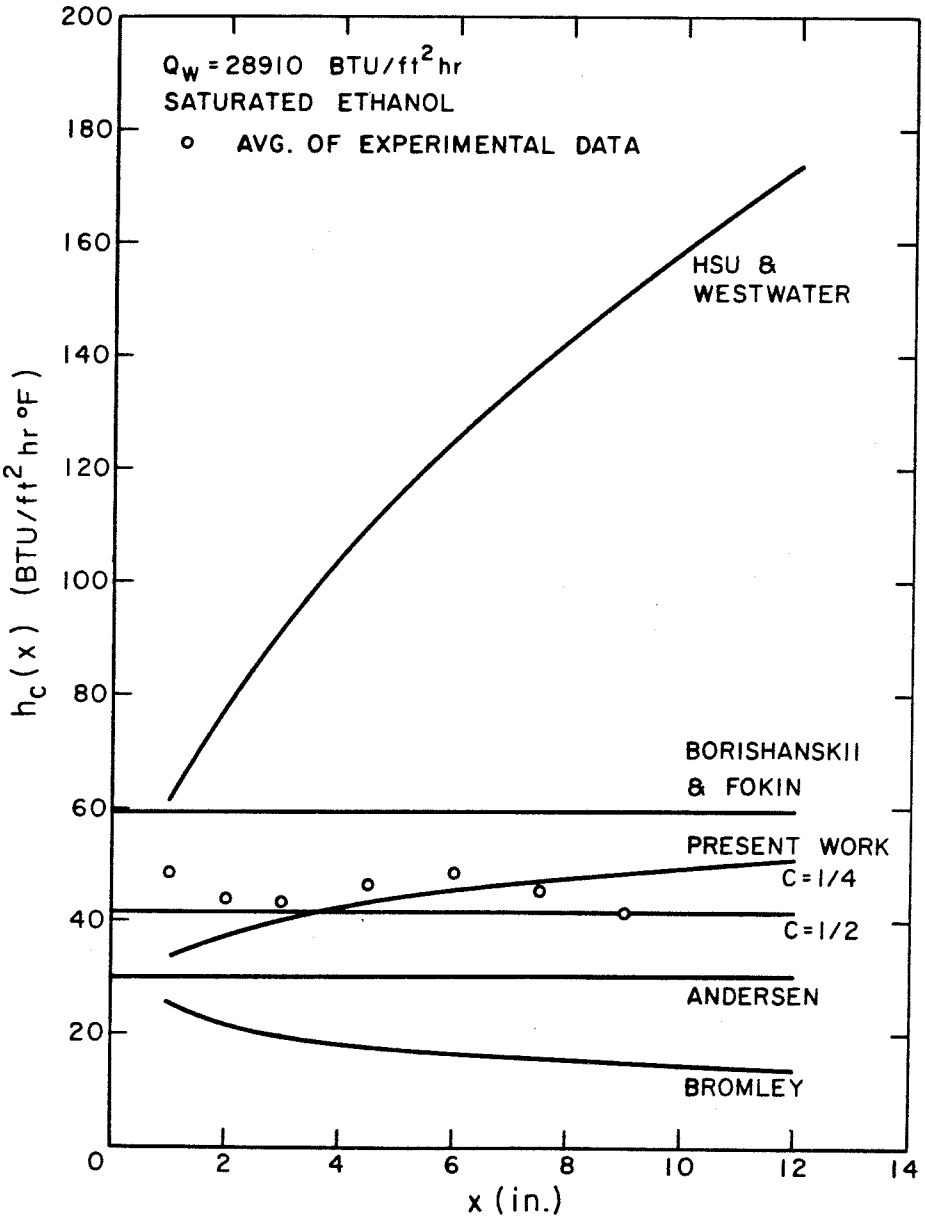

Figure 12. Convective Heat Transfer Coefficient vs. Vertical Position for Free Convection Film Boiling of Saturated Ethanol on a Vertical Cylinder

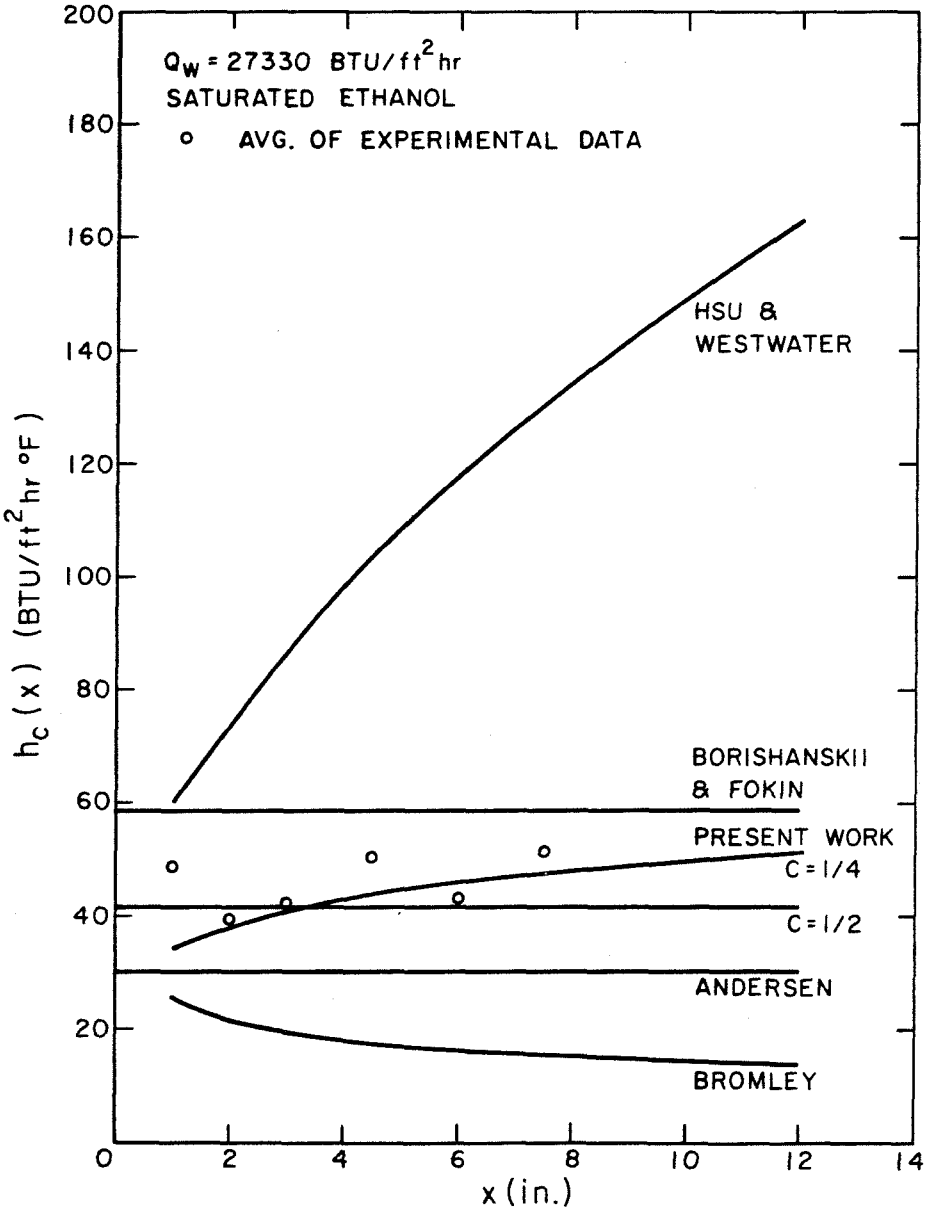

Figure 13. Convective Heat Transfer Coefficient vs. Vertical Position for Free Convection Film Boiling of Saturated Ethanol on a Vertical Cylinder

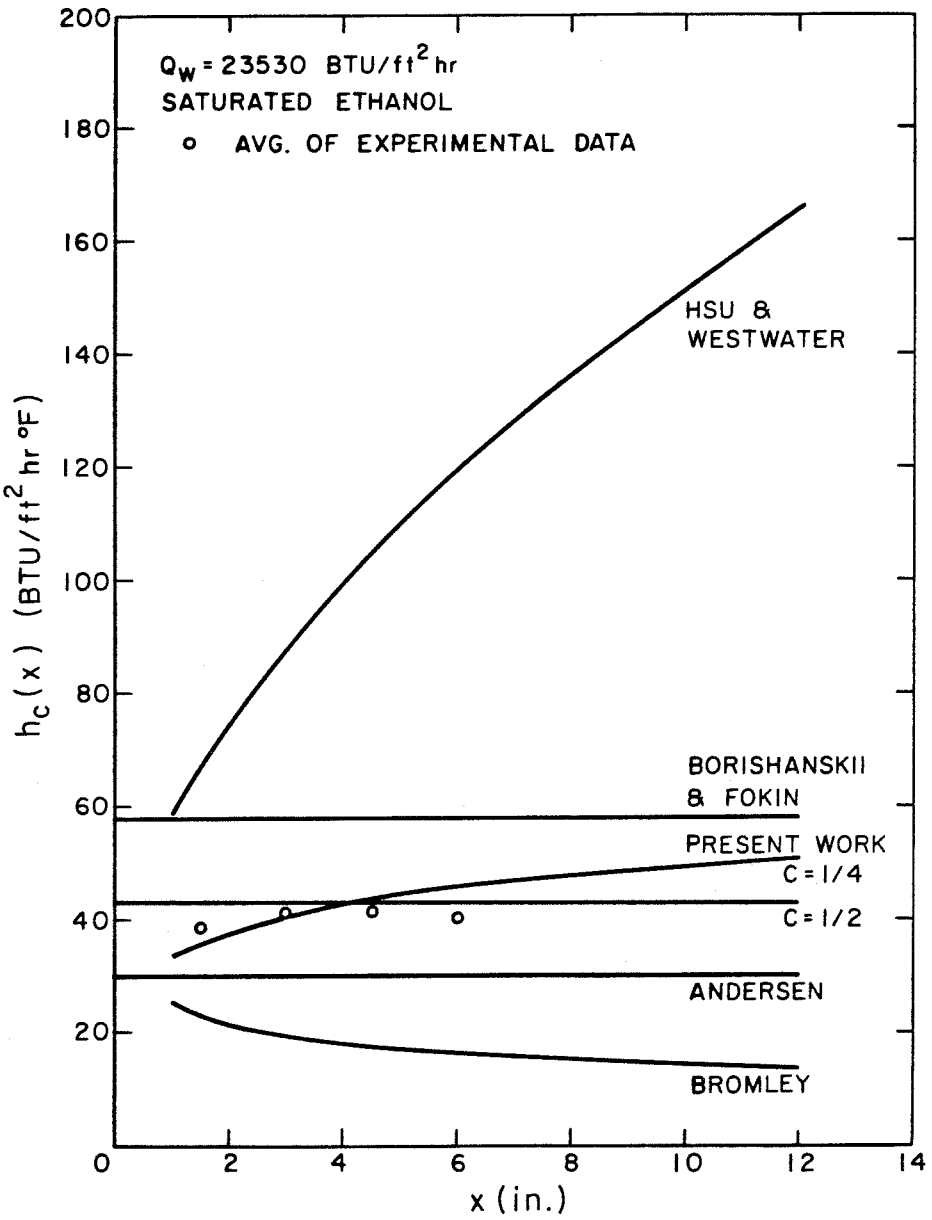

Figure 14. Convective Heat Transfer Coefficient vs. Vertical Position for Free Convection Film Boiling of Saturated Ethanol on a Vertical Cylinder

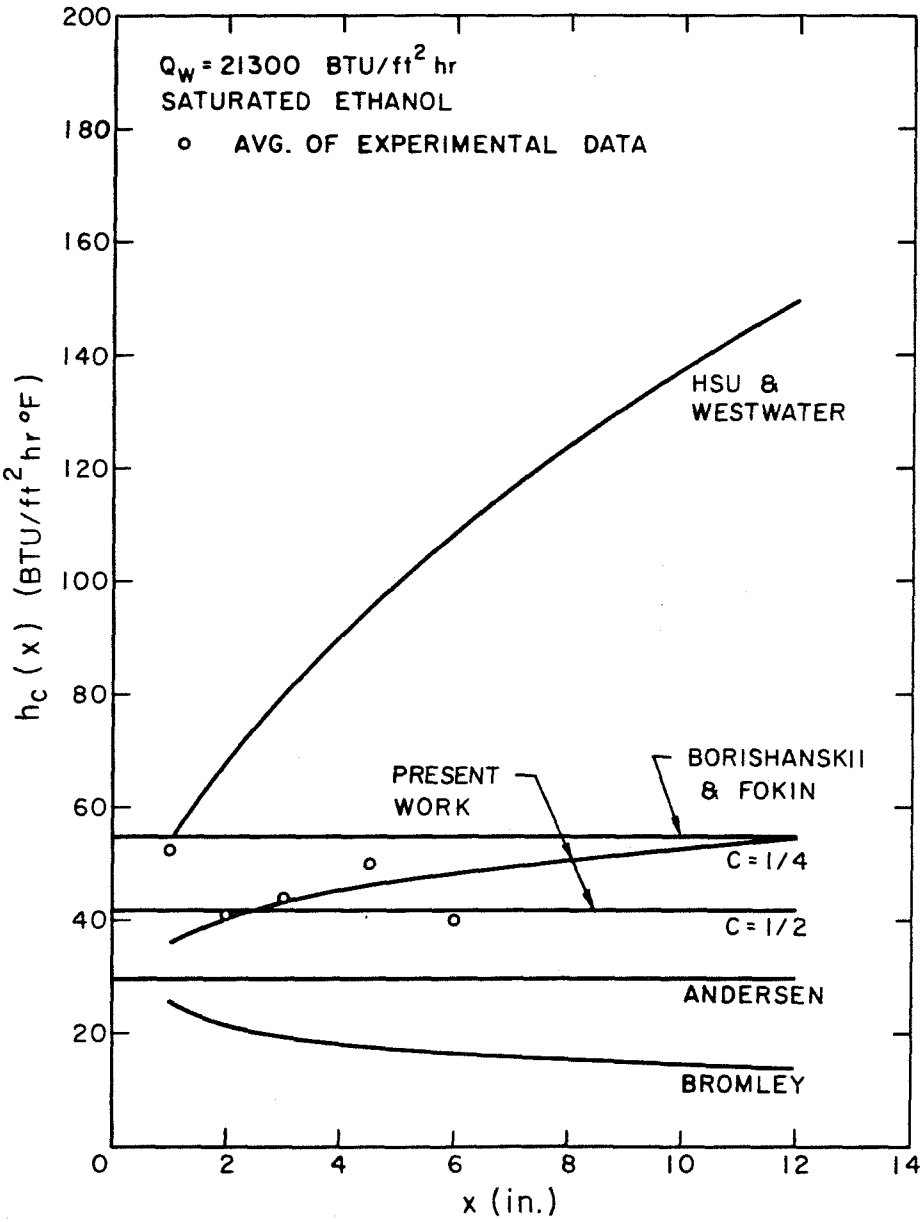

Figure 15. Convective Heat Transfer Coefficient vs. Vertical Position for Free Convection Film Boiling of Saturated Ethanol on a Vertical Cylinder

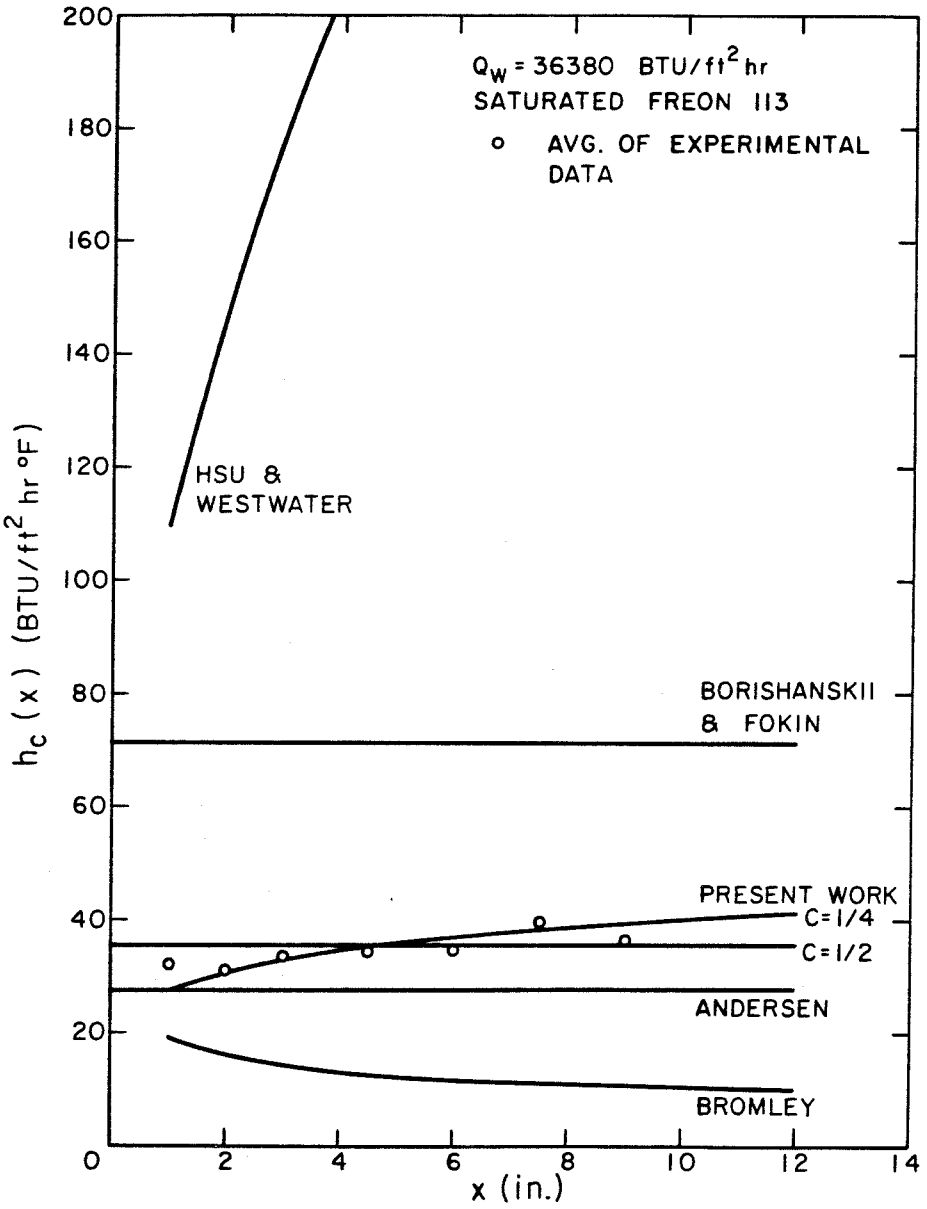

Figure 16. Convective Heat Transfer Coefficient vs. Vertical Position for Free Convection Film Boiling of Saturated Freon 113 on a Vertical Cylinder

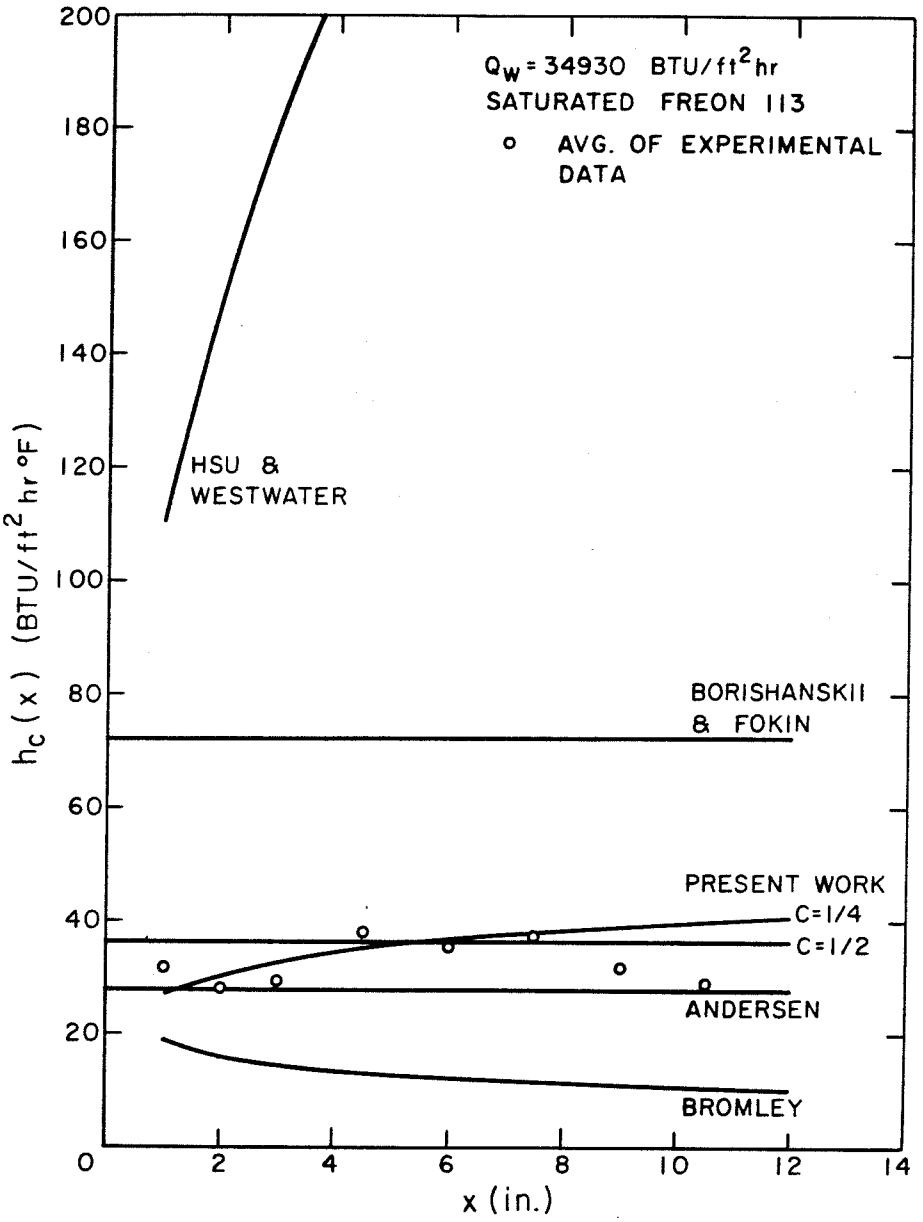

Figure 17. Convective Heat Transfer Coefficient vs. Vertical Position for Free Convection Film Boiling of Saturated Freon 113 on a Vertical Cylinder

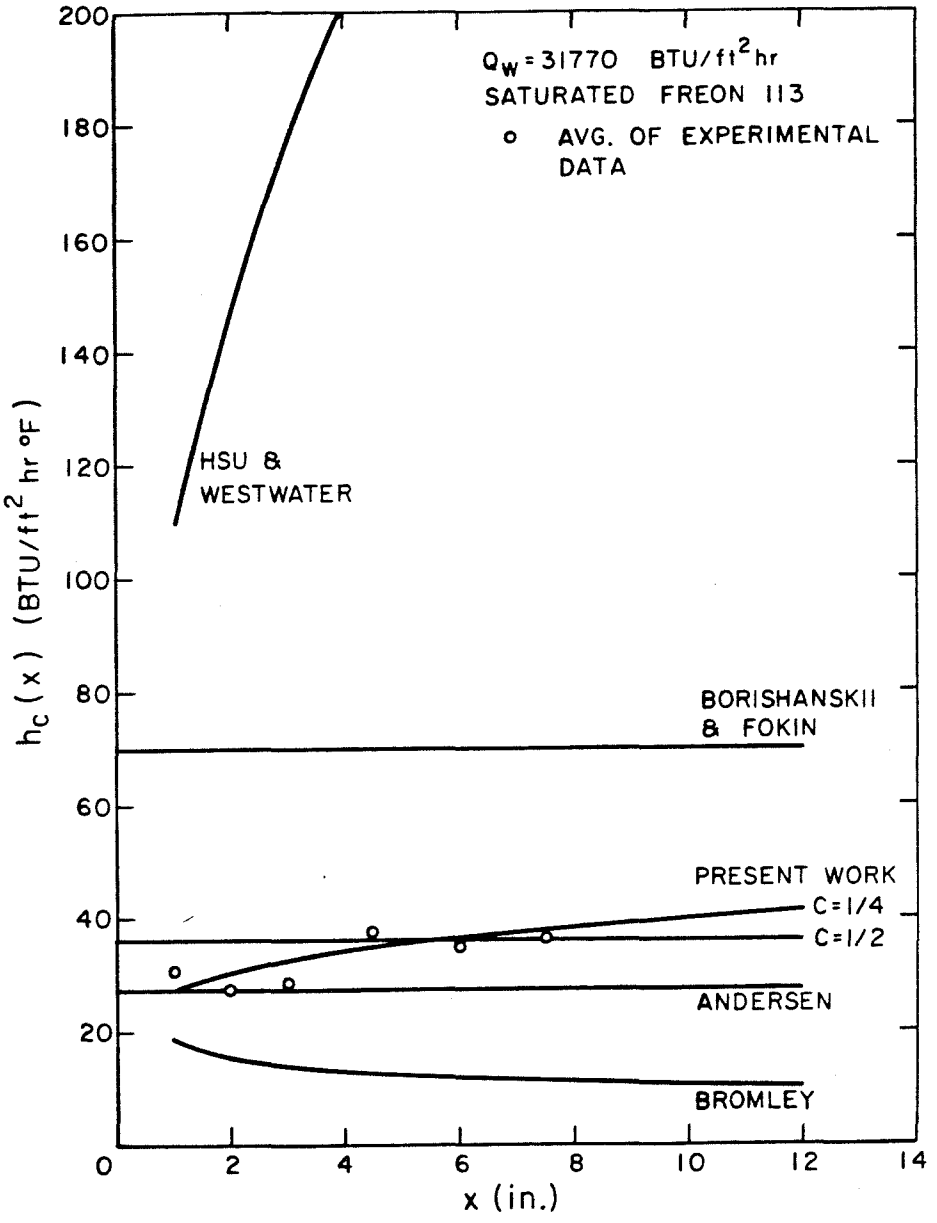

Figure 18. Convective Heat Transfer Coefficient vs. Vertical Position for Free Convection Film Boiling of Saturated Freon 113 on a Vertical Cylinder

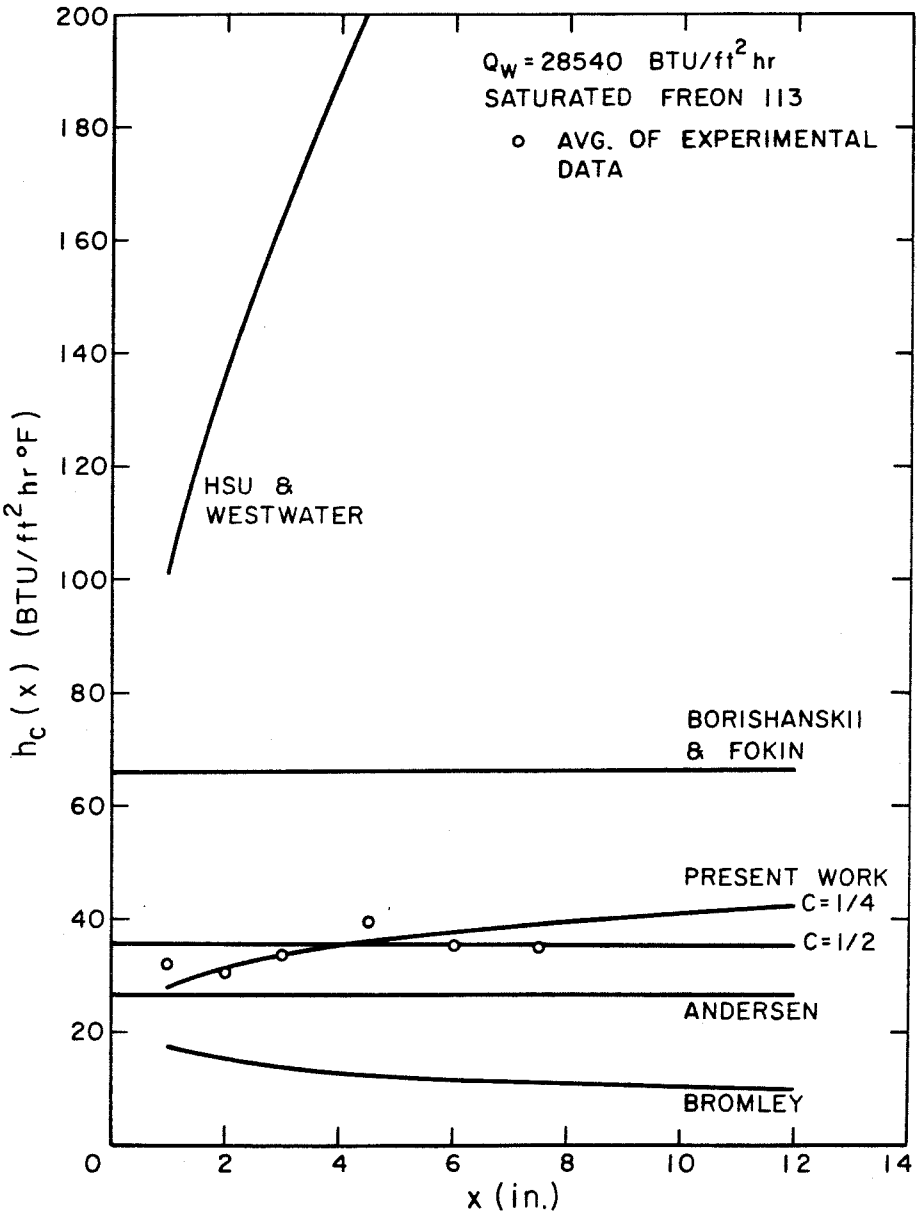

Figure 19. Convective Heat Transfer Coefficient vs. Vertical Position for Free Convection Film Boiling of Saturated Freon 113 on a Vertical Cylinder

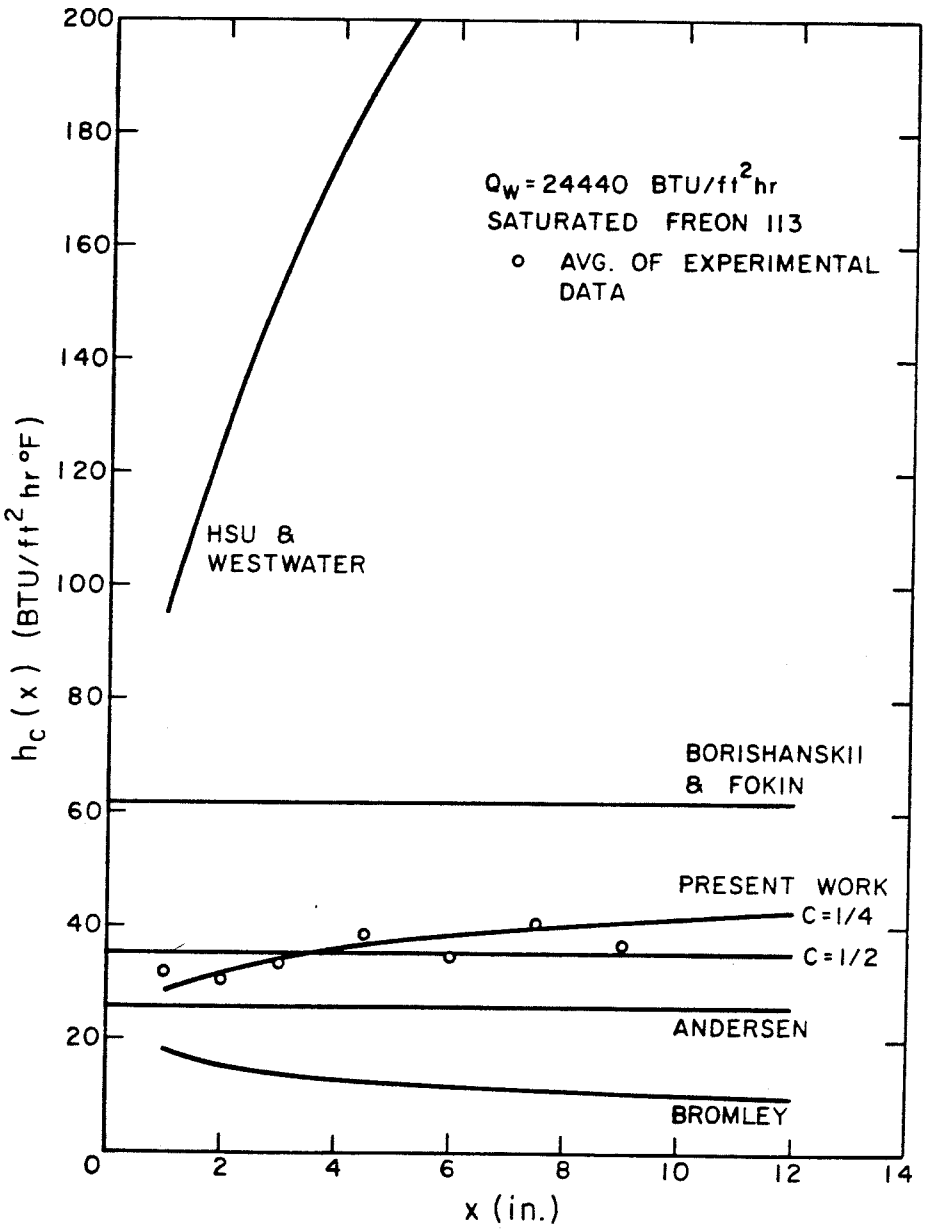

Figure 20. Convective Heat Transfer Coefficient vs. Vertical Position for Free Convection Film Boiling of Saturated Freon 113 on a Vertical Cylinder

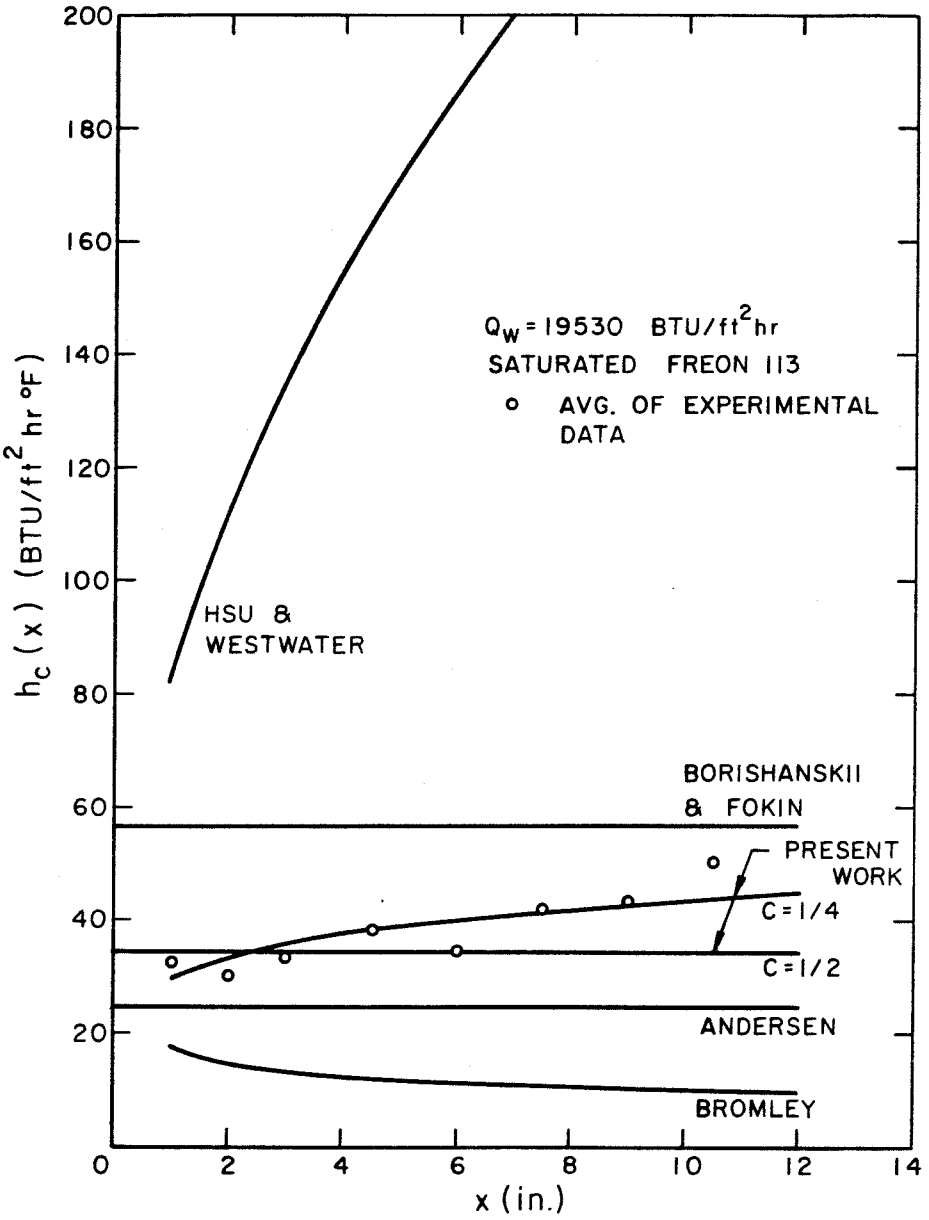

Figure 21. Convective Heat Transfer Coefficient vs. Vertical Position for Free Convection Film Boiling of Saturated Freon 113 on a Vertical Cylinder

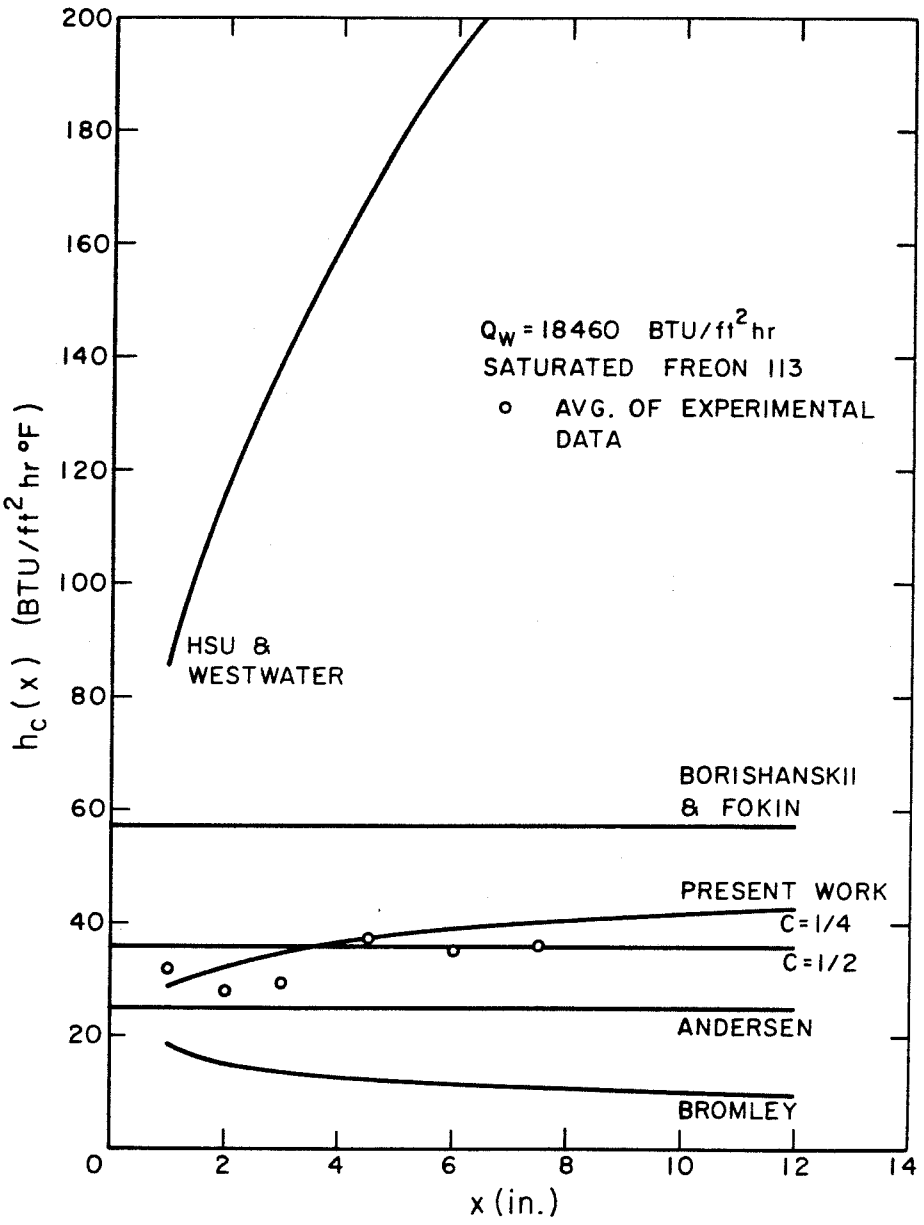

Figure 22. Convective Heat Transfer Coefficient vs. Vertical Position for Free Convection Film Boiling of Saturated Freon 113 on a Vertical Cylinder

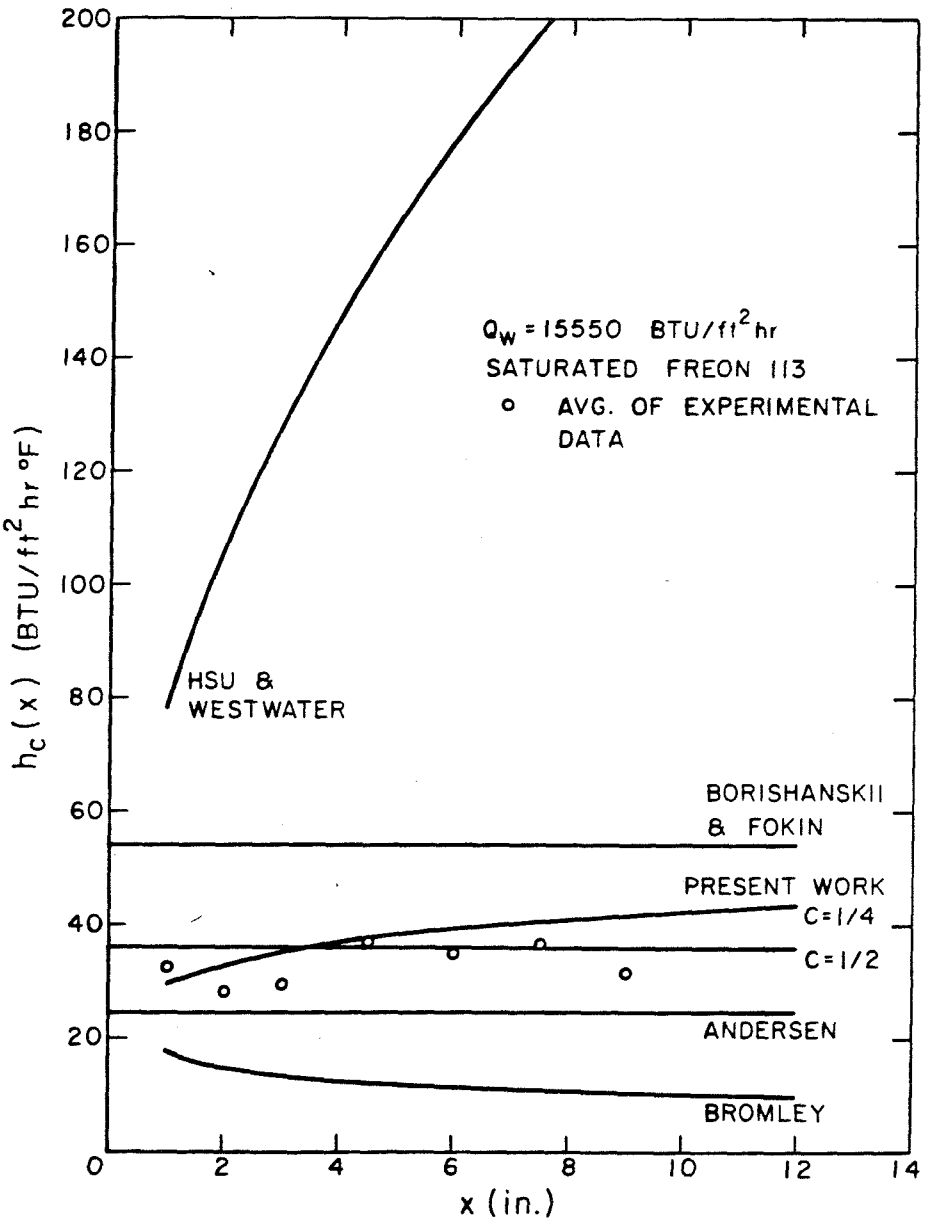

Figure 23. Convective Heat Transfer Coefficient vs. Vertical Position for Free Convection Film Boiling of Saturated Freon 113 on a Vertical Cylinder

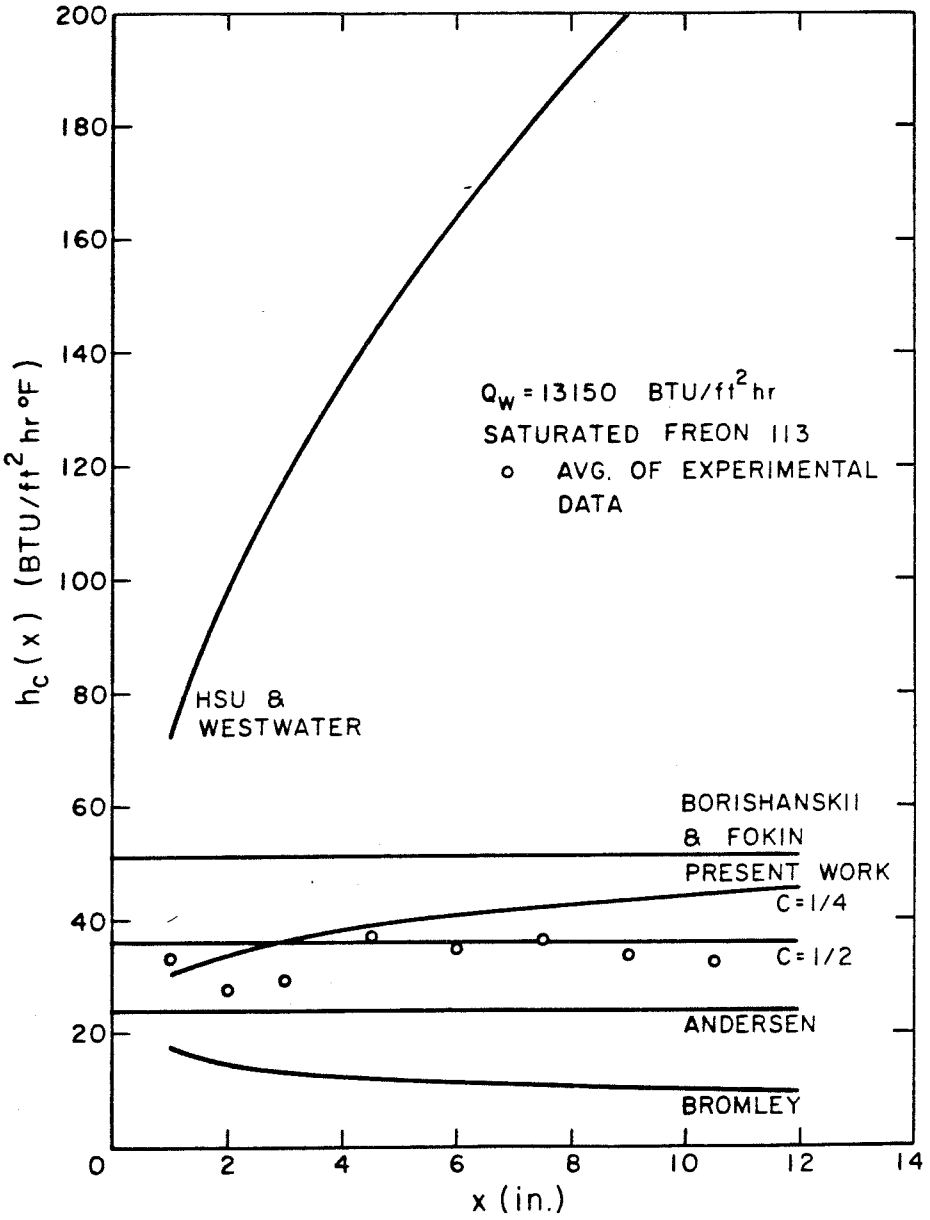

Figure 24. Convective Heat Transfer Coefficient vs. Vertical Position for Free Convection Film Boiling of Saturated Freon 113 on a Vertical Cylinder

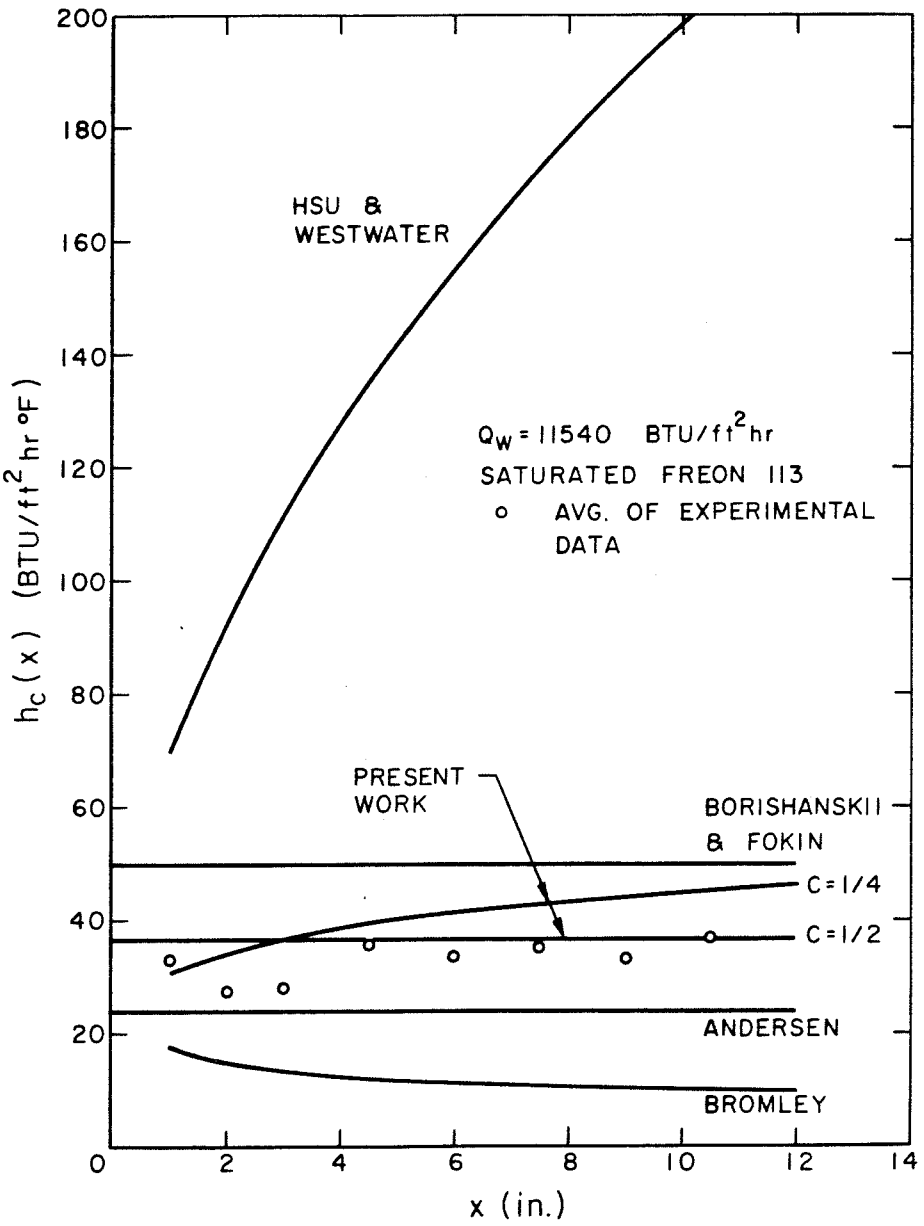

Figure 25. Convective Heat Transfer Coefficient vs. Vertical Position for Free Convection Film Boiling of Saturated Freon 113 on a Vertical Cylinder

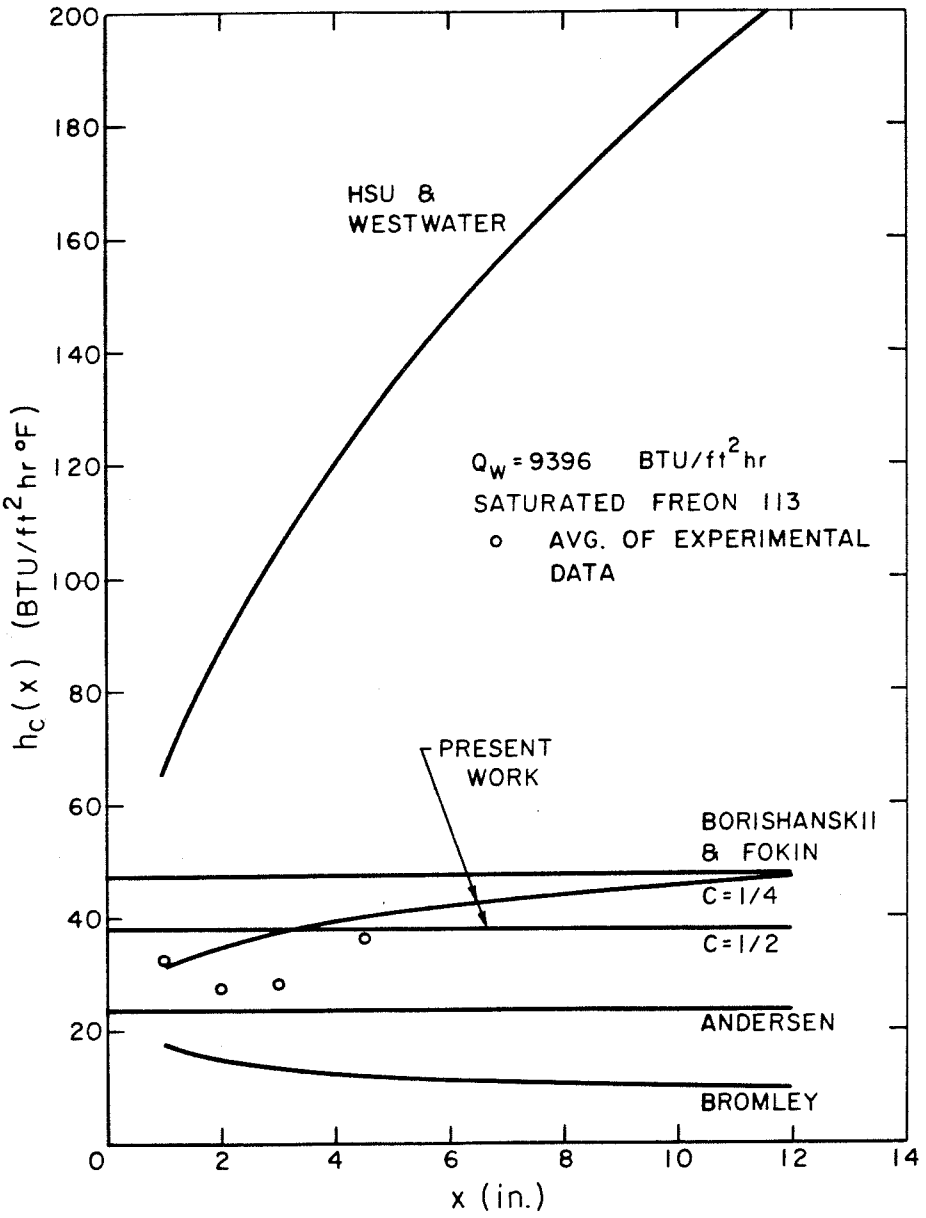

Figure 26. Convective Heat Transfer Coefficient vs. Vertical Position for Free Convection Film Boiling of Saturated Freon 113 on a Vertical Cylinder

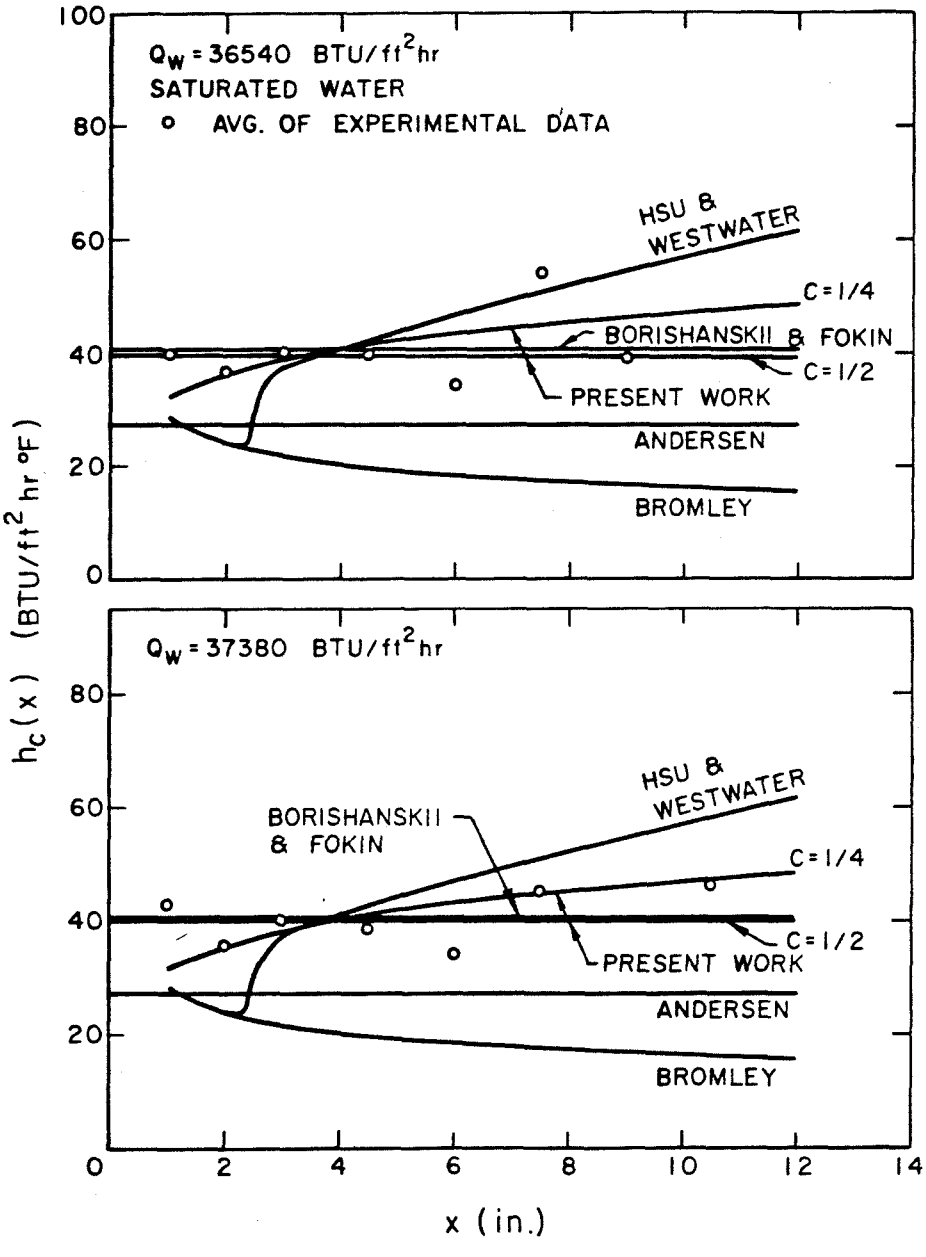

Figure 27. Convective Heat Transfer Coefficient vs. Vertical Position for Free Convection Film Boiling of Saturated Distilled Water on a Vertical Cylinder

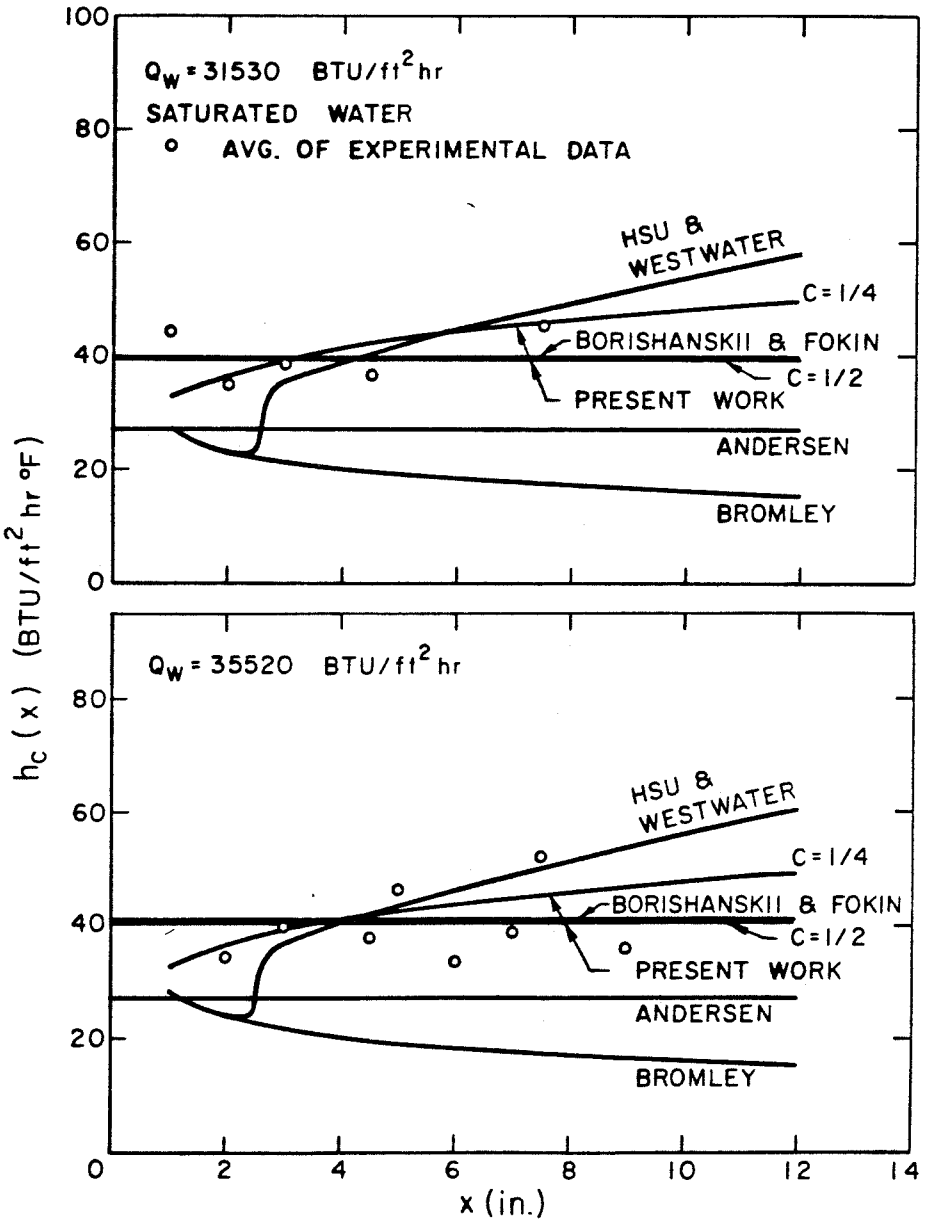

Figure 28. Convective Heat Transfer Coefficient vs. Vertical Position for Free Convection Film Boiling of Saturated Distilled Water on a Vertical Cylinder

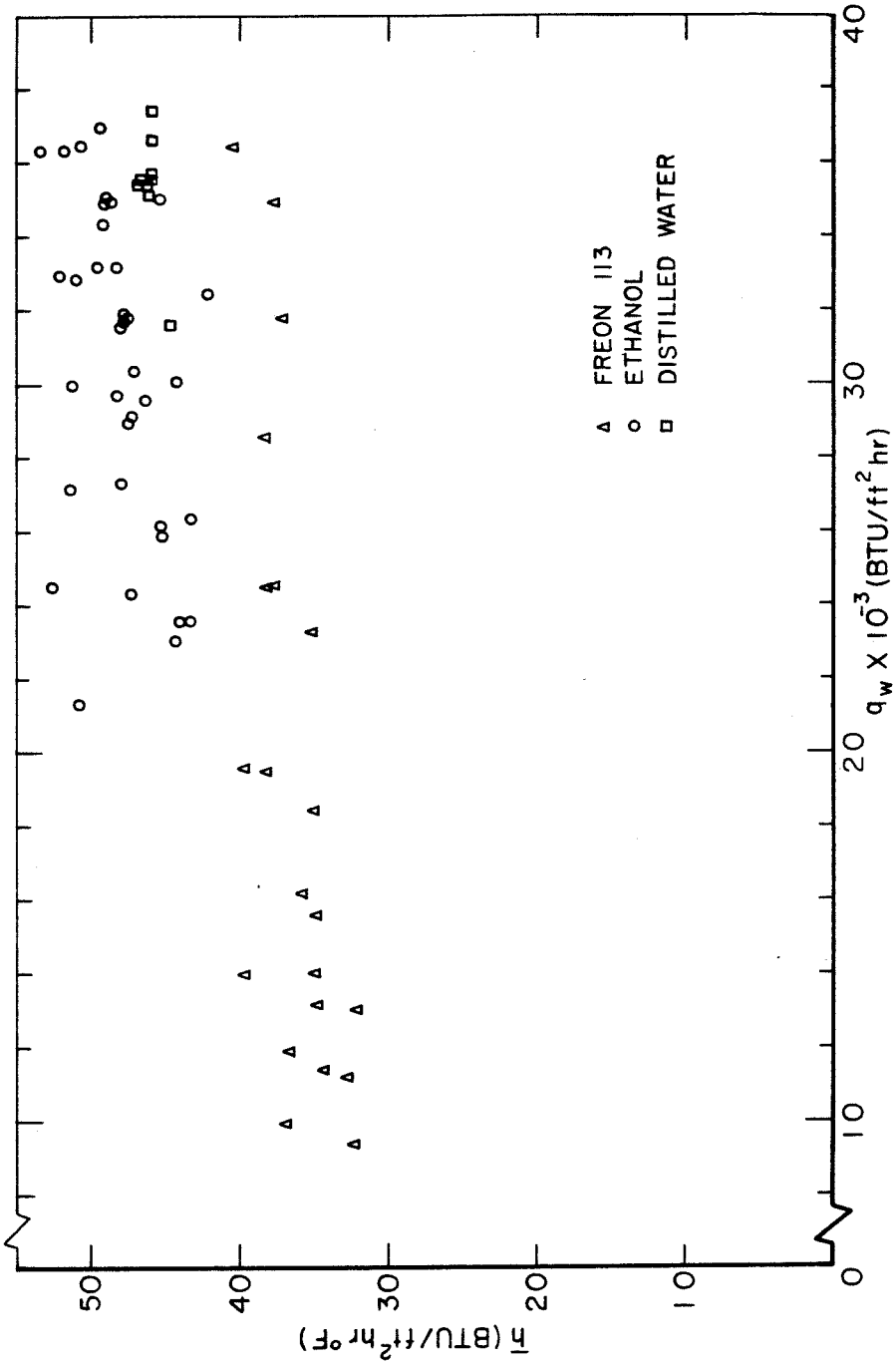

Figure 29. Average Convective Heat Transfer Coefficient vs. Wall Heat Flux for Free Convection Film Boiling of Three Saturated Liquids on a Vertical Cylinder

TABLE 3

Convective Heat Transfer Coefficient and Film Boiling Number Calculated from Eq. 96 and Experimentally Determined Values for Saturated Ethanol

Q_w $\left(\frac{BTU}{hr\ ft^2}\right)$	x (inches)	T_w (^oF)	$h_{c_{EXP}}$ $\left(\frac{BTU}{hr\ ft^2\ ^oF}\right)$	h_c[Eq 96] $\left(\frac{BTU}{hr\ ft^2\ ^oF}\right)$	$N_{FB_{EXP}}$	N_{FB}[Eq 96]	$\frac{N_{FB_{EXP}}}{N_{FB}[Eq\ 96]}$
35010	1.5	962	39.3	34.2	1.74	1.52	1.15
	3.0	923	41.9	39.0	1.87	1.74	1.07
32440	1.5	914	39.1	34.5	1.74	1.54	1.13
	3.0	879	41.5	39.3	1.86	1.76	1.06
30080	1.5	873	38.6	34.6	1.73	1.55	1.11
	3.0	837	41.2	39.6	1.85	1.78	1.04
26340	1.5	794	38.6	35.2	1.75	1.59	1.10
	3.0	766	40.8	40.1	1.86	1.82	1.02
23530	1.5	730	38.9	35.7	1.78	1.84	1.09
	3.0	703	41.2	40.7	1.90	1.87	1.01
34860	4.5	890	44.1	42.3	1.97	1.89	1.04
	6.06	914	42.4	44.0	1.89	1.96	0.96
	7.44	848	47.5	46.9	2.13	2.11	1.01
31550	4.5	836	43.5	42.7	1.96	1.92	1.02
	6.06	859	41.7	44.4	1.87	1.99	0.94
	7.44	793	47.1	47.4	2.13	2.14	0.99
29170	4.5	794	43.2	43.0	1.95	1.94	1.00
	6.06	817	41.3	44.7	1.86	2.02	0.93
	7.44	764	45.8	47.5	2.08	2.16	0.96
25880	4.5	731	43.0	43.6	1.97	1.99	0.99
	6.06	758	40.7	45.1	1.85	2.05	0.90
23040	4.5	676	42.8	44.1	1.98	2.04	0.97
	6.06	709	39.7	45.5	1.83	2.09	0.87
34980	4.5	909	42.9	42.0	1.91	1.87	1.02

Q_w $\frac{BTU}{hr\ ft^2}$	x (inches)	T_w (^oF)	$h_{c_{EXP}}$ $\frac{BTU}{hr\ ft^2\ ^oF}$	h_c[Eq 96] $\frac{BTU}{hr\ ft^2\ ^oF}$	$N_{FB_{EXP}}$	N_{FB}[Eq 96]	$\frac{N_{FB_{EXP}}}{N_{FB}[Eq\ 96]}$
34980	6.0	918	42.2	43.9	1.88	1.96	0.96
	7.5	841	48.2	47.2	2.17	2.12	1.02
31960	4.5	870	41.5	42.1	1.86	1.89	0.99
	6.0	874	41.2	44.1	1.85	1.98	0.93
	7.5	808	46.4	47.2	2.10	2.13	0.98
29540	4.5	826	41.2	42.4	1.86	1.91	0.97
	6.0	830	40.9	44.4	1.84	2.00	0.92
	7.5	773	45.6	47.4	2.07	2.15	0.96
26140	4.5	749	41.9	43.2	1.91	1.97	0.97
	6.0	764	40.6	45.0	1.85	2.04	0.90
	7.5	731	43.5	47.5	1.99	2.18	0.91
23530	4.5	698	41.6	43.7	1.92	2.01	0.95
	6.0	714	40.2	45.4	1.85	2.09	0.89
34360	1.0	854	46.2	33.4	2.08	1.50	1.38
	2.0	920	41.2	36.4	1.84	1.62	1.13
	3.0	931	40.5	38.8	1.80	1.73	1.04
	4.5	858	45.9	42.8	2.06	1.92	1.07
	6.0	842	47.2	45.3	2.12	2.04	1.04
	7.5	845	47.0	46.9	2.11	2.11	1.00
	9.0	861	45.7	48.0	2.05	2.16	0.95
	10.5	854	46.2	49.4	2.08	2.22	0.94
31640	1.0	827	44.4	33.4	2.00	1.50	1.33
	2.0	884	40.0	36.5	1.79	1.63	1.10
	3.0	896	39.2	38.8	1.75	1.74	1.01
	4.5	813	45.5	43.2	2.05	1.95	1.05
	6.0	795	47.1	45.7	2.13	2.07	1.03

Q_w $\frac{BTU}{hr\ ft^2}$	x (inches)	T_w (^oF)	$h_{c_{EXP}}$ $\frac{BTU}{hr\ ft^2\ ^oF}$	h_c[Eq 96] $\frac{BTU}{hr\ ft^2\ ^oF}$	$N_{FB_{EXP}}$	N_{FB}[Eq 96]	$\frac{N_{FB_{EXP}}}{N_{FB}[Eq\ 96]}$
31640	7.5	795	47.1	47.5	2.13	2.14	0.99
	9.0	826	44.4	48.2	2.00	2.17	0.92
	10.5	825	44.5	49.4	2.01	2.23	0.90
34940	1.0	891	44.2	32.9	1.98	1.47	1.34
	2.0	953	39.8	36.0	1.77	1.66	1.10
	3.0	955	39.6	38.5	1.76	1.71	1.03
	4.5	852	47.2	43.1	2.12	1.94	1.10
	6.0	836	48.6	45.6	2.19	2.05	1.07
	7.5	863	46.4	46.7	2.08	2.09	0.99
	9.0	905	43.4	47.2	1.92	2.11	0.91
	10.5	878	45.2	48.0	2.02	2.20	0.92
31780	1.0	832	44.2	33.3	1.99	1.50	1.33
	2.0	890	39.8	36.4	1.78	1.63	1.09
	3.0	895	39.5	38.9	1.76	1.74	1.02
	4.5	799	46.9	43.5	2.12	1.97	1.08
	6.0	777	49.0	46.2	2.22	2.09	1.06
	7.5	809	46.1	47.2	2.08	2.13	0.98
	9.0	850	47.8	47.6	1.92	2.14	0.90
	10.5	861	41.9	48.6	1.88	2.18	0.86
28900	1.0	769	44.9	33.8	2.04	1.54	1.33
	2.0	829	40.0	36.9	1.80	1.66	1.09
	3.0	833	39.7	39.4	1.79	1.77	1.01
	4.5	746	47.0	44.0	2.14	2.01	1.07
	6.0	727	48.8	46.7	2.24	2.14	1.05
	7.5	759	45.8	47.6	2.08	2.17	0.96
	9.0	805	41.9	47.9	1.89	2.16	0.87

Q_w $\frac{BTU}{hr\ ft^2}$	x (inches)	T_w (^oF)	$h_{c_{EXP}}$ $\frac{BTU}{hr\ ft^2\ ^oF}$	h_c[Eq 96] $\frac{BTU}{hr\ ft^2\ ^oF}$	$N_{FB_{EXP}}$	N_{FB}[Eq 96]	$\frac{N_{FB_{EXP}}}{N_{FB}[Eq\ 96]}$
36880	1.0	940	43.2	32.5	1.92	1.45	1.33
	2.0	1017	38.1	35.5	1.88	1.56	1.07
	4.5	857	49.7	43.4	2.23	1.95	1.15
	6.0	932	43.8	44.0	1.95	1.96	0.99
	7.5	866	48.9	47.0	2.19	2.11	1.04
	9.0	904	45.8	47.7	2.05	2.13	0.96
33120	1.0	867	43.4	33.0	1.95	1.48	1.32
	2.0	945	38.0	35.8	1.69	1.59	1.06
	4.5	796	49.4	43.9	2.23	1.98	1.12
	6.0	872	43.0	44.4	1.93	1.99	0.97
	7.5	819	47.3	47.2	2.13	2.13	1.00
30380	1.0	802	44.4	33.6	2.01	1.52	1.32
	2.0	885	38.2	36.2	1.71	1.62	1.05
	4.5	743	49.8	44.5	2.28	2.03	1.12
	6.0	822	42.8	44.8	1.93	2.02	0.96
	7.5	835	41.8	46.2	1.88	2.08	0.90
36290	1.0	889	46.2	33.2	2.07	1.48	1.39
	2.0	972	40.2	36.0	1.78	1.59	1.12
	3.0	930	43.1	39.1	1.92	1.74	1.10
	4.5	829	51.3	43.8	2.31	1.97	1.17
	6.0	894	45.8	44.6	2.05	2.00	1.03
	7.5	827	51.5	47.8	2.32	2.15	1.08
	9.0	844	49.9	48.8	2.24	2.20	1.02
	10.5	796	54.4	51.3	2.46	2.32	1.06
32880	1.0	826	46.3	33.6	2.09	1.51	1.38
	2.0	900	40.6	36.4	1.82	1.63	1.12

Q_w $\frac{BTU}{hr\ ft^2}$	x (inches)	T_w (^oF)	$h_{c_{EXP}}$ $\frac{BTU}{hr\ ft^2\ ^oF}$	h_c[Eq 96] $\frac{BTU}{hr\ ft^2\ ^oF}$	$N_{FB_{EXP}}$	N_{FB}[Eq 96]	$\frac{N_{FB_{EXP}}}{N_{FB}[Eq\ 96]}$
32880	3.0	860	43.6	39.7	1.96	1.78	1.10
	4.5	778	50.7	44.2	2.30	2.01	1.15
	6.0	837	45.4	45.1	2.04	2.03	1.01
	7.5	775	51.0	48.2	2.31	2.19	1.06
36430	1.0	905	45.2	33.0	2.02	1.47	1.37
	2.0	986	39.5	35.8	1.75	1.58	1.10
	3.0	946	42.2	38.9	1.87	1.73	1.08
	4.5	833	51.1	43.8	2.30	1.97	1.17
	6.0	904	45.2	44.5	2.02	1.98	1.02
	7.5	832	51.2	47.7	2.31	2.15	1.07
	9.0	837	50.8	49.0	2.28	2.21	1.04
	10.5	883	46.9	49.3	2.10	2.21	0.95
33190	1.0	833	48.2	33.6	2.08	1.51	1.38
	2.0	924	39.4	36.1	1.76	1.61	1.09
	3.0	880	42.5	39.4	1.90	1.76	1.08
	4.5	782	50.8	44.2	2.30	2.00	1.15
	6.0	849	44.9	44.9	2.02	2.02	1.00
	7.5	786	50.4	48.0	2.28	2.18	1.05
29650	1.0	759	47.0	34.2	2.14	1.56	1.38
	2.0	854	39.3	36.6	1.76	1.84	1.07
	3.0	812	42.5	40.0	1.92	1.80	1.06
	4.5	725	50.4	44.7	2.31	2.05	1.13
	6.0	789	44.4	45.4	2.01	2.05	0.98
27330	1.0	698	48.9	34.9	2.25	1.61	1.40
	2.0	803	39.5	37.0	1.78	1.67	1.07
	3.0	765	42.6	40.4	1.94	1.83	1.05

Q_w $\frac{BTU}{hr\ ft^2}$	x (inches)	T_w (^oF)	$h_{c_{EXP}}$ $\frac{BTU}{hr\ ft^2\ ^oF}$	h_c[Eq 96] $\frac{BTU}{hr\ ft^2\ ^oF}$	$N_{FB_{EXP}}$	N_{FB}[Eq 96]	$\frac{N_{FB_{EXP}}}{N_{FB}[Eq\ 96]}$
27330	4.5	682	50.6	45.2	2.34	2.09	1.12
	6.0	756	43.3	45.5	1.97	2.07	0.95
24310	1.0	617	52.0	36.0	2.44	1.69	1.45
	2.0	736	39.8	37.6	1.82	1.72	1.06
	3.0	702	42.8	41.0	1.97	1.89	1.04
	4.5	632	50.2	45.8	2.34	2.14	1.10
21300	2.0	658	41.0	38.5	1.90	1.79	1.07
	3.0	626	44.3	42.0	2.07	1.97	1.05
	4.5	578	50.1	46.6	2.37	2.20	1.07
36300	1.0	889	46.2	33.2	2.07	1.48	1.39
	2.0	968	40.5	36.0	1.80	1.60	1.12
	3.0	909	44.7	39.5	1.99	1.76	1.13
	4.5	823	51.8	44.0	2.34	1.98	1.18
	6.0	872	47.6	45.1	2.13	2.02	1.06
	7.5	791	55.0	48.7	2.49	2.20	1.13
	9.0	803	53.8	49.8	2.43	2.25	1.08
	10.5	778	56.3	51.8	2.55	2.35	1.09
32970	1.0	830	46.1	33.6	2.08	1.51	1.37
	2.0	898	40.9	36.5	1.83	1.63	1.12
	3.0	838	45.5	40.2	2.04	1.81	1.13
	4.5	763	52.3	44.6	2.38	2.03	1.17
	6.0	813	47.6	45.6	2.15	2.06	1.04
	7.5	724	56.5	49.6	2.59	2.27	1.14
	9.0	774	51.2	49.8	2.32	2.26	1.03
29930	1.0	764	47.0	34.1	2.14	1.55	1.38
	2.0	823	42.0	37.2	1.90	1.68	1.13
	3.0	774	46.1	40.8	2.09	1.85	1.13

Q_w $\frac{BTU}{hr\ ft^2}$	x (inches)	T_w (^oF)	$h_{c_{EXP}}$ $\frac{BTU}{hr\ ft^2\ ^oF}$	h_c[Eq 96] $\frac{BTU}{hr\ ft^2\ ^oF}$	$N_{FB_{EXP}}$	N_{FB}[Eq 96]	$\frac{N_{FB_{EXP}}}{N_{FB}[Eq\ 96]}$
29930	4.5	717	51.7	45.0	2.37	2.06	1.15
	6.0	771	46.4	45.8	2.11	2.08	1.01
	7.5	678	56.2	50.1	2.60	2.32	1.12
27180	1.0	693	49.1	34.9	2.26	1.61	1.41
	2.0	759	42.8	37.8	1.95	1.72	1.13
	3.0	702	48.2	41.7	2.22	1.92	1.15
	4.5	666	52.2	45.6	2.42	2.12	1.14
	6.0	719	46.5	46.4	2.13	2.13	1.00
	7.5	669	51.8	49.6	2.40	2.30	1.04
24440	1.0	616	52.5	36.1	2.45	1.69	1.46
	2.0	674	45.8	39.0	2.12	1.80	1.17
	3.0	622	51.7	43.1	2.42	2.02	1.20
	4.5	611	53.1	46.5	2.49	2.18	1.14
	6.0	660	47.2	47.2	2.19	2.19	1.00

TABLE 4

Convective Heat Transfer Coefficient and Film Boiling Number Calculated from Eq. 96 and Experimentally Determined Values for Saturated Freon 113

Q_w $\frac{BTU}{hr\ ft^2}$	x (inches)	T_w (^oF)	$h_{c_{EXP}}$ $\frac{BTU}{hr\ ft^2\ ^oF}$	h_c[Eq 96] $\frac{BTU}{hr\ ft^2\ ^oF}$	$N_{FB_{EXP}}$	N_{FB}[Eq 96]	$\frac{N_{FB_{EXP}}}{N_{FB}[Eq\ 96]}$
36380	1.0	1074	32.2	26.9	1.60	1.33	1.20
	2.0	1096	31.2	30.0	1.54	1.49	1.04
	3.0	1042	33.8	32.7	1.67	1.62	1.04
	4.5	939	39.6	36.2	1.95	1.78	1.09
	6.0	1022	34.9	36.9	1.72	1.82	0.94
	7.5	938	39.7	39.4	1.96	1.94	1.01
	9.0	989	36.7	39.9	1.81	1.97	0.92
14020	1.0	495	35.2	30.4	1.72	1.48	1.16
	2.0	502	34.5	34.0	1.68	1.66	1.02
	3.0	452	40.2	38.1	1.96	1.86	1.06
	4.5	445	41.1	41.0	2.01	2.00	1.00
	6.0	488	35.9	41.3	1.75	2.01	0.87
	7.5	433	42.8	45.2	2.09	2.21	0.95
19480	1.0	666	32.7	28.6	1.60	1.40	1.14
	2.0	677	32.0	32.0	1.56	1.56	1.00
	3.0	624	35.9	35.2	1.75	1.72	1.02
	4.5	572	40.6	39.0	1.98	1.90	1.04
	6.0	628	35.6	39.5	1.74	1.93	0.90
	7.5	595	38.4	41.8	1.88	2.04	0.92
24540	1.0	801	32.3	27.9	1.58	1.37	1.16
	2.0	817	31.4	31.1	1.54	1.53	1.01
	3.0	764	34.6	34.0	1.70	1.67	1.02
	4.5	682	40.6	37.9	1.98	1.85	1.07
	6.0	769	34.3	38.1	1.68	1.87	0.90

Q_w $\frac{BTU}{hr\ ft^2}$	x (inches)	T_w (^oF)	$h_{c_{EXP}}$ $\frac{BTU}{hr\ ft^2\ ^oF}$	h_c[Eq 96] $\frac{BTU}{hr\ ft^2\ ^oF}$	$N_{FB_{EXP}}$	N_{FB}[Eq 96]	$\frac{N_{FB_{EXP}}}{N_{FB}[Eq\ 96]}$
19530	1.0	667	32.8	28.6	1.80	1.40	1.14
	2.0	705	30.2	31.5	1.48	1.54	0.96
	3.0	654	33.7	34.6	1.65	1.69	0.97
	4.5	600	38.0	38.3	1.86	1.87	0.99
	6.0	640	34.7	39.2	1.70	1.92	0.89
	7.5	561	41.8	42.8	2.04	2.09	0.98
	9.0	545	43.5	44.6	2.12	2.18	0.98
	10.5	490	50.5	47.8	2.46	2.33	1.06
24440	1.0	807	31.8	27.8	1.56	1.36	1.14
	2.0	835	30.2	30.8	1.48	1.52	0.98
	3.0	780	33.4	33.8	1.64	1.66	0.99
	4.5	702	38.8	37.5	1.90	1.83	1.04
	6.0	756	35.0	38.3	1.71	1.88	0.91
	7.5	677	40.8	41.4	2.00	2.02	0.99
	9.0	729	36.8	41.5	1.80	2.03	0.89
28540	1.0	897	32.3	27.5	1.59	1.35	1.17
	2.0	926	30.8	30.5	1.52	1.50	1.01
	3.0	871	33.8	33.4	1.66	1.64	1.01
	4.5	776	39.9	37.2	1.96	1.82	1.07
	6.0	843	35.4	37.9	1.74	1.86	0.94
	7.5	850	35.0	39.2	1.72	1.93	0.89
13960	1.0	546	30.4	29.2	1.48	1.43	1.04
	2.0	548	30.3	32.8	1.48	1.60	0.92
	3.0	495	35.0	36.5	1.71	1.78	0.96
	4.5	453	39.9	40.6	1.95	1.98	0.98
	6.0	516	33.0	40.3	1.61	1.97	0.82

Q_w $\frac{BTU}{hr\ ft^2}$	x (inches)	T_w (^oF)	$h_{c_{EXP}}$ $\frac{BTU}{hr\ ft^2\ ^oF}$	h_c[Eq 96] $\frac{BTU}{hr\ ft^2\ ^oF}$	$N_{FB_{EXP}}$	N_{FB}[Eq 96]	$\frac{N_{FB_{EXP}}}{N_{FB}[Eq\ 96]}$
11860	1.0	469	31.9	30.3	1.56	1.48	1.05
	2.0	471	31.7	33.8	1.55	1.66	0.93
	3.0	420	37.6	38.3	1.84	1.87	0.98
	4.5	400	40.4	41.9	1.98	2.05	0.96
9951	1.0	392	34.7	32.0	1.70	1.56	1.08
	2.0	391	34.9	36.0	1.70	1.76	0.97
	3.0	340	43.4	41.4	2.12	2.03	1.05
	4.5	347	42.0	43.8	2.06	2.14	0.96
34930	1.0	1050	31.9	27.0	1.58	1.33	1.18
	2.0	1132	28.0	29.5	1.39	1.46	0.95
	3.0	1100	29.5	31.8	1.46	1.58	0.93
	4.5	934	38.2	36.0	1.88	1.78	1.06
	6.0	981	35.5	37.2	1.75	1.83	0.95
	7.5	945	37.5	39.1	1.85	1.93	0.96
	9.0	1050	31.9	38.9	1.58	1.92	0.82
	10.5	1109	29.1	39.1	1.44	1.94	0.74
31770	1.0	1002	30.8	27.0	1.52	1.33	1.14
	2.0	1073	27.4	29.6	1.36	1.46	0.93
	3.0	1044	28.8	31.9	1.42	1.58	0.90
	4.5	878	37.6	36.2	1.85	1.78	1.04
	6.0	922	35.0	37.4	1.72	1.84	0.94
	7.5	898	36.4	39.2	1.79	1.93	0.93
23240	1.0	786	31.2	27.8	1.53	1.36	1.12
	2.0	848	27.9	30.4	1.37	1.50	0.92
	3.0	824	29.1	32.9	1.43	1.62	0.89
	4.5	694	37.4	37.3	1.83	1.83	1.00
	6.0	738	34.2	38.3	1.68	1.88	0.89

Q_w $\frac{BTU}{hr\ ft^2}$	x (inches)	T_w (^oF)	$h_{c_{EXP}}$ $\frac{BTU}{hr\ ft^2\ ^oF}$	h_c[Eq 96] $\frac{BTU}{hr\ ft^2\ ^oF}$	$N_{FB_{EXP}}$	N_{FB}[Eq 96]	$\frac{N_{FB_{EXP}}}{N_{FB}[Eq\ 96]}$
13180	1.0	517	31.0	29.6	1.51	1.44	1.05
	2.0	565	27.2	32.1	1.33	1.57	0.85
	3.0	553	28.1	34.6	1.37	1.69	0.81
	4.5	463	36.4	39.9	1.78	1.95	0.91
9396	1.0	394	32.4	31.6	1.58	1.54	1.03
	2.0	438	27.6	33.8	1.35	1.64	0.82
	3.0	431	28.3	36.4	1.38	1.78	0.78
	4.5	367	36.2	42.1	1.77	2.06	0.86
11260	1.0	440	33.2	30.9	1.62	1.51	1.07
	2.0	492	28.1	33.0	1.37	1.61	0.85
	3.0	484	28.8	35.6	1.41	1.74	0.81
	4.5	420	35.6	40.6	1.74	1.98	0.88
11540	1.0	450	32.9	30.7	1.61	1.50	1.07
	2.0	508	27.5	32.7	1.34	1.60	0.84
	3.0	499	28.3	35.3	1.38	1.72	0.80
	4.5	425	35.9	40.6	1.75	1.98	0.88
	6.0	443	33.7	41.7	1.65	2.04	0.81
	7.5	430	35.2	43.9	1.72	2.14	0.80
	9.0	447	33.3	44.5	1.62	2.17	0.75
	10.5	416	37.0	47.2	1.81	2.30	0.78
13150	1.0	491	33.3	30.2	1.62	1.47	1.10
	2.0	554	27.9	32.3	1.36	1.58	0.86
	3.0	537	29.2	35.0	1.43	1.71	0.84
	4.5	456	37.1	40.1	1.81	1.86	0.93
	6.0	475	34.9	41.3	1.70	2.02	0.85
	7.5	462	36.4	43.4	1.78	2.12	0.84
	9.0	488	33.6	43.7	1.64	2.13	0.77
	10.5	496	32.8	44.5	1.60	2.17	0.74

Q_w $\frac{BTU}{hr\ ft^2}$	x (inches)	T_w (^oF)	$h_{c_{EXP}}$ $\frac{BTU}{hr\ ft^2\ ^oF}$	h_c[E 96] $\frac{BTU}{hr\ ft^2\ ^oF}$	$N_{FB_{EXP}}$	N_{FB}[Eq 96]	$\frac{N_{FB_{EXP}}}{N_{FB}[Eq\ 96]}$
15550	1.0	561	32.8	29.4	1.60	1.44	1.11
	2.0	624	28.1	31.7	1.38	1.55	0.89
	3.0	608	29.2	34.3	1.43	1.68	0.85
	4.5	515	37.1	39.2	1.81	1.91	0.95
	6.0	536	35.0	40.4	1.71	1.97	0.87
	7.5	520	36.6	42.5	1.79	2.07	0.86
	9.0	575	31.7	42.1	1.55	2.06	0.75
18460	1.0	652	31.8	28.6	1.56	1.40	1.11
	2.0	712	28.0	31.1	1.37	1.52	0.80
	3.0	691	29.3	33.6	1.43	1.64	0.87
	4.5	586	37.0	38.3	1.81	1.87	0.97
	6.0	610	35.0	39.6	1.71	1.93	0.89
	7.5	599	35.9	41.3	1.76	2.02	0.87
16160	1.0	566	33.8	29.5	1.65	1.44	1.14
	2.0	619	29.7	32.0	1.45	1.56	0.93
	3.0	598	31.2	34.7	1.52	1.70	0.90
	4.5	502	40.1	39.8	1.96	1.94	1.01
	6.0	543	35.8	40.5	1.75	1.98	0.89

TABLE 5

Convective Heat Transfer Coefficient and Film Boiling Number Calculated from Eq. 96 and Experimentally Determined Values for Saturated Distilled Water

Q_w $\frac{BTU}{hr\ ft^2}$	x (inches)	T_w (^oF)	$h_{c_{EXP}}$ $\frac{BTU}{hr\ ft^2\ ^oF}$	h_c[Eq 96] $\frac{BTU}{hr\ ft^2\ ^oF}$	$N_{FB_{EXP}}$	N_{FB}[Eq 96]	$\frac{N_{FB_{EXP}}}{N_{FB}[Eq\ 96]}$
37380	1.0	982	43.1	32.6	3.87	2.78	1.32
	2.0	1095	35.8	34.7	3.08	2.99	1.03
	3.0	1021	40.4	38.5	3.45	3.29	1.05
	4.5	1060	37.9	40.4	3.25	3.46	0.94
	7.5	956	45.0	46.2	3.83	3.94	0.97
	10.5	938	46.4	49.4	3.94	4.20	0.94
31530	1.0	860	44.2	33.8	3.72	2.84	1.31
	2.0	990	35.0	35.5	2.98	3.02	0.99
	3.0	934	38.6	39.0	3.28	3.32	0.99
	4.5	964	36.6	41.1	3.12	3.50	0.89
	7.5	847	45.3	47.6	3.81	4.00	0.95
36540	1.0	1012	39.9	32.0	3.41	2.74	1.25
	2.0	1064	36.6	35.1	3.14	3.01	1.04
	3.0	1008	40.2	38.6	3.43	3.29	1.04
	4.5	1012	39.9	41.2	3.41	3.52	0.97
	6.0	1104	34.3	41.4	2.96	3.57	0.83
	7.5	838	54.1	49.0	4.54	4.12	1.10
	9.0	1025	39.1	45.9	3.34	3.92	0.85
35610	2.0	1082	34.5	34.6	2.97	2.98	1.00
	3.0	1016	38.5	38.2	3.29	3.27	1.01
	4.5	1025	37.9	40.7	3.24	3.48	0.93
	6.0	1095	33.8	41.4	2.91	3.56	0.82
	7.5	842	52.2	48.7	4.38	4.09	1.07
	9.0	1055	36.1	45.1	3.09	3.86	0.80

Q_w $\frac{BTU}{hr\ ft^2}$	x (inches)	T_w (^oF)	$h_{c_{EXP}}$ $\frac{BTU}{hr\ ft^2\ ^oF}$	h_c[Eq 96] $\frac{BTU}{hr\ ft^2\ ^oF}$	$N_{FB_{EXP}}$	N_{FB}[Eq 96]	$\frac{N_{FB_{EXP}}}{N_{FB}[Eq\ 96]}$
35430	3.0	986	40.3	38.8	3.43	3.30	1.04
	5.0	912	45.7	43.8	3.88	3.71	1.04
	7.0	1010	38.7	44.1	3.30	3.77	0.88
	3.0	964	41.8	39.2	3.56	3.34	1.07
	5.0	903	46.5	44.0	3.93	3.73	1.06
	7.0	1012	38.5	44.1	3.29	3.76	0.87
35080	3.0	986	39.8	38.7	3.39	3.30	1.03
	5.0	916	44.9	43.7	3.81	3.70	1.03
	7.0	1021	37.5	43.8	3.20	3.74	0.86
35490	3.0	1025	37.8	38.1	3.23	3.25	0.99
	5.0	938	43.8	43.3	3.72	3.68	1.01

TABLE 6

Convective Heat Transfer Coefficient and Film Boiling Number Calculated from Eq. 97 and Experimentally Determined Values for Saturated Ethanol

Q_w $\frac{BTU}{hr\ ft^2}$	$\bar{T}_w$ (^oF)	$\bar{h}_{c_{EXP}}$ $\frac{BTU}{hr\ ft^2\ ^oF}$	h_c[Eq 97] ANAL $\frac{BTU}{hr\ ft^2\ ^oF}$	$\overline{N_{FB_{EXP}}}$	N_{FB}[Eq 97] ANAL	$\frac{\overline{N_{FB_{EXP}}}}{N_{FB}[Eq\ 97]_{ANAL}}$
35010	942	40.6	41.4	1.80	1.84	0.98
32440	896	40.3	41.8	1.80	1.87	0.96
30080	855	39.9	42.2	1.79	1.89	0.94
26340	780	39.7	42.8	1.80	1.94	0.93
23530	717	40.0	43.1	1.83	1.98	0.93
34860	884	44.6	40.7	2.00	1.82	1.10
31550	829	44.0	41.2	1.98	1.86	1.07
29170	791	43.4	41.6	1.96	1.88	1.04
25880	744	41.8	42.4	1.91	1.93	0.99
23040	692	41.2	42.9	1.90	1.98	0.96
34980	889	44.4	40.7	1.98	1.82	1.09
31960	851	42.9	41.4	1.93	1.86	1.04
29540	810	42.5	41.8	1.92	1.88	1.02
26140	748	42.0	42.3	1.91	1.93	0.99
34360	871	44.9	40.7	2.01	1.82	1.10
31640	833	43.9	41.2	1.98	1.86	1.06
34940	892	44.1	40.8	1.97	1.82	1.08
31780	839	43.6	41.3	1.96	1.86	1.06
36880	919	44.7	40.5	1.99	1.80	1.10
33120	860	43.9	41.0	1.97	1.84	1.07
30380	817	43.2	41.5	1.95	1.87	1.04
36290	873	47.5	40.1	2.13	1.80	1.18
32880	829	46.1	40.7	2.08	1.83	1.13

Q_w $\frac{BTU}{hr\ ft^2}$	$\bar{T}_w$ (^oF)	$\bar{h}_{c_{EXP}}$ $\frac{BTU}{hr\ ft^2\ ^oF}$	h_c[Eq 97] ANAL $\frac{BTU}{hr\ ft^2\ ^oF}$	$\overline{N_{FB_{EXP}}}$	N_{FB}[Eq 97] ANAL	$\frac{\overline{N_{FB_{EXP}}}}{N_{FB}[Eq\ 97]_{ANAL}}$
36433	891	46.2	40.3	2.07	1.80	1.15
33190	842	45.5	40.8	2.04	1.83	1.12
29650	788	44.4	41.4	2.01	1.87	1.07
27330	741	44.7	41.6	2.04	1.90	1.07
24310	686	44.3	42.1	2.04	1.95	1.05
21300	592	48.3	42.0	2.27	1.98	1.15
36300	854	49.1	39.8	2.20	1.79	1.23
32970	806	48.2	40.3	2.18	1.82	1.20
29330	755	47.9	40.7	2.18	1.85	1.18
27175	701	48.3	41.0	2.22	1.89	1.17
24440	637	49.9	41.1	2.33	1.92	1.21

TABLE 7

Convective Heat Transfer Coefficient and Film Boiling Number Calculated from Eq. 97 and Experimentally Determined Values for Saturated Freon 113

Q_w $\frac{BTU}{hr\ ft^2}$	$\bar{T}_w$ (^oF)	$\bar{h}_{c_{EXP}}$ $\frac{BTU}{hr\ ft^2\ ^oF}$	$_c$[Eq 97] $\frac{BTU}{hr\ ft^2\ ^oF}$	$\overline{N_{FB_{EXP}}}$	N_{FB}[Eq 97]	$\frac{\overline{N_{FB_{EXP}}}}{\overline{N_{FB[Eq\ 97]}}}$
36380	1040	35.3	35.5	1.74	1.75	1.00
14020	469	38.1	34.9	1.86	1.70	1.09
19480	627	35.6	35.0	1.74	1.71	1.02
19530	608	34.4	35.5	1.69	1.74	0.97
24440	755	35.0	35.3	1.72	1.73	0.99
28540	860	34.4	35.7	1.69	1.76	0.96
11860	440	35.1	36.1	1.71	1.76	0.97
9951	368	38.3	36.5	1.87	1.78	1.05
34930	1038	32.5	36.3	1.60	1.79	0.90
31770	970	32.4	36.3	1.60	1.79	0.89
23240	778	31.7	36.3	1.56	1.78	0.87
13180	528	30.0	37.0	1.47	1.80	0.81
9396	408	30.8	38.0	1.50	1.86	0.81
11260	459	31.2	37.1	1.52	1.81	0.84
11540	452	32.7	36.7	1.50	1.79	0.89
13150	493	32.9	36.2	1.60	1.76	0.91
15550	563	32.7	36.0	1.60	1.76	0.91

TABLE 8

Convective Heat Transfer Coefficient and Film Boiling Number Calculated from Eq. 97 and Experimentally Determined Values for Saturated Distilled Water

Q_w $\frac{BTU}{hr\ ft^2}$	$\bar{T}_w$ (^oF)	$\bar{h}_{c_{EXP}}$ $\frac{BTU}{hr\ ft^2\ ^oF}$	h_c[Eq 97] $\frac{BTU}{hr\ ft^2\ ^oF}$	$\overline{N_{FB_{EXP}}}$	N_{FB}[Eq 97]	$\frac{\overline{N_{FB_{EXP}}}}{\overline{N_{FB[Eq\ 97]}}}$
37380	1025	40.1	39.5	3.43	3.38	1.01
31530	919	39.6	40.7	3.36	3.45	0.98
36540	1009	40.1	39.7	3.42	3.39	1.01
35610	989	40.3	39.8	3.43	3.40	1.01
35430	969	41.4	39.8	3.46	3.40	1.02
35080	974	40.6	39.9	3.46	3.40	1.02
35490	987	40.3	39.9	3.43	3.40	1.01

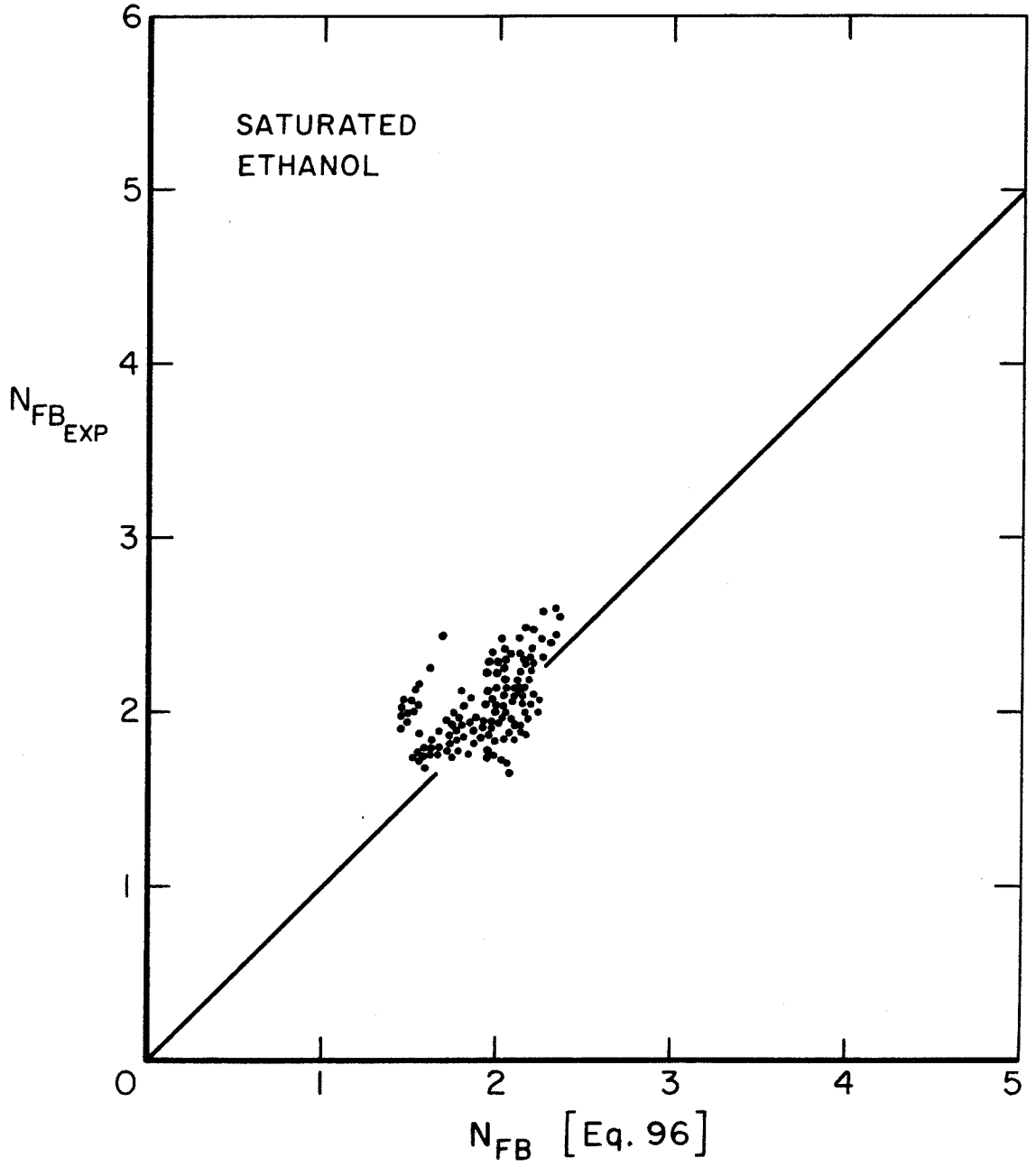

Figure 30. Comparison of Film Boiling Number Calculated from Eq.96 to Experimentally Determined Value, $N_{FB_{EXP}}$, for Film Boiling of Saturated Ethanol

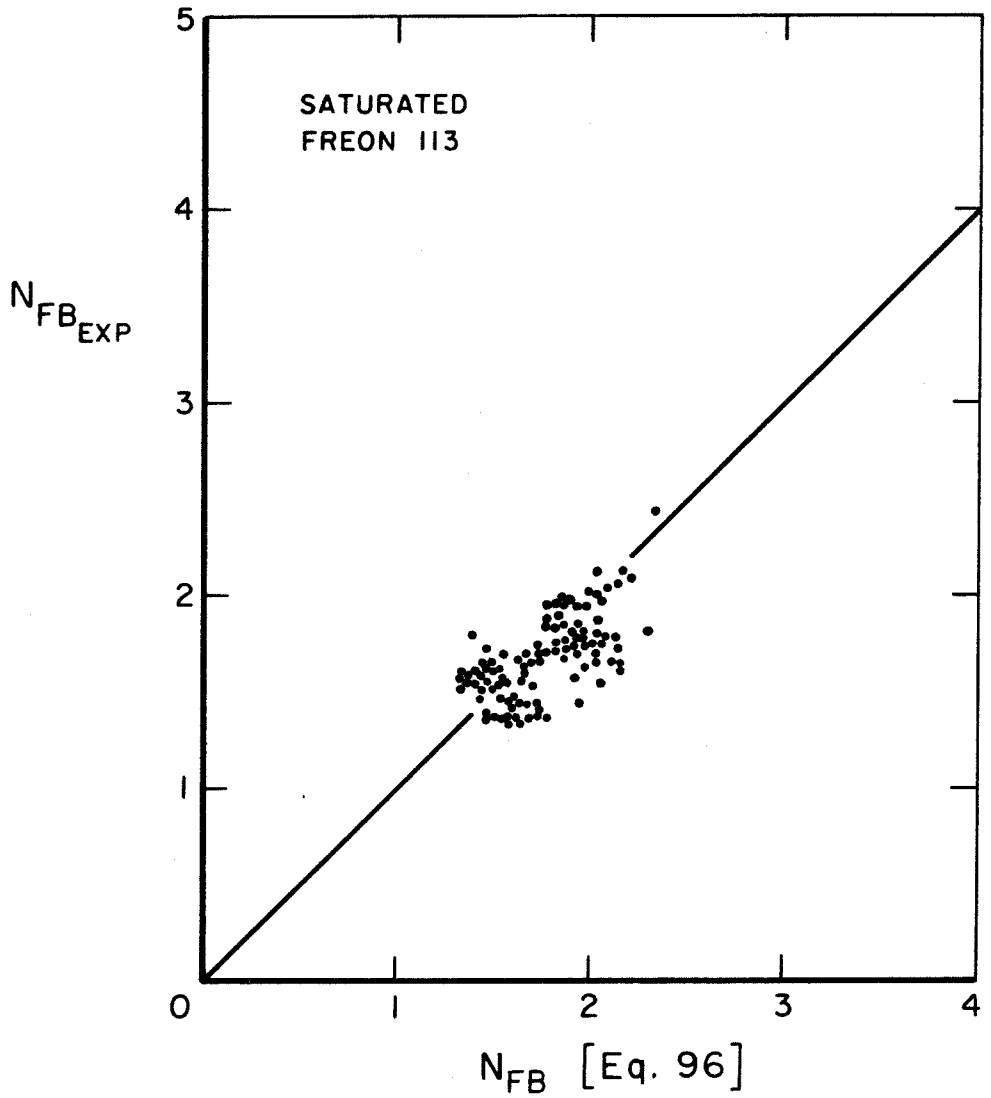

Figure 31. Comparison of Film Boiling Number Calculated From Eq.96 to Experimentally Determined Value, $N_{FB_{EXP}}$, for Film Boiling of Saturated Freon 113

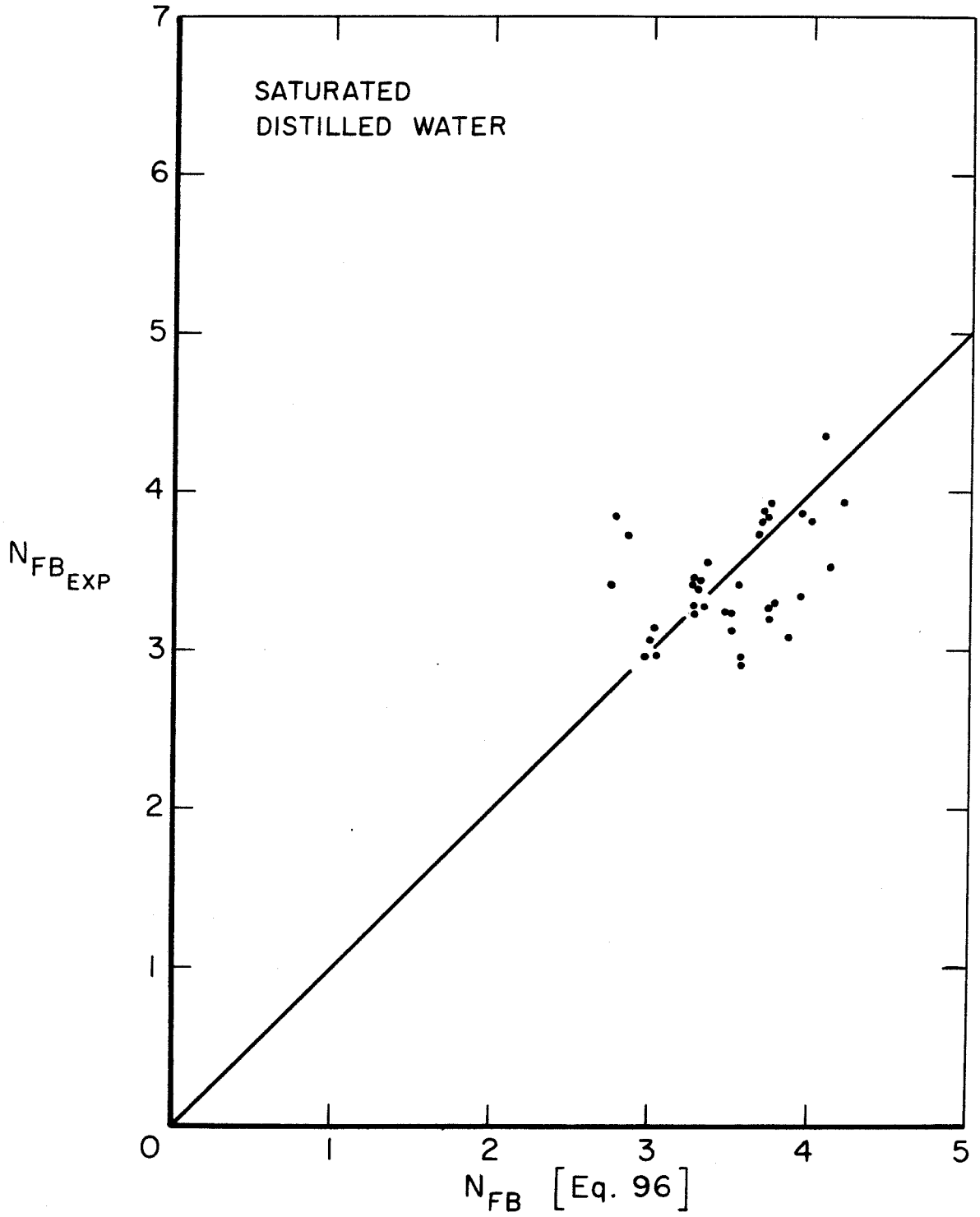

Figure 32. Comparison of Film Boiling Number Calculated From Eq.96 To Experimentally Determined Value, $N_{FB_{EXP}}$, for Film Boiling of Saturated Distilled Water

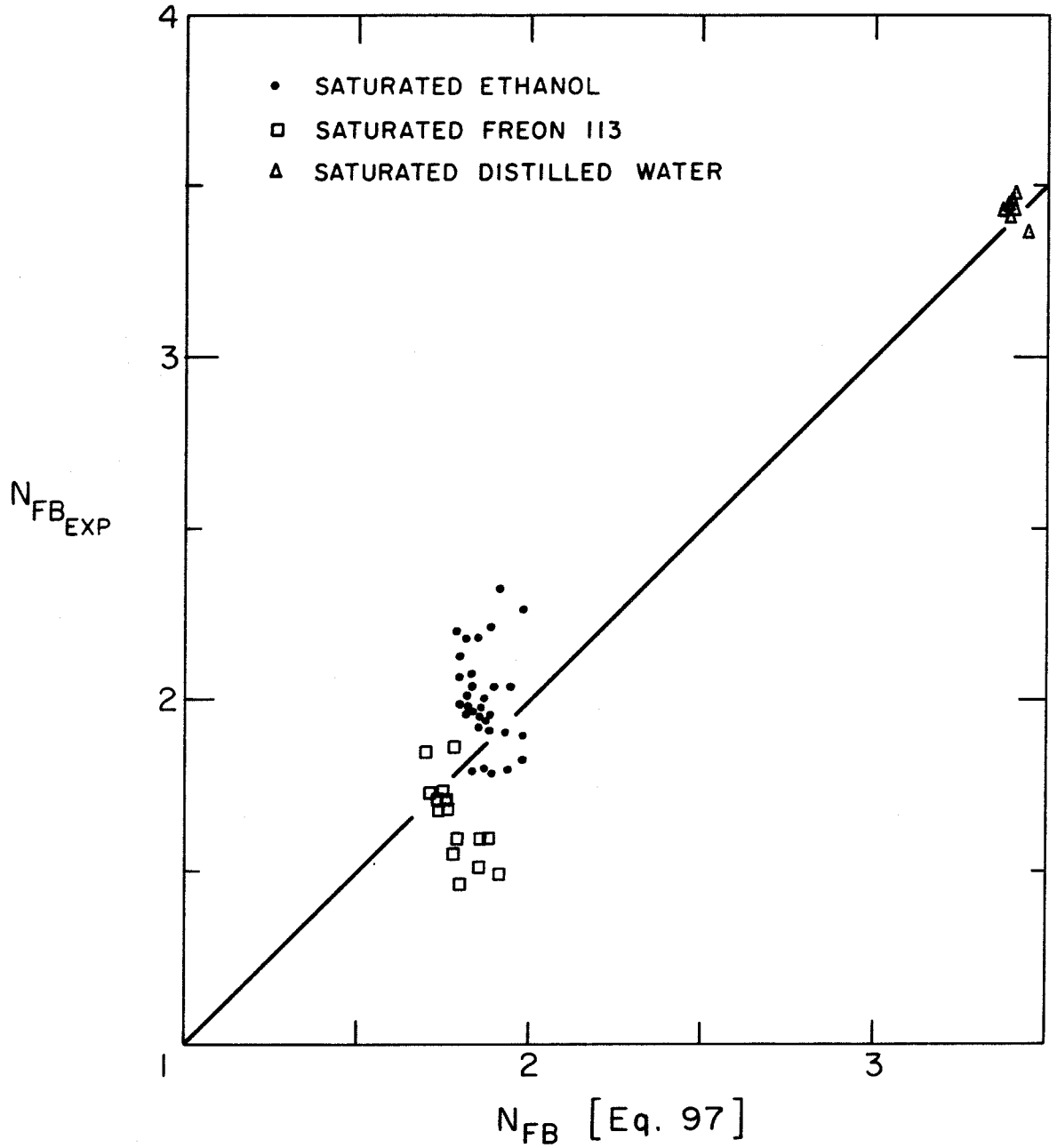

Figure 33. Comparison of Film Boiling Number Calculated From Eq.97 to Experimentally Determined Value, $N_{FB_{EXP}}$, for Film Boiling of Three Saturated Fluids

APPENDIX C

INTERFACIAL WAVE CHARACTERISTICS

TABLE 9. PHOTOGRAPHIC EXPERIMENTAL DATA

SATURATED ETHANOL, $Q_W = 35870 \frac{BTU}{hr\ ft^2}$

x(in)	Re_δ	$\overline{\lambda}_{EXP}$(in)	$\overline{C}^*_{R_{EXP}}$ ($\frac{in}{s}$)	$\delta_{MIN}(10^{-3}in)$	$\overline{\eta}_{EXP}$(in)
0.34	116	0.38	20.2	4.4	0.06
1.56	526	0.48	21.9	12.0	0.15
2.75	926	0.59	13.0	13.3	0.29
3.81	1280	0.74	15.8	14.8	0.38
6.56	2210	0.94	14.3	16.7	0.61

SATURATED ETHANOL, $Q_W = 23110 \frac{BTU}{hr\ ft^2}$

x(in)	Re_δ	$\overline{\lambda}_{EXP}$(in)	$\overline{C}^*_{R_{EXP}}$ ($\frac{in}{s}$)	$\delta_{MIN}(10^{-3}in)$	$\overline{\eta}_{EXP}$(in)
0.34	82.2	0.35	16.1	2.7	0.05
1.56	377	0.57	16.1	4.0	0.12
2.75	665	0.70	16.2	8.7	0.25
3.81	921	0.75	18.0	9.7	0.26
5.19	1260	0.87	19.2	10.0	6.32
6.56	1590	1.16	23.0	12.0	0.39

TABLE 9. (CONTINUED)

SATURATED FREON 113, $Q_W = 20060 \frac{BTU}{hr\ ft^2}$

x(in)	Re_δ	$\overline{\lambda}_{EXP}$(in)	$\overline{C}^*_{R_{EXP}}$ ($\frac{in}{s}$)	$\delta_{MIN}(10^{-3}in)$	$\overline{\eta}_{EXP}$(in)
0.33	291	0.21	-	-	0.03
0.75	661	0.31	13.3	6.6	0.06
1.56	1380	0.44	13.1	10.7	0.16
2.75	2420	0.68	12.1	13.3	0.27
3.81	3360	0.65	19.7	-	0.28
5.19	4580	0.75	15.2	18.7	0.36
6.56	5780	1.10	16.8	24.7	0.56
7.97	7030	0.95	11.8	28.7	0.74

SATURATED FREON 113, $Q_W = 11040 \frac{BTU}{hr\ ft^2}$

x(in)	Re_δ	$\overline{\lambda}_{EXP}$(in)	$\overline{C}^*_{R_{EXP}}$ ($\frac{in}{s}$)	$\delta_{MIN}(10^{-3}in)$	$\overline{\eta}_{EXP}$(in)
0.50	261	0.43	14.2	3.3	0.04
1.56	816	0.56	14.4	8.7	0.10
3.81	1990	0.80	11.5	12.0	0.29

TABLE 9. (CONTINUED)

SATURATED DISTILLED WATER, $Q_W = 35430 \frac{BTU}{hr\ ft^2}$

x(in)	Re_δ	$\bar{\lambda}_{EXP}$(in)	$\bar{C}^*_{R_{EXP}}$ $(\frac{in}{s})$	$\delta_{MIN}(10^{-3}in)$	$\bar{\eta}_{EXP}$(in)
0.50	28.6	0.48	46.6	2.6	0.09
1.78	102	0.88	33.8	4.6	0.20
3.22	184	1.03	23.0	6.6	0.31
4.66	266	0.99	30.9	6.6	0.36
6.09	348	1.16	27.0	7.2	0.46

TABLE 10. RESULTS OF LINEARIZED STABILITY THEORY

SATURATED ETHANOL, $Q_W = 35870 \frac{BTU}{hr\ ft^2}$

x(in)	Re_δ	$\overline{\lambda}_{EXP}$(in)	λ_C(in)	λ_D(in)	$\overline{\delta}(10^{-3}$in)	$u_o(\frac{in}{s})$	Real $[\omega_D^*](\frac{rad}{s})$
0.34	116	0.38	4.61	0.64	5.80	490	697
1.56	526	0.48	31.7	5.03	14.0	920	542
2.75	926	0.59	66.2	10.7	19.5	1160	368
3.81	1280	0.74	101	16.2	23.6	1340	294
6.56	2210	0.94	209	33.8	32.4	1670	202

SATURATED ETHANOL, $Q_W = 23110 \frac{BTU}{hr\ ft^2}$

x(in)	Re_δ	$\overline{\lambda}_{EXP}$(in)	λ_C(in)	λ_D(in)	$\overline{\delta}(10^{-3}$in)	$u_o(\frac{in}{s})$	Real $[\omega_D^*](\frac{rad}{s})$
0.34	82.2	0.35	2.97	0.40	4.27	382	1850
1.56	377	0.57	20.7	3.14	10.4	721	666
2.75	665	0.70	43.2	6.68	14.5	913	454
3.81	921	0.75	66.2	10.3	17.5	1050	363
5.19	1260	0.87	99.7	15.7	20.9	1190	292
6.56	1590	1.16	136	21.0	24.0	1310	250

TABLE 10. (CONTINUED)

SATURATED FREON 113, $Q_W = 20060 \frac{BTU}{hr\ ft^2}$

x(in)	Re_δ	$\bar{\lambda}_{EXP}$(in)	λ_C(in)	λ_D(in)	$\bar{\delta}(10^{-3}$in)	$u_o(\frac{in}{s})$	Real $[\omega_D^*](\frac{rad}{s})$
0.33	291	0.21	4.46	0.76	4.14	302	1240
0.75	661	0.31	13.0	2.28	6.69	426	708
1.56	1380	0.44	34.7	5.97	10.3	578	426
2.75	2420	0.68	75.7	12.5	14.3	732	285
3.81	3360	0.65	120	19.0	17.3	838	226
5.19	4580	0.75	186	28.2	20.7	954	181
6.56	5780	1.10	261	38.2	23.7	1050	152
7.97	7030	0.95	346	49.1	26.6	1140	132

SATURATED FREON 113, $Q_W = 11040 \frac{BTU}{hr\ ft^2}$

x(in)	Re_δ	$\bar{\lambda}_{EXP}$(in)	λ_C(in)	λ_D(in)	$\bar{\delta}(10^{-3}$in)	$u_o(\frac{in}{s})$	Real $[\omega_D^*](\frac{rad}{s})$
0.50	261	0.43	4.23	0.68	3.57	261	1270
1.56	816	0.56	19.1	3.03	6.92	420	582
3.81	1990	0.80	65.3	9.67	11.7	609	311
6.00	3140	-	124	17.4	15.2	736	244

TABLE 10. (CONTINUED)

SATURATED DISTILLED WATER, $Q_W = 35430 \frac{BTU}{hr\ ft^2}$

x(in)	Re_δ	$\overline{\lambda}_{EXP}$(in)	λ_C(in)	λ_D(in)	$\overline{\delta}(10^{-3}$in)	$u_o(\frac{in}{s})$	Real $[\omega_D^*](\frac{rad}{s})$
0.5	28.6	0.48	3.48	0.30	4.27	679	2390
1.78	102	0.88	17.2	1.72	8.96	1150	1030
3.22	184	1.03	36.2	3.82	12.7	1480	696
4.66	266	0.99	57.9	6.33	15.7	1720	544
6.09	348	1.16	81.3	9.06	18.4	1920	456

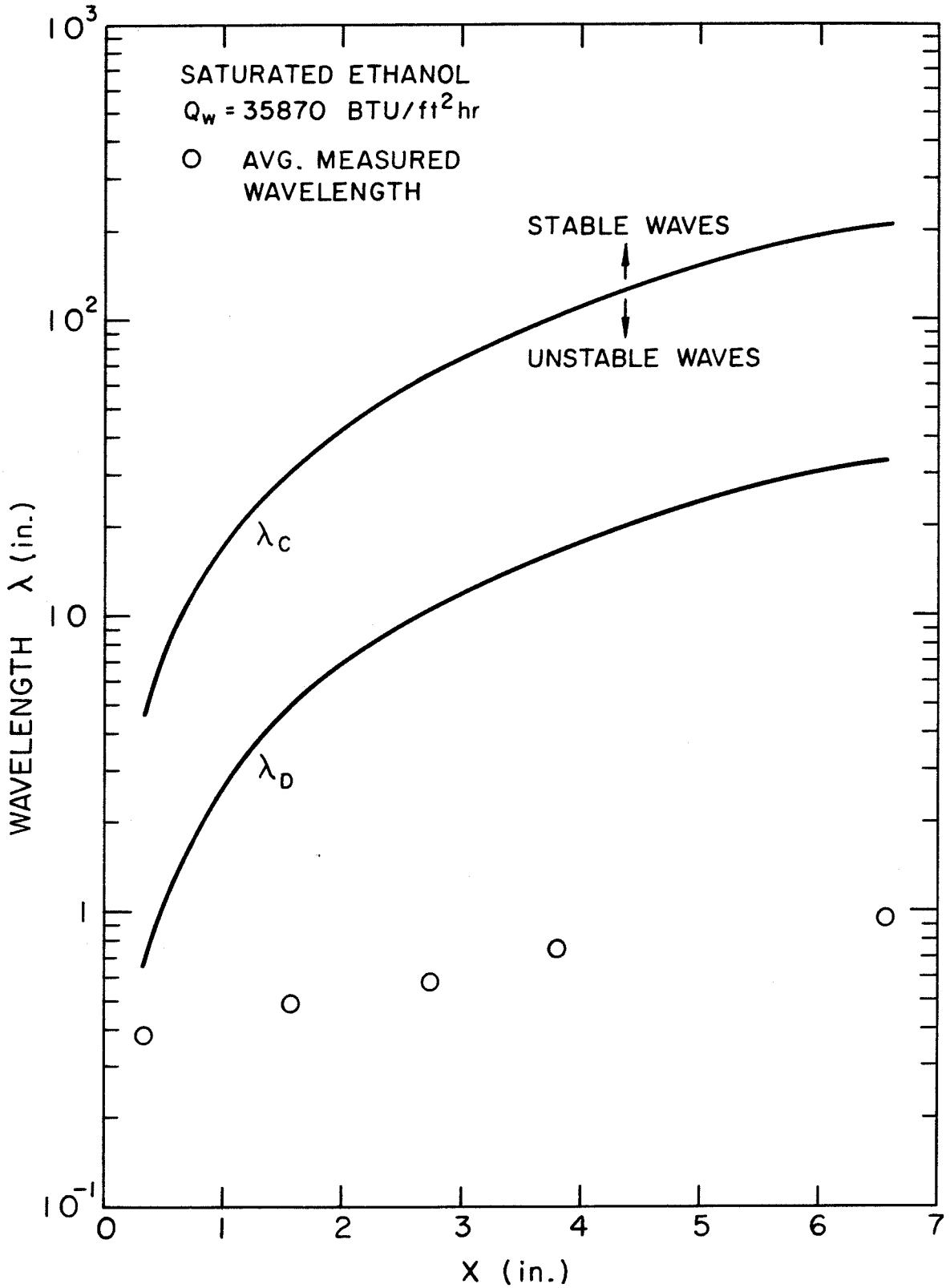

Figure 34. Measured Average Wavelength vs. Vertical Position and Comparison to Theory for Film Boiling of Saturated Ethanol on a Vertical Cylinder

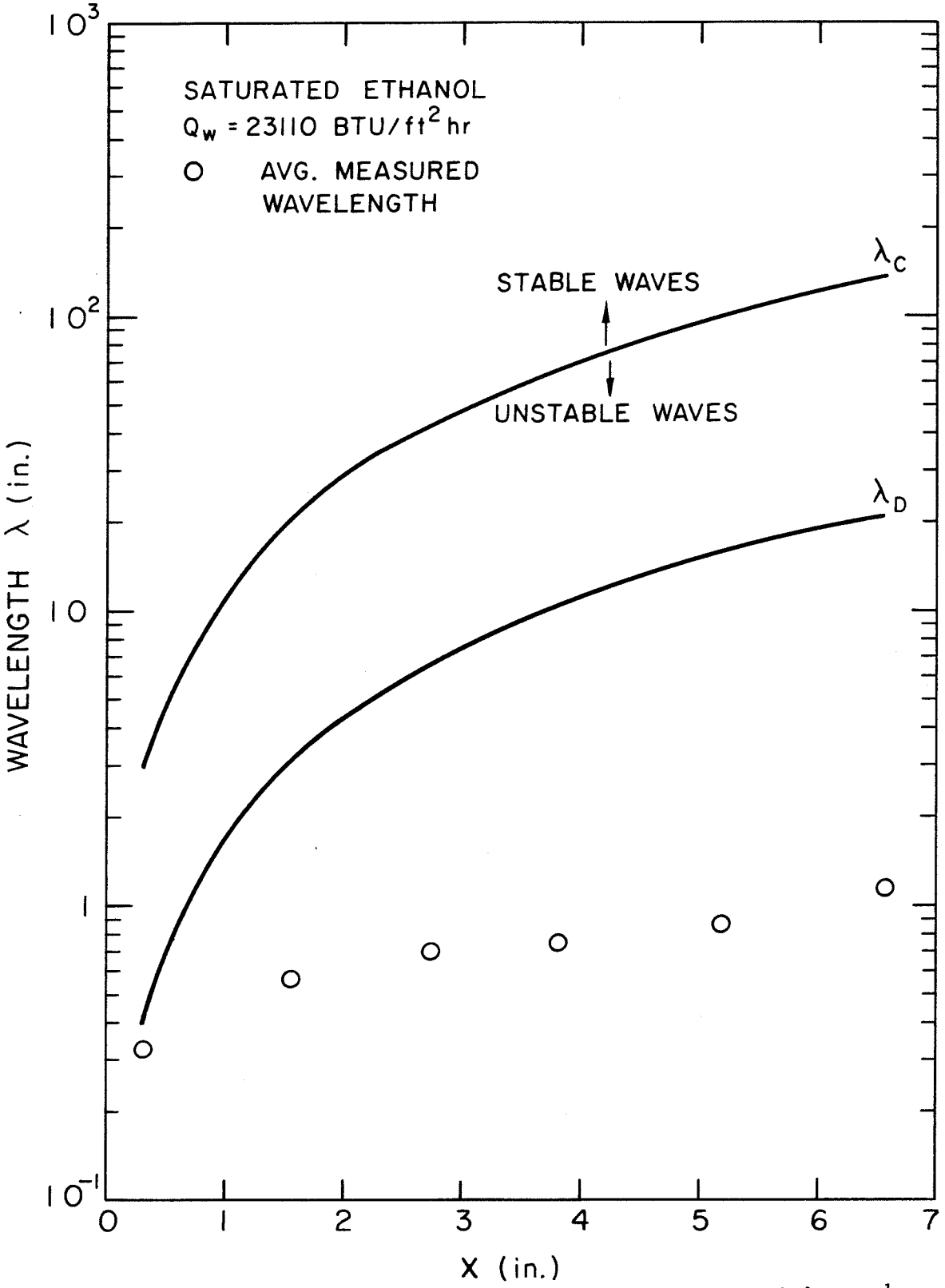

Figure 35. Measured Average Wavelength vs. Vertical Position and Comparison to Theory for Film Boiling of Saturated Ethanol on a Vertical Cylinder

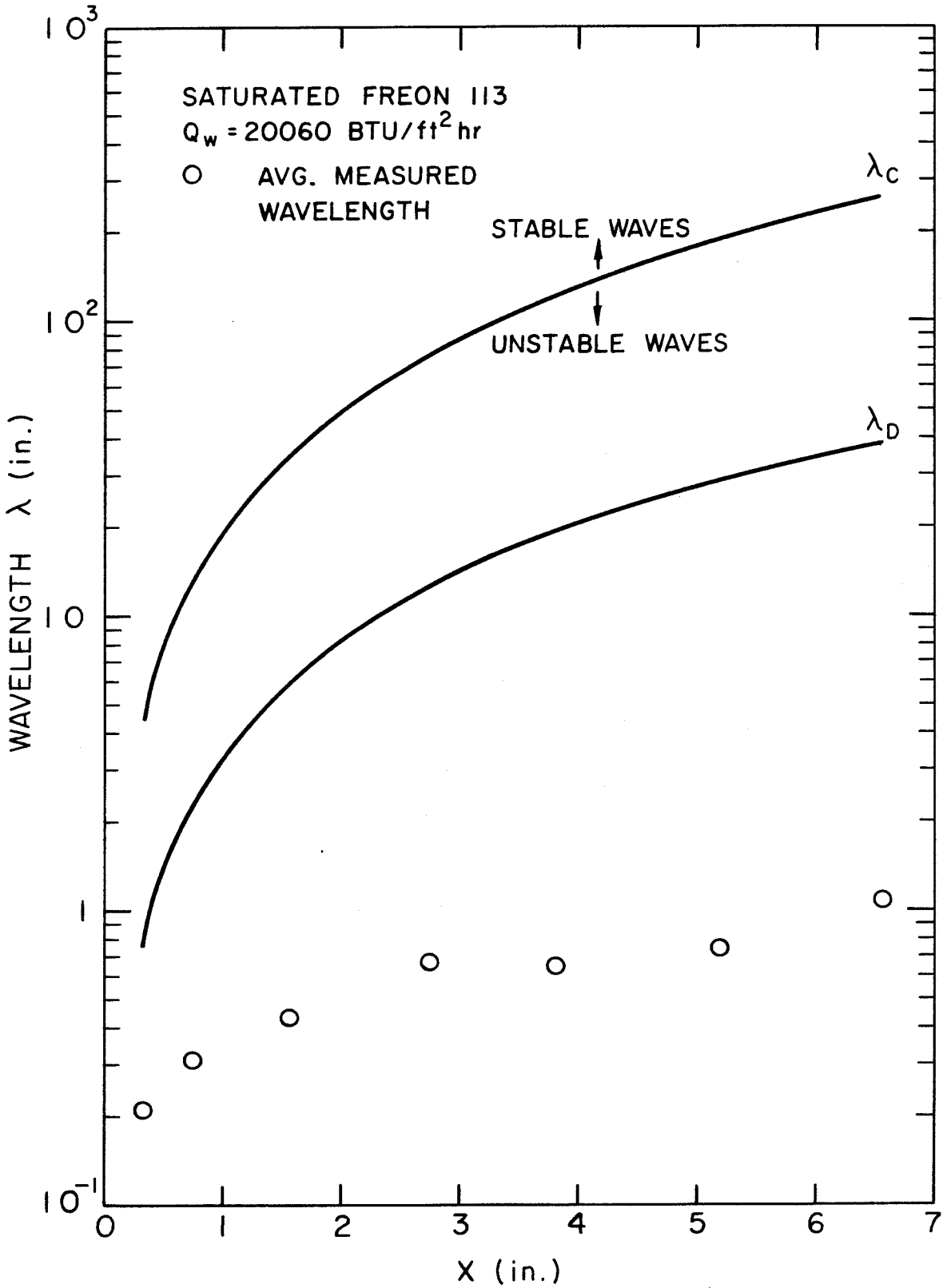

Figure 36. Measured Average Wavelength vs. Vertical Position and Comparison to Theory for Film Boiling of Saturated Freon 113 on a Vertical Cylinder

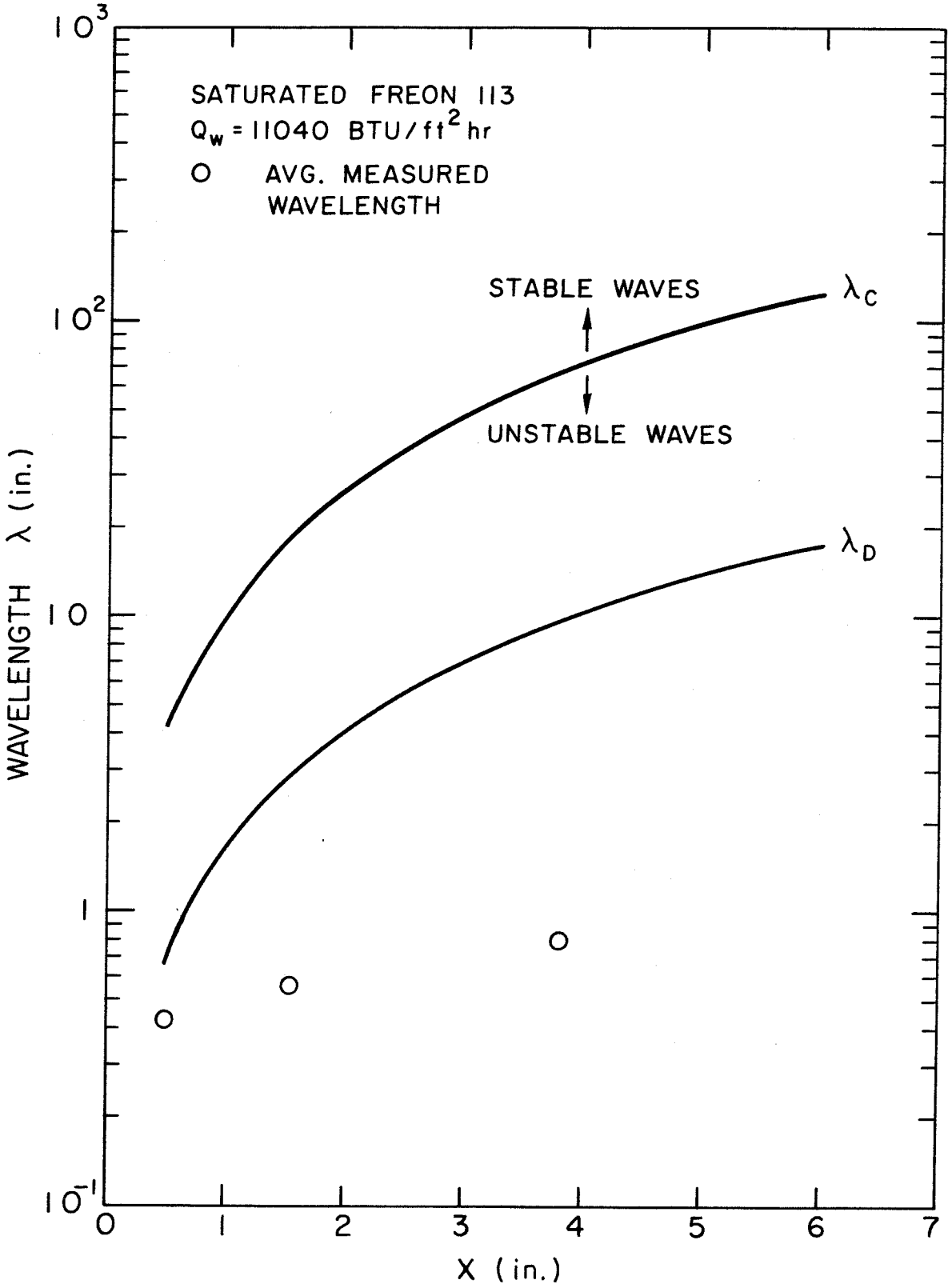

Figure 37. Measured Average Wavelength vs. Vertical Position and Comparison to Theory for Film Boiling of Saturated Freon 113 on a Vertical Cylinder

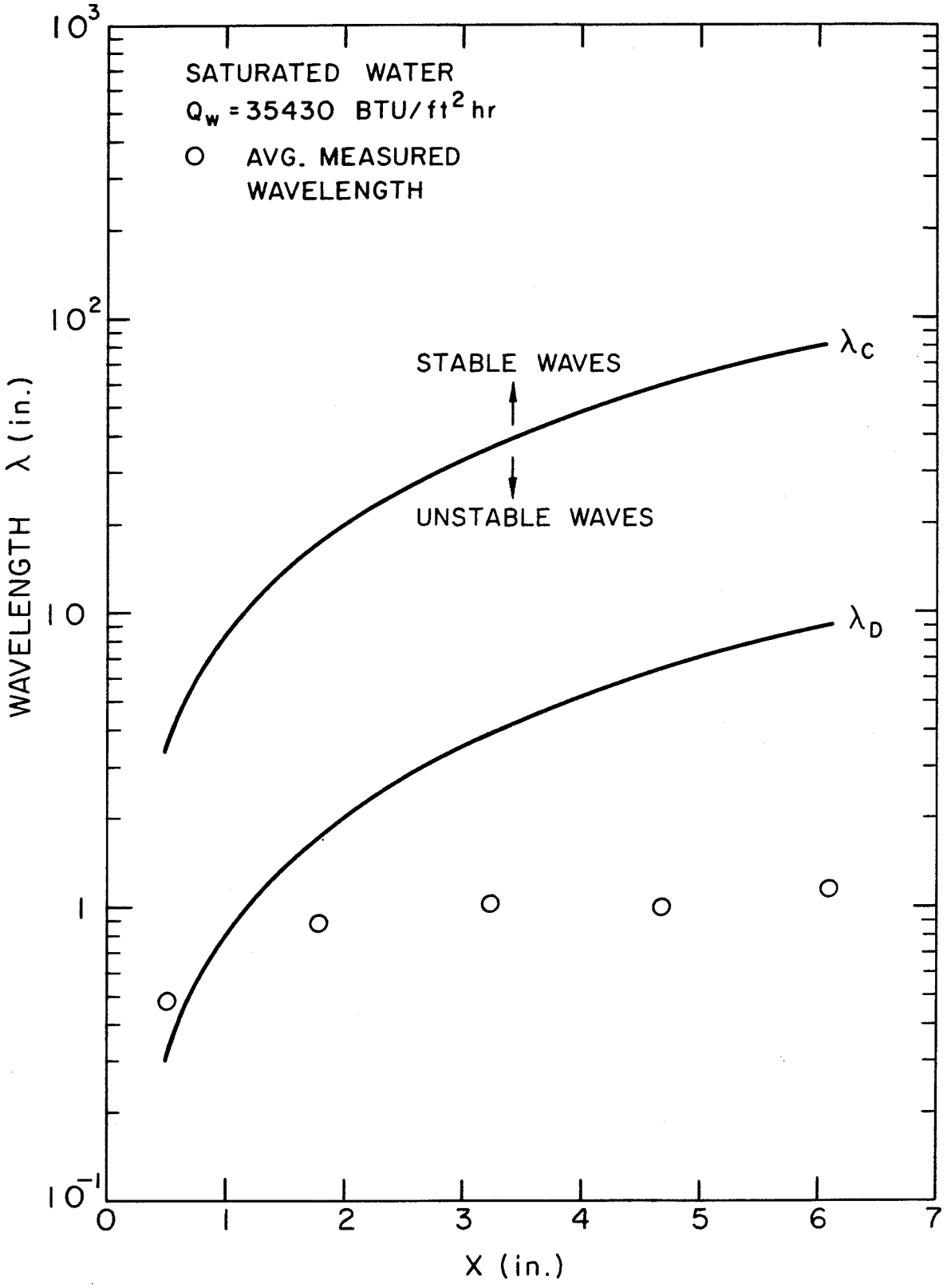

Figure 38. Measured Average Wavelength vs. Vertical Position and Comparison to Theory for Film Boiling of Saturated Distilled Water on a Vertical Cylinder

TABLE 11. COMPARISON OF STABILITY THEORY TO INTERFACIAL WAVE DATA ON THE BASIS OF GROWTH RATES

SATURATED ETHANOL, $Q_W = 35870 \frac{BTU}{hr\ ft^2}$

x(in)	Re_δ	$\alpha_D (10^2)$	$\bar{\alpha}_{EXP} (10^2)$	$Im(\omega_D) (10^3)$	$Im[\omega(\bar{\alpha}_{EXP})] (10^3)$	$\frac{Im[\omega(\bar{\alpha}_{EXP})]}{Im(\omega_D)}$
0.34	116	5.66	9.56	9.91	9.44	0.952
1.56	526	1.75	18.3	3.94	1.86	0.473
2.75	926	1.14	20.8	2.73	1.00	0.366
3.81	1280	0.895	19.9	2.19	0.737	0.336
6.56	2210	0.602	21.6	1.51	0.412	0.274

SATURATED ETHANOL, $Q_W = 23110 \frac{BTU}{hr\ ft^2}$

x(in)	Re_δ	$\alpha_D (10^2)$	$\bar{\alpha}_{EXP} (10^2)$	$Im(\omega_D) (10^3)$	$Im[\omega(\bar{\alpha}_{EXP})] (10^3)$	$\frac{Im[\omega(\bar{\alpha}_{EXP})]}{Im(\omega_D)}$
0.34	82.2	6.76	7.67	11.9	11.8	0.997
1.56	377	2.08	11.4	4.70	2.96	0.631
2.75	665	1.36	12.9	3.26	1.61	0.494
3.81	921	1.06	14.6	2.62	1.10	0.419
5.19	1260	0.840	15.2	2.12	0.794	0.374
6.56	1590	0.720	13.0	1.80	0.674	0.373

TABLE 11. (CONTINUED)

SATURATED FREON 113, $Q_W = 20060 \frac{BTU}{hr\ ft^2}$

x(in)	Re_δ	$\alpha_D(10^2)$	$\overline{\alpha}_{EXP}(10^2)$	$Im(\omega_D)(10^3)$	$Im[\omega(\overline{\alpha}_{EXP})](10^3)$	$\frac{Im[\omega(\overline{\alpha}_{EXP})]}{Im(\omega_D)}$
0.33	291	3.41	12.3	7.64	5.66	0.742
0.75	661	1.85	13.6	4.42	2.45	0.554
1.56	1380	1.08	14.8	2.63	1.14	0.431
2.75	2420	0.720	13.3	1.73	0.676	0.391
3.81	3360	0.570	16.8	1.34	0.440	0.328
5.19	4580	0.460	17.3	1.05	0.319	0.303
6.56	5780	0.390	13.6	0.872	0.281	0.322
7.97	7030	0.340	17.6	0.743	0.206	0.278

SATURATED FREON 113, $Q_W = 11040 \frac{BTU}{hr\ ft^2}$

x(in)	Re_δ	$\alpha_D(10^2)$	$\overline{\alpha}_{EXP}(10^2)$	$Im(\omega_D)(10^3)$	$Im[\omega(\overline{\alpha}_{EXP})](10^3)$	$\frac{Im[\omega(\overline{\alpha}_{EXP})]}{Im(\omega_D)}$
0.50	261	3.32	5.21	7.83	7.48	0.955
1.56	816	1.44	7.80	3.59	2.28	0.636
3.81	1990	0.758	9.18	1.86	0.879	0.474

TABLE 11. (CONTINUED)

SATURATED DISTILLED WATER, $Q_W = 35434 \frac{BTU}{hr\ ft^2}$

x(in)	Re_δ	$\alpha_D (10^2)$	$\bar{\alpha}_{EXP} (10^2)$	$Im(\omega_D) (10^{-})$	$Im[\omega(\bar{\alpha}_{EXP})] (10^3)$	$\frac{Im[\omega(\bar{\alpha}_{EXP})]}{Im(\omega_D)}$
0.50	28.6	9.02	5.59	10.7	10.4	0.973
1.78	102	3.28	6.40	5.28	4.97	0.941
3.22	184	2.08	7.70	3.76	2.94	0.782
4.66	266	1.56	9.93	3.03	1.89	0.624
6.09	348	1.27	9.96	2.59	1.46	0.564

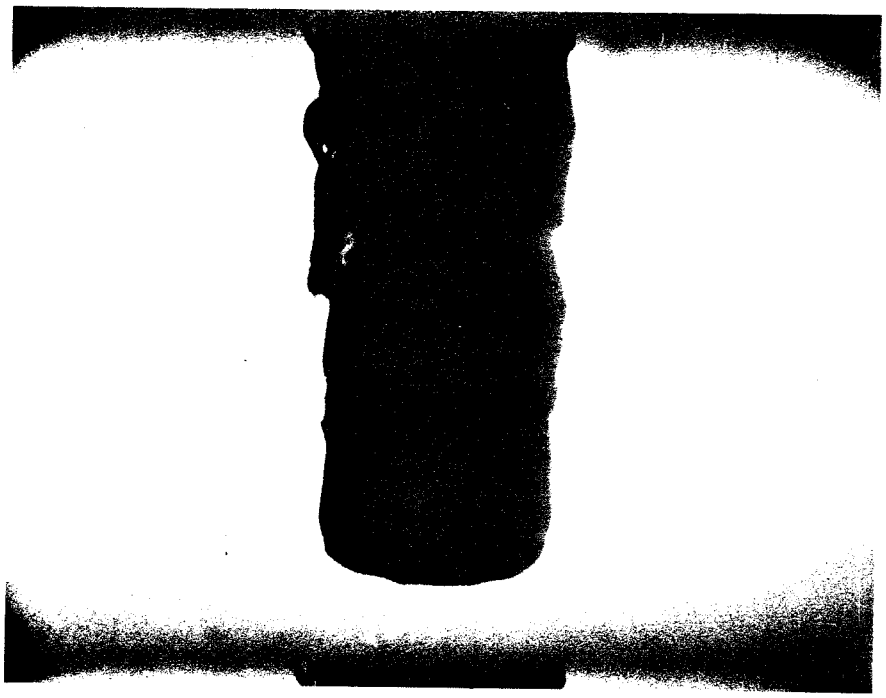

Figure 39. Free Convection Film Boiling of Saturated Ethanol on a 0.5 in. Diameter Vertical Cylinder at a Heat Flux of 35780 BTU/hr ft^2 from 0.41 in. Below to 1.03 in. Above the Lower End of the Cylinder

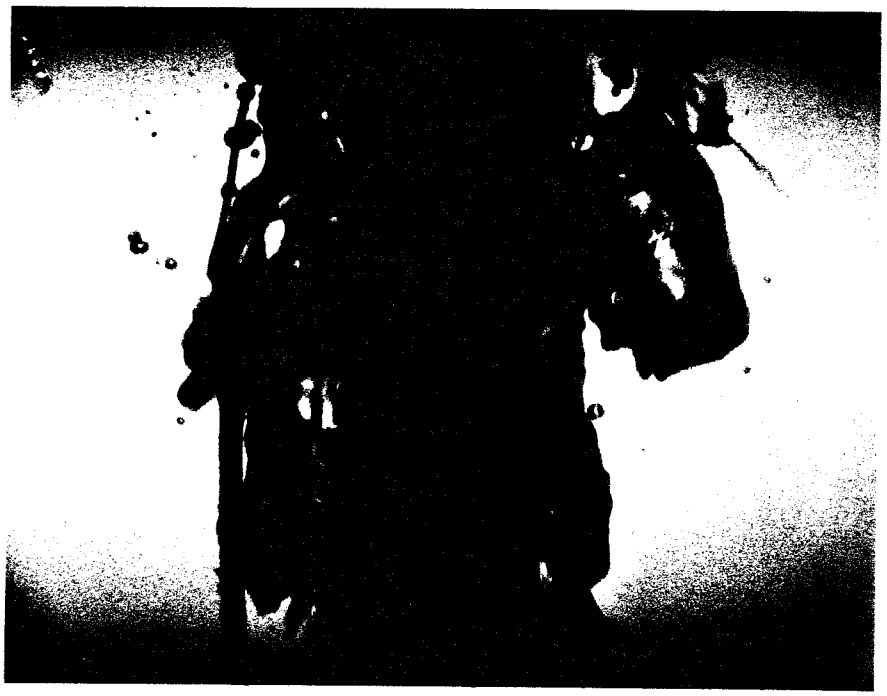

Figure 40. Free Convection Film Boiling of Saturated Ethanol on a 0.5 in. Diameter Vertical Cylinder at a Heat Flux of 35780 BTU/hr ft^2 from 2.06 in. to 3.44 in. Above the Lower End of the Cylinder

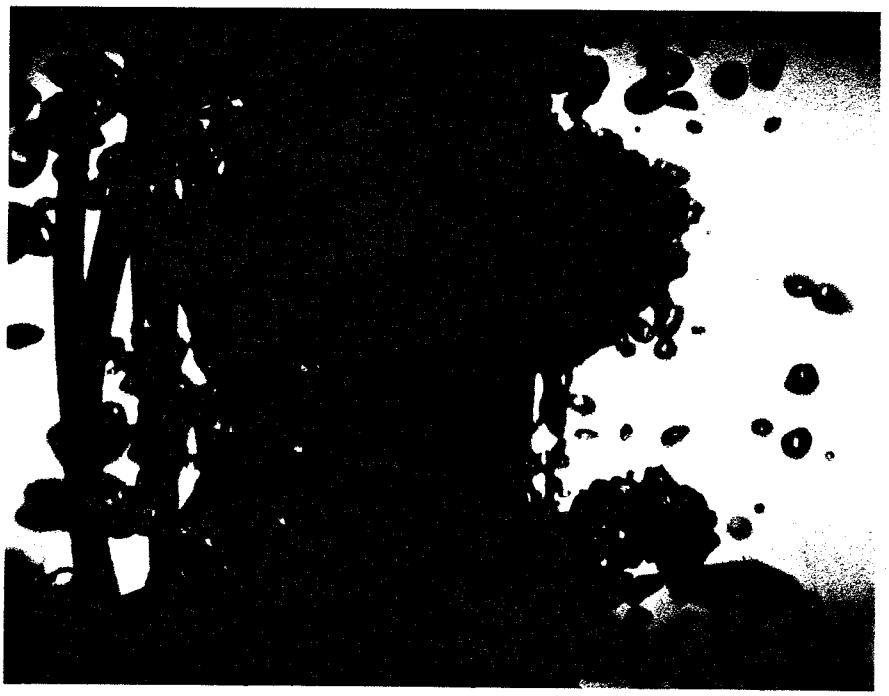

Figure 41. Free Convection Film Boiling of Saturated Ethanol on a 0.5 in. Diameter Vertical Cylinder at a Heat Flux of 35780 BTU/hr ft^2 from 5.88 in. to 7.25 in. Above the Lower End of the Cylinder

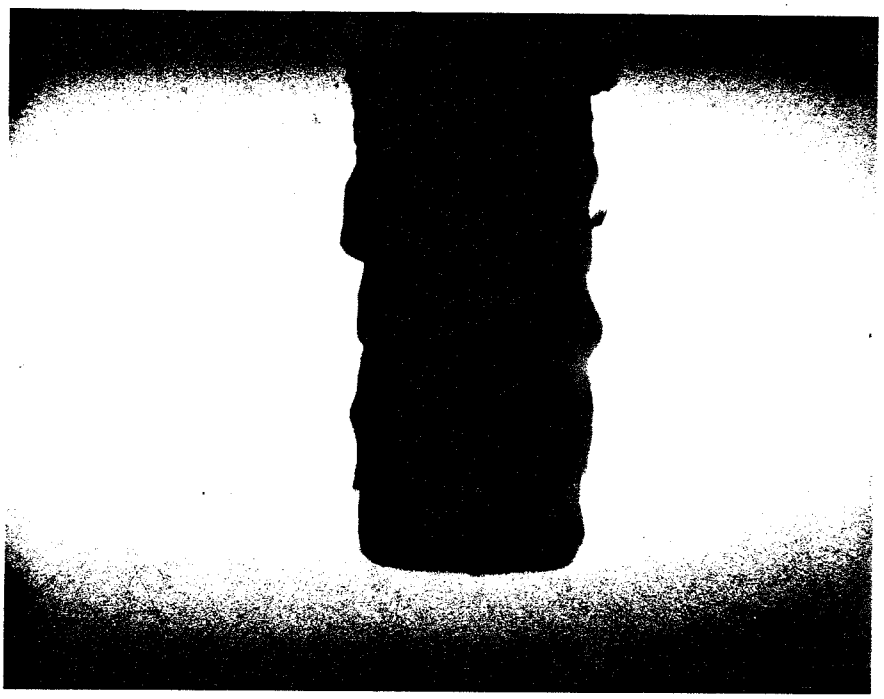

Figure 42. Free Convection Film Boiling of Saturated Freon 113 on a 0.5 in. Diameter Vertical Cylinder at a Heat Flux of 20060 BTU/hr ft^2 from 0.41 in. Below to 1.03 in. Above the Lower End of the Cylinder

Figure 43. Free Convection Film Boiling of Saturated Freon 113 on a 0.5 in. Diameter Vertical Cylinder at a Heat Flux of 20060 BTU/hr ft^2 from 0.88 in. to 2.25 in. Above the Lower End of the Cylinder

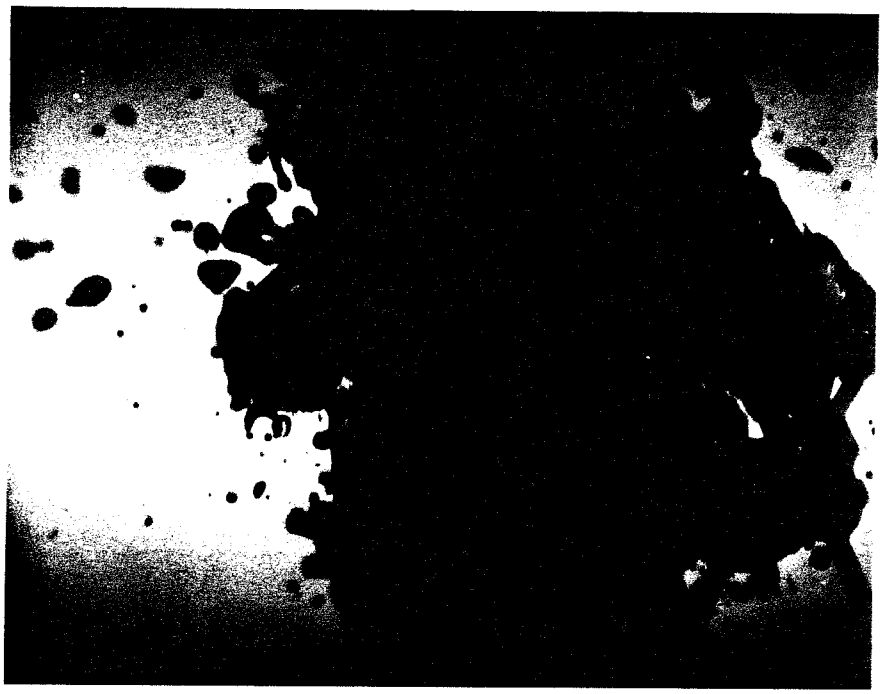

Figure 44. Free Convection Film Boiling of Saturated Freon 113 on a 0.5 in. Diameter Vertical Cylinder at a Heat Flux of 20060 BTU/hr ft^2 from 4.50 in. to 5.88 in. Above the Lower End of the Cylinder

Figure 45. Free Convection Film Boiling of Saturated Distilled Water on a 0.5 in. Diameter Vertical Cylinder at a Heat Flux of 35430 BTU/hr ft^2 from 0.06 in. to 1.44 in. Above the Lower End of the Cylinder

Figure 46. Free Convection Film Boiling of Saturated Distilled Water on a 0.5 in. Diameter Vertical Cylinder at a Heat Flux of 35430 BTU/hr ft^2 from 2.06 in. to 3.44 in. Above the Lower End of the Cylinder

Figure 47. Free Convection Film Boiling of Saturated Distilled Water on a 0.5 in. Diameter Vertical Cylinder at a Heat Flux of 35430 BTU/hr ft^2 from 4.5 in. to 5.88 in. Above the Lower End of the Cylinder

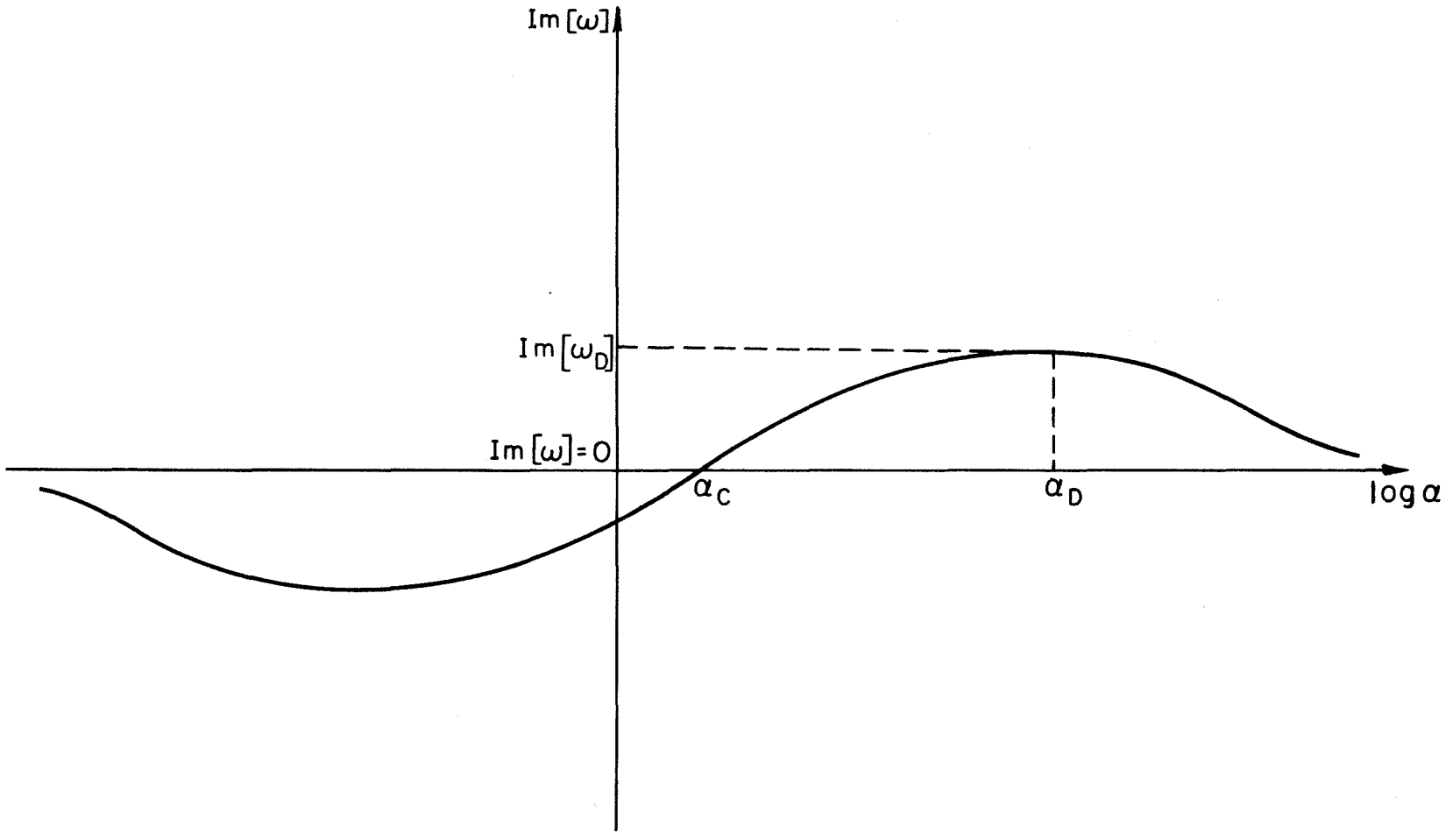

Figure 48. Imaginary Part of Dimensionless Frequency as a Function of Dimensionless Wave Number: General Form of Theoretical Result

APPENDIX D

ESTIMATE OF EXPERIMENTAL ERROR

APPENDIX D

ESTIMATE OF EXPERIMENTAL ERROR

A. Heat Transfer Measurements

1. Heat Flux Rate

Basic Measurements

	Measurement	Minimum Accuracy
Test Section Diameter, D	0.500 in.	1%
Test Section Length, L	12.0 in.	2%
Test Section Current, I	(amperes)	1%
Test Section Voltage, V	(volts)	0.1%
Power Factor (determined from Phase Angle Between Test Section Voltage and Current), $\cos\theta$	1.0	3%

Calculation of Heat Transfer Rate:

$$q_w = \frac{IV\cos\theta}{\pi DL} = 26.06\, IV \quad \frac{BTU}{hr\ ft^2}$$

Additional errors in the value of q_w may be caused by the following:

1. Nonuniformity of heating coils — guaranteed less than 2%.
2. Axial conduction in test section, given by

$$\frac{\Delta q_{AC}}{q_w} = \frac{k_m t \frac{d^2T}{dx^2}}{q_w}$$

where k_m = the thermal conductivity of the sheath material of the test section $30 \frac{BTU}{hr\,ft^2\,^\circ F}$,

t = the thickness of the sheath material = 0.0052 ft.

The quantity d^2T/dx^2 was obtained from thermocouple measurements. The maximum value of $\Delta q_{AC}/q_w$ for all experimental measurements is 0.05 (5%).

Thus, the maximum possible error in q_w is

$$\frac{\Delta q_w}{q_w} = \frac{\Delta I}{I} + \frac{\Delta V}{V} + \frac{\Delta(\cos\theta)}{\cos\theta} + \frac{\Delta D}{D} + \frac{\Delta L}{L} + \frac{\Delta q_{AC}}{q_w} + 2\% = 14.1\%$$

2. Temperature Difference

	Measurement	Minimum Accuracy
Calibration Coefficient,	$\frac{\text{millivolts}}{^\circ F}$	5%
Voltage difference between thermocouple on test section and reference junction, ΔV (this includes errors induced by averaging nonsteady voltage readings)	(millivolts)	1%

Calculation of thermocouple temperature:

$$T_{tc} = 32^\circ F + \beta \Delta V$$

where T_{tc} is the temperatue of the wall at the point of thermocouple attachment. Maximum possible error in $T_{tc} - T_S$ due to measurements is,

$$\frac{\Delta(T_{tc}-T_S)}{T_{tc}-T_S} = \frac{\Delta\beta}{\beta} + \frac{\delta\Delta V}{\Delta V} = 6\% \quad .$$

Additionally, there is an error in temperature measurement induced by the presence of the thermocouple on the test section. Heat is conducted away from the surface through the thermocouple leads and transferred to the surrounding liquid by convection. This causes the temperature of the surface in the neighborhood of the attachment point of the thermocouple to be lower than it would be in the absence of thermocouple attachment.

In order to quantify the maximum error in temperature due to conduction in the thermocouple leads, the sheath material of the test section is approximated by a massive solid at uniform temperature, T_w, in a natural convection environment. Although the sheath is not extremely thick compared to the thermocouple wire diameter, temperature errors induced by the thermocouple leads will be much smaller than those indicated by an analysis assuming the sheath of the test section to be an isothermal, thin flat plate in a free convection environment, since there is a very large heat source on the inside of the sheath. Thus, it is felt that the actual configuration more closely resembles an isothermal semi-infinite solid of high thermal conductivity with respect to temperature perturbations induced by the presence of the thermocouple. The problem of temperature measurement error on a convectively cooled, relatively massive solid has been solved in [59], and the results are presented and discussed in [57]. The results are presented in terms of three dimensionless groups. These are:

1. The dimensionless temperature error;

$$\frac{T_w - T_{tc}}{T_w - T_S} \quad ,$$

where $T_w - T_{tc}$ is the measurement error,

2. $$\frac{\sqrt{\frac{\widetilde{kA}}{R}}\ \tanh\{(\widetilde{kA}R)^{-\frac{1}{2}}L\}}{\pi r_{tc} k_m} \qquad (*)$$

where

$$\widetilde{kA} = k_{tc}A_{tc} + k_i A_i$$

$$R = \frac{1}{h_{tc} 2\pi r_i} + \frac{\ln\left(\frac{r_i}{r_{tc}}\right)}{2\pi k_i}$$

and k_m = thermal conductivity of the test section sheath

k_{tc} = thermal conductivity of the thermocouple material

A_{tc} = cross-sectional area of the thermocouple metal

k_i = thermal conductivity of the insulation on the thermocouple leads

A_i = cross-sectional area of insulation

r_{tc} = radius of thermocouple metal

r_i = outside radius of thermocouple insulation

h_{tc} = convective heat transfer coefficient between thermocouple lead and surrounding fluid.

The numerator of (*) comes from fin theory.

3. The Biot number of the solid,

$$\frac{h_s r_{tc}}{k_m}$$

where h_s = the heat transfer coefficient between the test section and the vapor film.

The results of this analysis are presented graphically in (57). The "worst case" values of the Biot number, and the quantity (*) are computed using the following values:

$$k_m = 30 \frac{BTU}{hr\,ft\,^\circ F} \quad ; \quad k_{tc} = 17 \frac{BTU}{hr\,ft\,^\circ F}$$

$$h_s = 30 \frac{BTU}{hr\,ft^2\,^\circ F} \quad ; \quad h_{tc} = 20 \frac{BTU}{hr\,ft^2\,^\circ F}$$

$$k_i = 0.1 \frac{BTU}{hr\,ft\,^\circ F} \quad ; \quad r_{tc} = 8.33 \times 10^{-4}\,ft$$

$$r_i = 0.00108\,ft \quad ; \quad L = 0.5\,ft \quad ;$$

giving

$$B_i = 1.67 \times 10^{-3}$$

and the quantity

$$(*) = 2.79 \times 10^{-2} \quad ,$$

and, from 57 ,

$$\frac{T_w - T_{tc}}{T_w - T_S} = \frac{\delta T_{tc}}{\Delta T_S} = 2\% \quad .$$

Since there are two thermocouple wires attached, the maximum possible error in ΔT_S is obtained by assuming the cooling effects of each wire to be additive. Thus,

$$\frac{\delta \Delta T_S}{\Delta T_S} = \frac{\delta (T_{tc} - T_S)}{(T_{tc} - T_S)} + 2 \frac{\delta \Delta T_{tc}}{\Delta T_S} = 10\% \quad .$$

3. Heat Transfer Coefficient

The heat transfer coefficient is calculated from the measured heat flux and temperature difference according to:

$$h = \frac{q_w}{\Delta T_S} \quad .$$

So, the maximum possible error in h is estimated to be

$$\frac{\delta h}{h} = \frac{\delta q_w}{q_w} + \frac{\delta \Delta T_S}{\Delta T_S} = 24.1\% \quad .$$

B. Photographic Measurements

The experimental errors involved in the extraction of data from the high-speed motion pictures are considered to be insignificant in comparison to the scatter of the quantities measured. The data reported for interfacial wave characteristics represent averages of many measurements for each quantity. The errors in measurement may be as large as 5% or so due to aberrations in the lens systems of the camera and film viewer combined with any possible errors in specification of the film speed. However, the statistical nature of the data was such that the standard deviation of data points was consistently greater than 20% of the mean value, and thus,

a detailed analysis of the measurement errors is considered to be of little value. The manner in which the results have been interpreted is reported in Section VII-B, in which the photographic measurements have been discussed.

APPENDIX E

FURTHER COMMENTS AND CONSIDERATIONS ON STABILITY ANALYSIS OF SECTION IV

APPENDIX E

FURTHER COMMENTS AND CONSIDERATIONS ON STABILITY ANALYSIS OF SECTION IV

A. The Kelvin-Helmholtz Approach

A Kelvin-Helmholtz approach to the stability of disturbances on the vapor liquid interface in film boiling is based on the following assumptions:

1. The vapor flow satisfies the potential flow equations.
2. The base flow in the vapor is at a uniform velocity, u_0.
3. $\gamma = \frac{\rho_v}{\rho_L} << \frac{2\pi\delta}{\lambda_D} << 1$.

The result of this type of analysis [61] for the most unstable, or "most dangerous" wavelength, λ_D, is:

$$\lambda_D = 2\pi\sqrt{\frac{3\sigma\delta}{\rho_v u_0^2}} \quad . \tag{98}$$

To compare this result to experimental measurements, the following conditions for film boiling of saturated water were selected:

$$q_w = 35430 \frac{BTU}{hr\,ft^2} = 1.12 \times 10^8 \frac{erg}{s\text{-}cm^2}$$

$$T_w = 975^oF = 797^oK$$

$$x = 0.5 \text{ in.} = 1.27 \text{cm}$$

giving,

$$\delta=2.44\times10^{-3}\text{cm} \quad ; \quad \rho_v=3.75\times10^{-4}\ \frac{g}{cm^3} \quad ;$$

$$u_0=1725\ \frac{cm}{s} \quad ; \quad \sigma=58.9\ \frac{dyne}{cm} \quad .$$

Thus, from a Kelvin-Helmholtz analysis,

$$\lambda_{D_{K-H}}=0.124\text{cm}=0.049\text{ in.} \quad .$$

Experimentally, the average observed wavelength under the above conditions was, however,

$$\overline{\lambda}_{EXP}=0.48\text{ in.}$$

and the results of Section IV, when applied to these conditions give:

$$\lambda_D=0.297\text{ in.} \quad .$$

For the same conditions, at a higher elevation, namely $x=3.22$ in. (6.18cm), we have

$$\delta=6.20\times10^{-3}\text{cm}$$

and

$$u_0=3750\ \frac{cm}{s}$$

giving

$$\lambda_{D_{K-H}} = 9.05 \times 10^{-2} \text{cm} = 0.036 \text{ in.}$$

whereas, the average observed wavelength was,

$$\overline{\lambda}_{EXP} = 1.03 \text{ in.}$$

and, the results of Section IV give,

$$\lambda_D = 3.82 \text{ in.} \quad .$$

It can easily be seen that the results of a Kelvin-Helmholtz approach not only drastically underpredict interfacial wavelengths, but also predict a "most dangerous" wavelength which decreases with increasing elevation, while the data exhibits the opposite trend.

It is felt that the Kelvin-Helmholtz approach to the present stability problem is inadequate. This is believed to be primarily due to the fact that there is significant mass transfer at the vapor-liquid interface which should be included when the momentum theorem is applied at that boundary, and which cannot be accounted for in the context of a Kelvin-Helmholtz analysis. Additionally, while the surface tension force is the primary stabilizing influence under the assumptions associated with a Kelvin-Helmholtz analysis, it is felt that this force is, in the present phenomenon, negligible compared to the forces associated with the acceleration of the liquid phase and the effects of intense vaporization at the interphase boundary. The linearized stability analysis presented in Section IV was first completed with surface tension included, and the numerical results were unchanged when the surface tension was set equal

to zero.

B. Region of Applicability of Equation (92)

In Section IV the following dispersion relation for interfacial disturbances was derived (Eq.(92)):

$$\frac{\alpha Re}{12\gamma}\omega^2+\left\{\frac{\alpha Re}{6}+i\left(1+\frac{Sh}{3}\right)\right\}\omega-\frac{Sh}{Pe}-i\alpha\left(2+\frac{7}{10}Sh\right)$$

$$-\alpha^2 Re\left\{\frac{1}{5}-\frac{1}{6}\frac{Sh^2}{Pe^2}(1-\gamma)\right\}=0 \quad .$$

In the linearized stability analysis, the following expansions were made for the disturbance quantities, $\varphi(y)$ and $S(y)$ (Eqs.82 and 83):

$$\varphi(y)=\varphi_0(y)+\alpha\varphi_1(y)+\alpha^2\varphi_2(y)+\ldots$$

$$S(y)=S_0(y)+\alpha S_1(y)+\alpha^2 S_2(y)+\ldots$$

Equations (82) and (83) were substituted into the disturbance equations, and successive terms in the power series were obtained by equating terms containing like powers of α. Additionally, terms containing factors of order α^2 and higher were considered to be negligibly small compared to those containing α^0 or α^1.

Thus, the results of this stability analysis will only be valid when the expansions (82) and (83) represent convergent power series, and when

$$\alpha^n\varphi_n(y) \ll \varphi_0(y) \qquad n=1,2,3\ldots$$

$$\alpha^n S_n(y) << S_0(y) \qquad n=1,2,3...$$

From Section IV, we have

$$\varphi_0(y) = -2\varepsilon y^2 \tag{84}$$

$$S_0(y) = \varepsilon y \tag{85}$$

$$\varphi_1(y) = -i\varepsilon Re\left[\frac{2}{15}y^5 - \frac{c}{6}y^4 - \left\{\frac{\alpha c^2}{6\gamma} + \frac{1}{3}\frac{Sh^2}{Pe^2}(1-\gamma)\right\}y^3 + \left\{\frac{\alpha c^2}{4\gamma} + \frac{1}{3}(c-1) + \frac{1}{2}\frac{Sh^2}{Pe^2}(1-\gamma)\right\}y^2\right] \tag{86}$$

$$S_1(y) = i\varepsilon Pe\left[-\frac{1}{5}y^5 + \frac{1}{2}y^4 - \frac{c}{6}y^3 + \left(\frac{c}{6} - \frac{3}{10}\right)y\right] \tag{87}$$

Since the stability criterion (92) is developed from the following interfacial condition, Eq.(89)

$$\frac{Sh}{Pe}\left[S_0(1) + \alpha S_1(1)\right] = i\alpha\left[\varphi_0(1) + \alpha\varphi_1(1) + \varepsilon c\right] \quad ,$$

an indication of the region of validity of (92) can be obtained by examining the conditions under which

$$|\alpha\varphi_1(1)| < |\varphi_0(1)|$$

and

$$|\alpha S_1(1)| < |S_0(1)| \quad .$$

Thus, it is desirable to have:

$$\left|i\alpha Re\left[-\frac{1}{5}+\frac{c}{12}+\frac{\alpha c^2}{12\gamma}+\frac{1}{6}\frac{Sh^2}{Pe^2}(1-\gamma)\right]\right| < 2 \qquad (99)$$

and,

$$\left|i\alpha Pe\left[\frac{7}{10}-\frac{c}{3}\right]\right| < 1 \quad . \qquad (100)$$

Recalling that $\omega=\alpha c$ and noting that $\frac{Sh^2}{Pe^2} << 1$, (99) and (100) reduce to

$$\left|-\frac{1}{5}\alpha+\frac{\omega}{12}+\frac{\omega^2}{12\gamma}\right| < \frac{2}{Re} \qquad (101)$$

and,

$$\left|\frac{7}{10}\alpha-\frac{\omega}{3}\right| < \frac{1}{Pe} \quad . \qquad (102)$$

The values of α and ω which are calculated from Eq.(92) can be used in (101) and (102) to determine the approximate region of validity of these results.

For the stability boundary, we have $\alpha=\alpha_c=\frac{2\pi\delta}{\lambda_c}$ and $\omega=\omega_c$, and $Im[\omega_c]=0$. In this case, the left hand sides of (101) and (102) are sufficiently small for all values of Re and Pe occurring in the course of this experimental investigation. Thus, the theoretical values of λ_c, the critical wavelength, are considered to be sufficiently accurate for the purposes of this investigation.

A different conclusion, however, has to be drawn for the "most

dangerous" wavelength. The "most dangerous" wavelength (i.e., the most unstable wavelength) is that for which the imaginary part of the frequency ($\omega=\omega_D$) is at a maximum. The corresponding wave number is defined by $\alpha_D = \frac{2\pi\bar{\delta}}{\lambda_D}$. In this case, inequalities (101) and (102) give limiting values of Re and Pe above which accurate results cannot be expected. When calculated values of α_D and ω_D for the range of Re and Pe occurring in the experiments undertaken in this study are substituted into the approximate convergence criteria (101) and (102), the inequalities are, in general, satisfied for $Re \lesssim 300$ and $Pe \lesssim 20$. Since the Prandtl numbers are near unity for the vapors of water, ethanol and Freon 113, the limitation on the validity of Eq.(92) for calculation of the most dangerous wavelength can be expressed approximately as:

$$Re \lesssim 20.$$

Thus, for Reynolds numbers greater than 20 or so, the expansions (82) and (83) do not represent convergent power series when the calculated values of α_D and ω_D are used. Since the terms $\varphi_n(y)$ and $S_n(y)$ contain the factors Re^n and Pe^n, respectively, the fact that there result limitations on the values of Re and Pe is not unexpected. Also, these limitations are consistent with the use of the equations of motion and energy for laminar flow in the derivation of Eq.(92), since for large Re and Pe, the flow will be turbulent, and these governing equations will not be applicable.

The Reynolds numbers of the vapor film occurring in this investigation were generally greater than twenty, and the applicability of the analysis to waves of length λ_D is questionable. However, as shown

earlier, the results of the analysis are applicable to waves of the critical wavelength, λ_c, even when the Reynolds number is large. It is therefore felt that the mechanisms of wave generation might be properly modeled in the derivation of Eq.(92), and that the results provide information which might be helpful in the understanding of the stability conditions.

On the basis of these findings, the following conclusions can be made:

1. Equation (92) is useful for determination of the critical wavelengths, or stability boundary, even in the region where the vapor flow is turbulent.
2. Equation (92) should not be expected to predict "most dangerous" wavelengths accurately for vapor film Reynolds numbers greater than twenty or so.
3. Evaporation at the vapor-liquid interface is an important feature in the generation of interfacial disturbances.